Science Advances
AAAS

Supplementary Materials for

Tibetan terrestrial and aquatic ecosystems collapsed with cryosphere loss inferred from sedimentary ancient metagenomics

Sisi Liu *et al.*

Corresponding author: Ulrike Herzschuh, ulrike.herzschuh@awi.de; Sisi Liu, sisi.liu@awi.de

Sci. Adv. **10**, eadn8490 (2024)
DOI: 10.1126/sciadv.adn8490

The PDF file includes:

Other Supplementary Material for this manuscript includes the following:

Supplementary Text

Modern and late Pleistocene/Holocene site setting

The modern climate conditions are indicated by mean annual temperature (MAT) of 6.6℃, mean July temperature (MJT) of 14.3℃, mean January temperature of -3.9℃, and over 90% of annual rainfall (about 560 mm) occurring in May−October according to the closest meteorological station at Garze (31.62° N, 100.00° E, at 3,522 m a.s.l.) that is located ~ 80 km northeast of Lake Naleng. According to the observed temperature lapse rate (0.55°C 100 m^{-1}) in the Hengduan Mountains (*127*), the MAT and MJT are estimated to be 2.9°C and 10.6°C at the lake, respectively.

We simulated permafrost extent over the past 22,000 years at a resolution of 500 years (Fig. S1) with integration of our published glacier dynamics (*45*). The modeled glaciers dominated the lake catchment before 15 ka (median 86.4%) and rapidly disappeared by 14 ka with slight advances in the eastern margin at 12.5 ka (0.8% and 0.02 Gt, Fig. S12A, B), which agrees with the clay content (mean grain size < 2 μm) of lake sediments (*96*). Before 14 ka, the permafrost extent accounted for a median value of 10.0% over the lake catchment; that is, permafrost was well developed in the glacier-free areas (median 67.9%, Fig. S12C) and lowland (4100−4500, median 62.6%, Fig. S12D) in particular. In contrast, the simulated permafrost within the lowland extensively shrank at 14 ka (7.5% remaining) and finally disappeared after 12.5 ka. The highland (4500−4900 m a.s.l.) hosted permafrost until 10 ka (Fig. S12E). Despite permafrost being restored, it was simulated in the highland only during the late Holocene (median 9.3%).

Library preparation

All libraries were quantified using quantitative real-time Polymerase chain reaction (qPCR) with 1 μL diluted library (1:20) (*103*). In total, 24 μL library and PCR no template controls were processed by PCR amplification and indexing as described in Gansauge and Meyer (*103*) with 11−14 cycles (Table S4) using the index primer sequences P5 (01-06, 11, 15-18, 46, 51, 64, 67, 72) and P7 (20, 21, 26, 27, 29, 40, 57, 60, 65, 82, 88, 91-96). After purification with the MinElute PCR Purification Kit (Qiagen, Germany), the initial quality control of amplified libraries was performed using the 4200 TapeStation system (Agilent, G2991AA). A total of four amplified libraries (ESL028, ESL034, ESL061, and ESL079) having high peak of adapter dimers with ~150 bp were selected to be cut out of an agarose gel (2%) after separation by electrophoresis, and then purified with E.Z.N.A.® MicroElute Gel Extraction Kit (Omega Bio-tek®). Afterwards, qPCR, indexing PCR, PCR purification, and quality control were performed for these libraries. No unexpected adapter peak was found. Two library blanks, JK125_LB and JK126_LB, without gene bands in TapeStation quality checking were not considered for shotgun sequencing.

Biota of the Tibetan Plateau: a compilation

For seed-bearing plants (phylum: Streptophyta), we downloaded species occurrence data from (i) the Global Biodiversity Information Facility (GBIF, accessed 24.10.2022, source data: (*128*)) with the following filters used: 'Geometry POLYGON ((73.499 24.814,104.672 24.814,104.672 39.826,73.499 39.826,73.499 24.814))', 'HasCoordinate is true', 'HasGeospatialIssue is false', 'TaxonKey is Tracheophyta' (Selecting Tracheophyta to ensure that taxa are not overlooked); (ii) Biodiversity the Hengduan Mountains and adjacent areas of south-central China (accessed

24.10.2022, http://hengduan.huh.harvard.edu/fieldnotes) with information on coordination and elevation; (iii) Flora of China (accessed 24.10.2022, ref. (*129*)) with a range of elevation; and (iv) publications with information on elevation (*130*, *131*). The species occurrences obtained from GBIF were cropped using a merged polygon of the Tibetan Plateau (*132*) and the Hengduan Mountains (*133*) using 'over()' in the 'sp' package (v. 1.5.1, refs. (*134*, *135*)). Elevation information was extracted from the SRTM 30m Digital Elevation Database based on the coordinates of the occurrences using the 'extract()' function in the 'raster' package (v. 3.6.11, ref. (*136*)). The SRTM 30m data was downloaded using the 'SRTM-Downloader' plugin in QGIS (v. 3.24.1-Tisler, https://www.qgis.org/en/site/, ref. (*137*)). For species lacking a family name, the family name was obtained using tax_name(db = "ncbi", get = c("family")) in the 'taxize' package (v. 0.9.98, ref. (*138*)). A family list, including occurrences found at elevations above 3000 m a.s.l. (referred to as high elevation region), was compiled based on these four databases. This list was then passed to the 'get_uid()' in the 'taxize' package (v. 0.9.98, ref. (*138*) to retrieve the taxonomy ID. As a result, the plant taxa list contains 1,615 genera and 259 families.

For mammals, we compiled the taxa list from the mammals of China (*139*) and GBIF (accessed 24.10.2022, source data: (*140*)), using the same filters as those used for vascular plants, except for the filter 'TaxonKey is Mammalia'. After retrieving the taxonomy ID and elevation information, 105 genera and 32 families were obtained. We further excluded bats (Hipposideridae, Vespertilionidae, and Rhinolophidae) and Hominidae and Camelidae.

For freshwater fish, we collected the occurrences for 15 orders of China's freshwater fish (*141*) from Fishbase hosted by GBIF (accessed 22.02.2023, source data: (*142*)) with 'TaxonKey is one of (Cypriniformes, Clupeiformes, Salmoniformes, Anguilliformes, Siluriformes, Cyprinodontiformes, Beloniformes, Gadiformes, Gasterosteiformes, Mugiliformes, Synbranchiformes, Perciformes, Scorpaeniformes, Pleuronectiformes, Tetraodontiformes). The inventory of freshwater fish was compiled following the same approach used for plants and mammals, resulting in a total of 134 genera and 62 families.

Permafrost simulation

A number of researches has demonstrated a temperature-driven permafrost distribution in the Tibetan Plateau, reviewed by Yang et al. (*143*). Although the soil-surface temperature (-20 cm) has been recognized to be more closely related to permafrost than air temperature (*144*), both variables have a strong linear relationship in the Tibetan permafrost regions (*145*). Due to a lack of paleo and present-day soil-surface temperature records, we used air temperature to simplify the generalized linear model (GLM). Modern estimates of the mean annual air temperature (MAAT) were derived from WorldClim (version 2, data for 1970−2000 C.E., ref. (*146*)) with 30 seconds (~1 km^2 spatial resolution). The SRTM 30-m digital elevation data was downloaded from NASA's server using QGIS (v. 3.24.1-Tisler, https://www.qgis.org/en/site/, ref. (*137*)) with the inherent plugin of SRTM-Downloader (v 3.1.17). To match the present-day permafrost distribution, we used a wider region of our study area with an extent of 31.11 ± 0.5° N and 99.75 ± 0.5° E to crop both spatial datasets using the 'crop' function. Then, they were projected to coordinate reference systems (crs) of Asia North Albers Equal Area Conic (crs = 102025) to minimize the geographic distortions using the 'projectRaster' function. The present-day permafrost distribution originated from the Map of Permafrost Distribution on the Tibetan Plateau v. 2017 (crs = 102025), which is simulated based on the temperature at the top of permafrost and validated by ground-based observations (*6*). Subsequently, spatial datasets were downscaled to a fine resolution of 30 m using

the ‘resample’ function with bilinear interpolation that weights the four nearest pixels to the original spatial pixel. The present-day relationship between permafrost distribution and MAAT was built using the ‘glm’ function with a Gaussian family. Such a relationship is statistically significant with a *P* value (t-test, 999 permutations) < 2e-16, suggesting that it is suitable for interpolation in a paleo temperature setting.

The past spatial temperature was simulated based on multi-proxy reconstructed paleo-temperature (*113*, *114*) and the 30 m SRTM digital elevation data (*45*). The permafrost distributions for 22−0 ka at 500-year intervals were predicted using the ‘predict.glm’ function with parameters of type = “response” and se.fit = TRUE. We extracted the threshold (0.22052) of permafrost presence by comparing the permafrost distribution at 0 ka to present-day. Hence, any pixel with a value ≥ 0.22052 was considered to contain permafrost. Then, we converted the simulated permafrost to binary spatial data and calculated the number of permafrost pixels per 100-m elevation bin under the effect of modeled glacier extent within lake catchment (*45*). The results are shown in Fig. S12C. We further calculated the number of permafrost pixels within 4100−4500 m a.s.l. and 4500−4900 m a.s.l to present the permafrost extent within lowland (Fig. S12D) and highland (Fig. S12E), respectively. The boundary of 4500 m a.s.l. was defined based on the reachable slope degree (38°) of yak-grazing (*147*). Most catchment areas above 4500 m are either far from inflows or with steep slopes (> 38°, Fig. S1). The functions for spatial data processing and simulation come from the R package ‘raster’ (version 3.5-15) (*136*) and ‘stats’ (*126*).

The composition of Proteobacteria has been reported to be distinct in soil sections in the Tibetan permafrost regions, of which Alphaproteobacteria dominate in the active layer and Gammaproteobacteria dominate in the permafrost layer (*148*). Thus, we calculated the compositional changes of Proteobacteria. Consequently, our simulated results align with the high percentages of Gammaproteobacteria before 14 ka and the pronounced decline afterward (Fig. S9A, B). Also, the percentages of Alphaproteobacteria imply that the active layers were possibly thinner in the pre-14 ka period and increased in thickness afterwards (Fig. S9C).

SedaDNA preservation and provenance assessment

The differences in sediment types and mineralogies are reported to affect DNA sources, absorption, and recovery, thereby weakening the comparison of DNA-inferred community changes across time (*48*, *149*, *150*). However, we assert that our inferences from the Lake Naleng sedaDNA record across time are both comparable and robust. The presence or absence of taxa DNA is most likely attributed to ecological changes, with limited influence from the depositional environment. The DNA preserved across sediment layers most likely tracks the biological information originating from diverse habitats within the catchment, transported via fluvial processes through time, including the influence of glacial melting before 14 ka. This reasoning is explained as follows.

First, we did not observe noticeable biases induced by lithology and sediment accumulation (Fig. S5), as neither the samples nor the taxa cluster along sediment types, and there is no skew along sedimentation rates in the PCA plots (Fig. S6).

Second, the lake-sediment source remained consistent and primarily originates from catchment area, supported by the observed uniformity in grain-size fractions and elemental components (Fig. S5). More specifically, the input of fine-grained detrital materials (clay to silt-sized particles) in the lake aligns with characteristics typical of unaltered sediments in a partly glaciated catchment

in the Tibetan alpine regions (*151*). Furthermore, the major element concentrations (SiO_2 and Al_2O_3) reflect the chemical composition of the granitic and granodiorite parent rock in the lake catchment. A previous study (*96*) discussed the deposition of lake sediments, emphasizing the direct erosion of soils derived from local sources (e.g., slopes, terraces, and topographic depressions near rivers and lakes) over time. This process was coupled with the input of local unaltered detrital sediments via glacial dynamics before 14.5 ka (*96*). We, therefore, assume that lake sediments continuously accumulated detrital materials eroded from the local environment.

Third, the capacity and recovery of DNA-mineral binding across time are comparable. The lake catchment area is characterized by Miocene granite and granodiorite, primarily made up of quartz, mica, and feldspar. This composition aligns with the mineral composition of a modern sediment sample from Lake Naleng, as determined by X-ray diffraction (XRD), which includes mica (48%), quartz (33%), chlorite (12%), and feldspar (7%) (*152*). By analogy, we deduce that a similar composition of minerals characterizes the core sediments over time, as there are no notable shifts in grain-size fractions and element concentrations throughout the core's entirety. Despite non-clay minerals (e.g., mica, quartz, chlorite, and feldspar) having relatively lower DNA adsorption capacities compared to clay minerals (e.g., smectite and illite), a high amount of DNA (40%) adsorbed to non-clay minerals is recoverable, whereas clay minerals yield up to 10% extraction of adsorbed DNA (*48*, *150*).

Fourth, read fragmentation induced by carbonates as seen for calcite (*149*) and clay minerals (if applicable) is rather unlikely. The catchment area lacks calcareous rocks (e.g., calcite) and the lake-sediment core contains very low carbonate content (< 1%, Fig. S5). So far, it is unclear if clay minerals would induce fragmentation as well. Nevertheless, we observed an insignificant relationship (Spearman's rho = -0.19, Bonferroni adjusted *P*-value = 0.246) between weighted average read length (as a proxy of fragmentation) and clay-size fraction (as a proxy of clay minerals). A low standard deviation (6 bp) of weighted average read length further implies less variability in preservation conditions of DNA over time. On the other hand, weighted average read length does not significantly explain the composition turnovers of terrestrial vegetation (adjusted R^2 = 1.9%, *P*-value = 0.113), terrestrial mammalian (adjusted R^2 = 0.2%, *P*-value = 0.2), and aquatic communities (not relevant due to negative adjusted R^2 = -0.18%), suggesting that observed DNA degradation with time (Fig. S4) has contributed minimally to ecological interpretation.

Fifth, redeposition is considered rather unlikely due to the bowl-shaped structure of the lake basin, as well as relatively rapid sedimentation rates and prevailing stable chemical burial conditions.

Co-existence of alternative states in lake system

The distribution of macrophyte and phytoplankton can be horizontal, such as in Taihu (in eastern China, ref. (*153*)), or vertical, such as in Son Kol (in the central Tien Shan, ref. (*154*)). Both lakes are mesotrophic with either a large surface area (Taihu) or deep-water body (Son Kol). Similar to Lake Naleng, palynological and non-pollen palynomorph (*69*) as well as biogeochemical parameters (TOC, TP, and C/N ration, ref. (*96*)) indicate moderate nutrient levels and high lake level during 14.5−3.6 ka. These characteristics could provide suitable habitats for both macrophytes and phytoplankton. Submerged plants require nutrients and light to grow and can usually be found in the littoral zones where light can penetrate the water column, while cyanobacteria can use atmospheric nitrogen and other nutrients such as phosphorus, and can be found in deeper waters where they can access these nutrients.

Figs S1 – S16

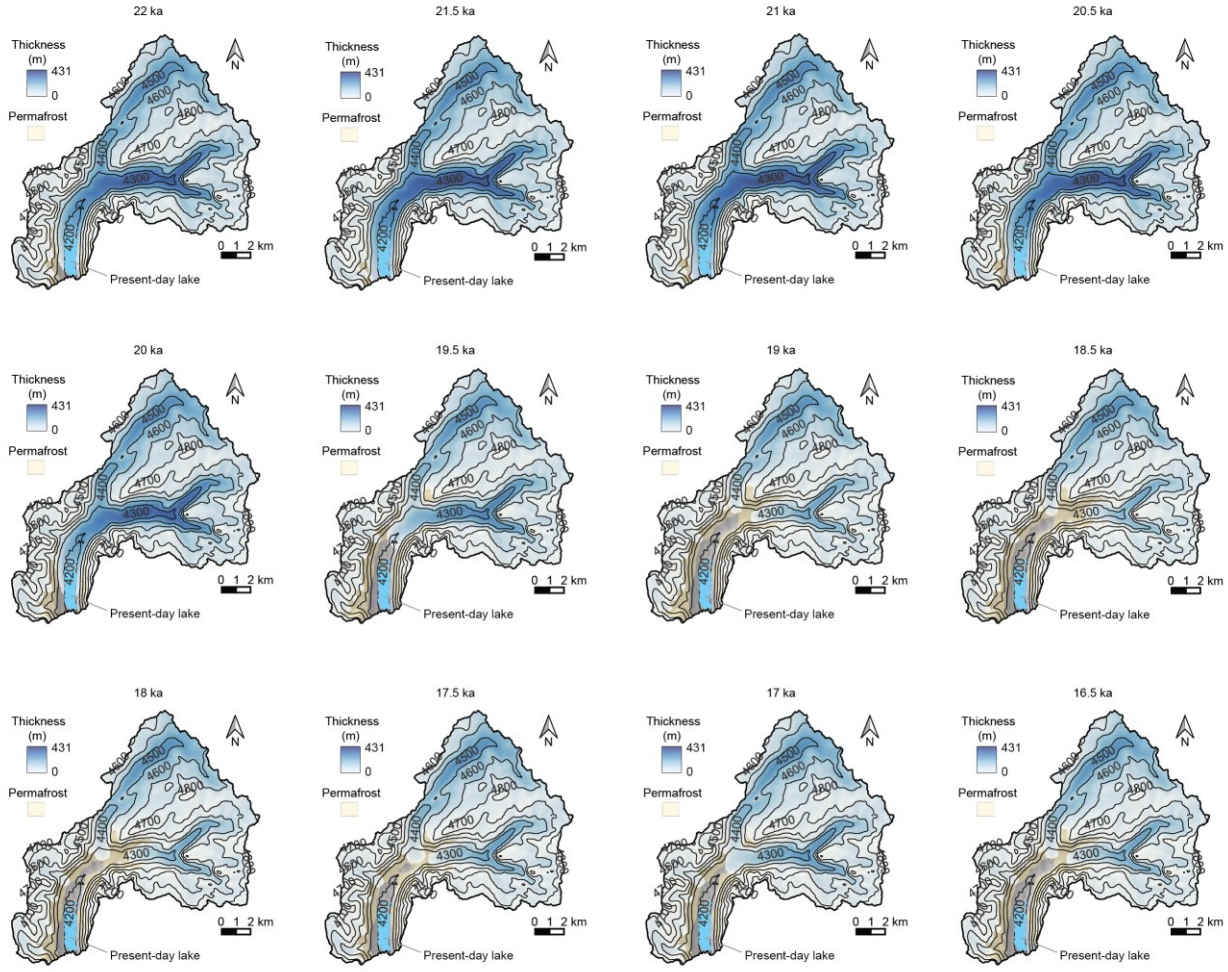
22 ka
21.5 ka
21 ka
20.5 ka
20 ka
19.5 ka
19 ka
18.5 ka
18 ka
17.5 ka
17 ka
16.5 ka
Thickness (m)
431
0
Permafrost
N
0 1 2 km
Present-day lake

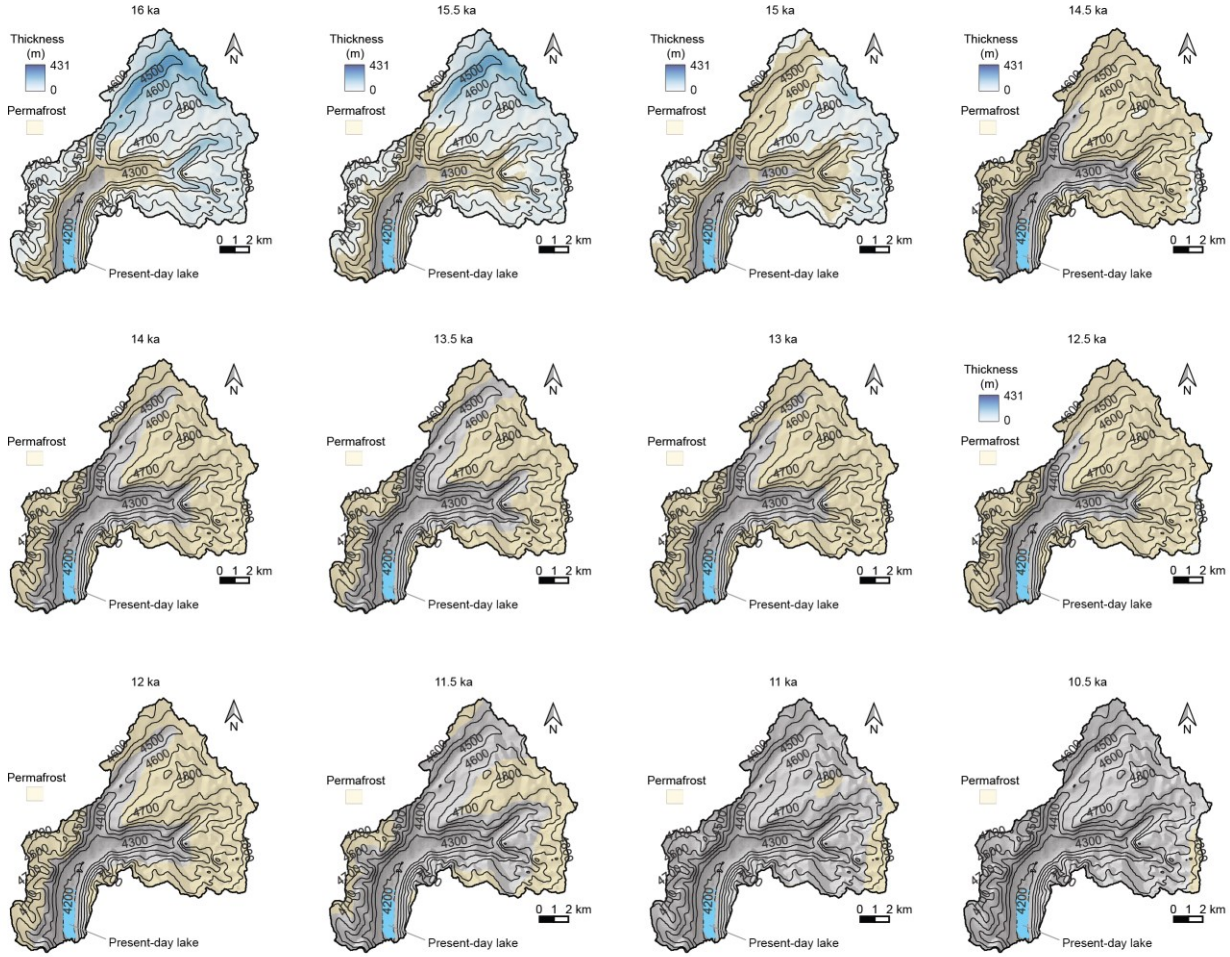
16 ka
15.5 ka
15 ka
14.5 ka
14 ka
13.5 ka
13 ka
12.5 ka
12 ka
11.5 ka
11 ka
10.5 ka
Thickness (m)
431
0
Permafrost
N
0 1 2 km
Present-day lake
4600
4500
4800
4700
4400
4300
4200

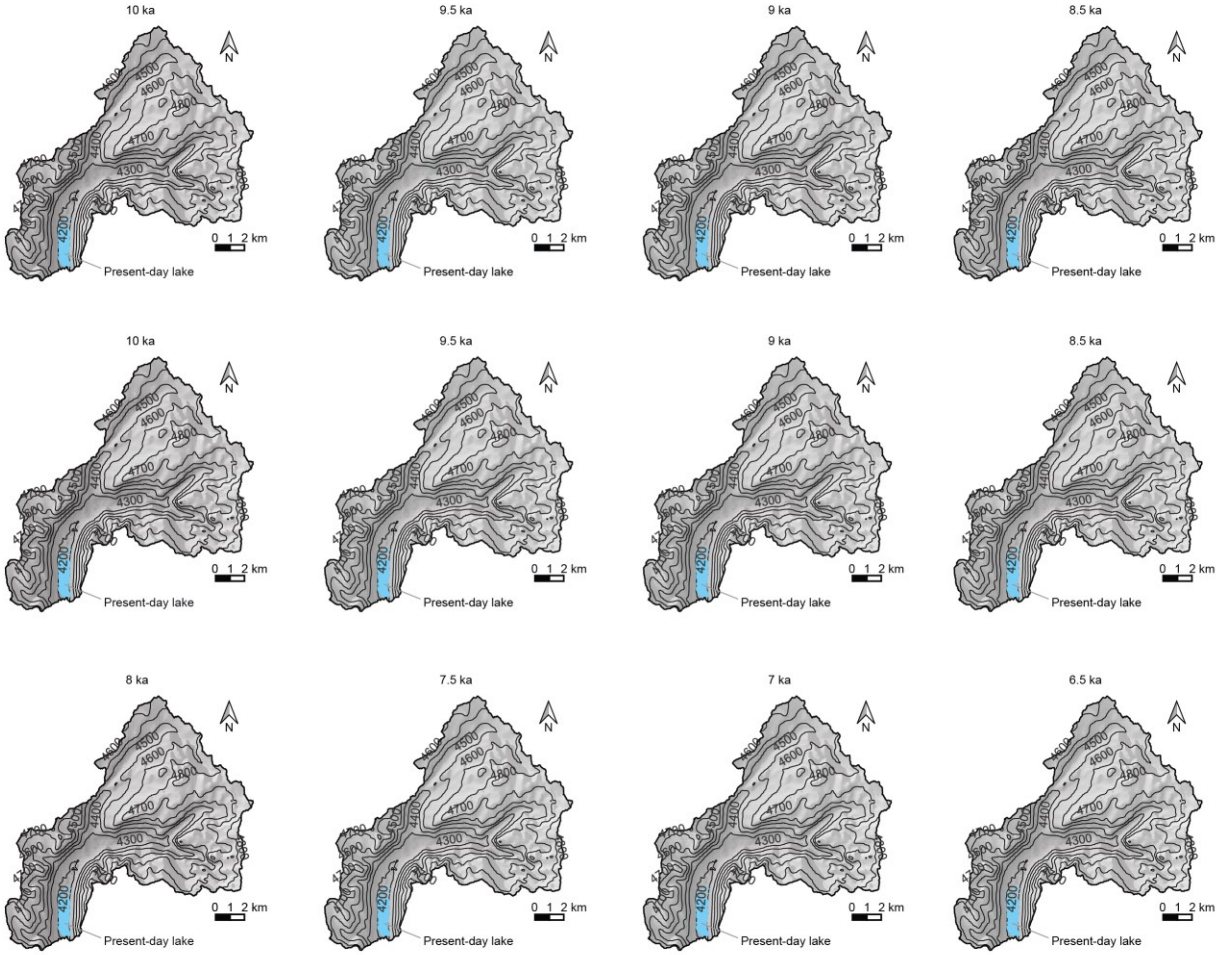
10 ka
9.5 ka
9 ka
8.5 ka
10 ka
9.5 ka
9 ka
8.5 ka
8 ka
7.5 ka
7 ka
6.5 ka
N
4600
4500
4800
4700
4400
4300
4200
0 1 2 km
Present-day lake

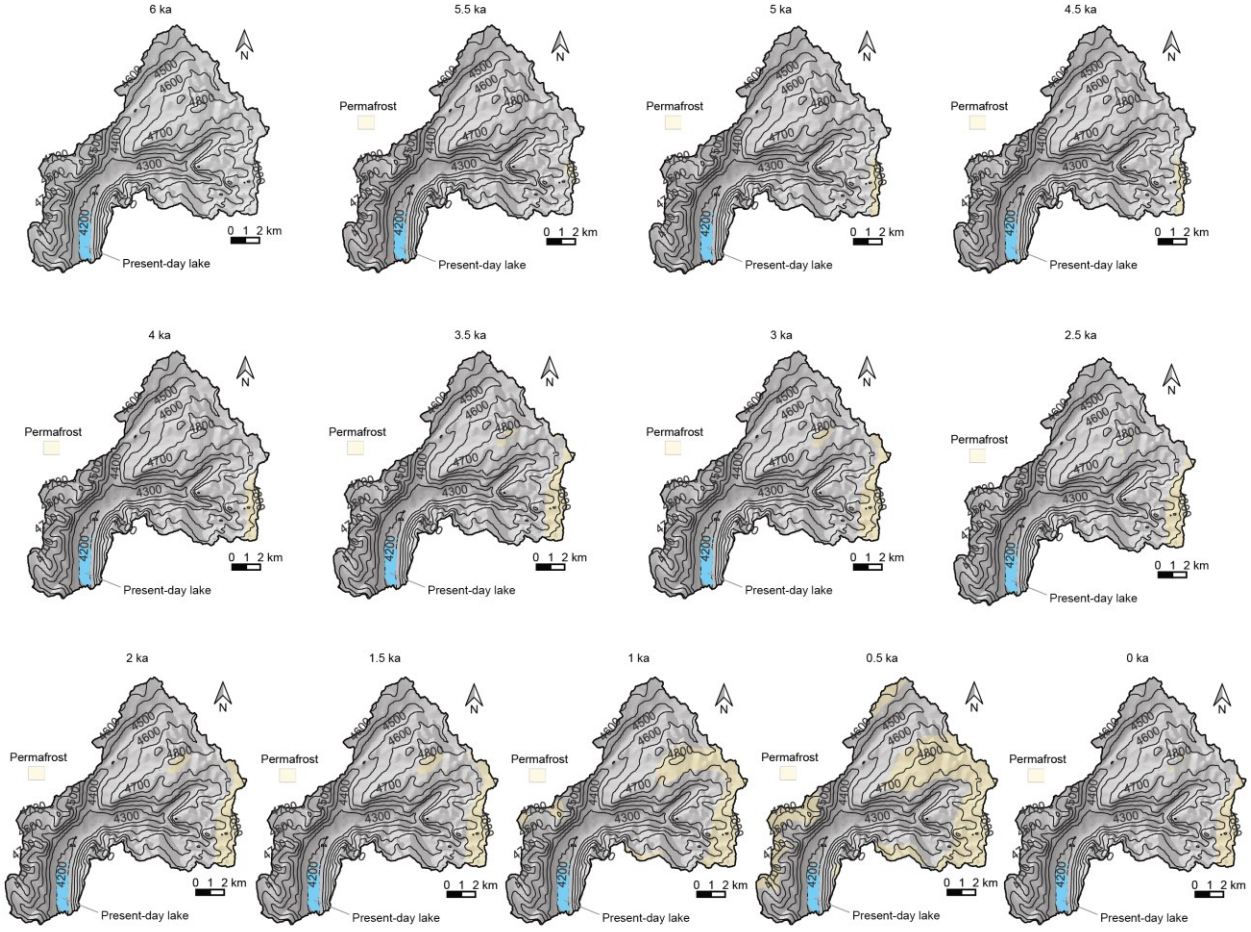

Fig. S1. Simulated permafrost extent (by taking glacier dynamics into account, ref. (*45*)) within Lake Naleng's catchment during 22−0 ka at a 500-year resolution, indicating substantial loss of permafrost and glaciers since 14 ka and only a small portion of permafrost restoration in the highlands during the late Holocene.

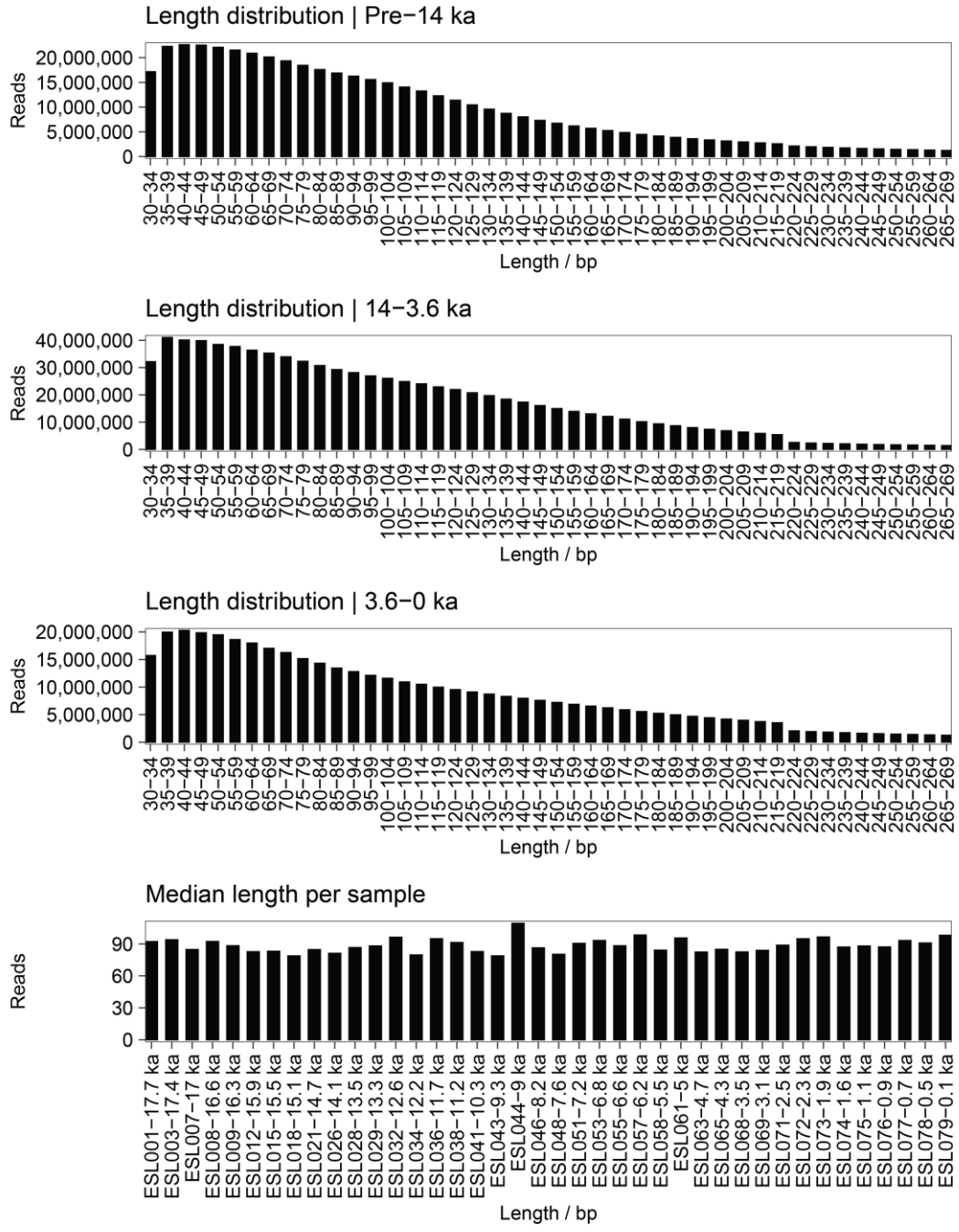

Fig. S2. Length distribution of reads of three time-intervals and median read length across time. The DNA fragments exhibit highly degraded profiles with left-skewed distributions, and there are no discernible differences in read length observed across time.

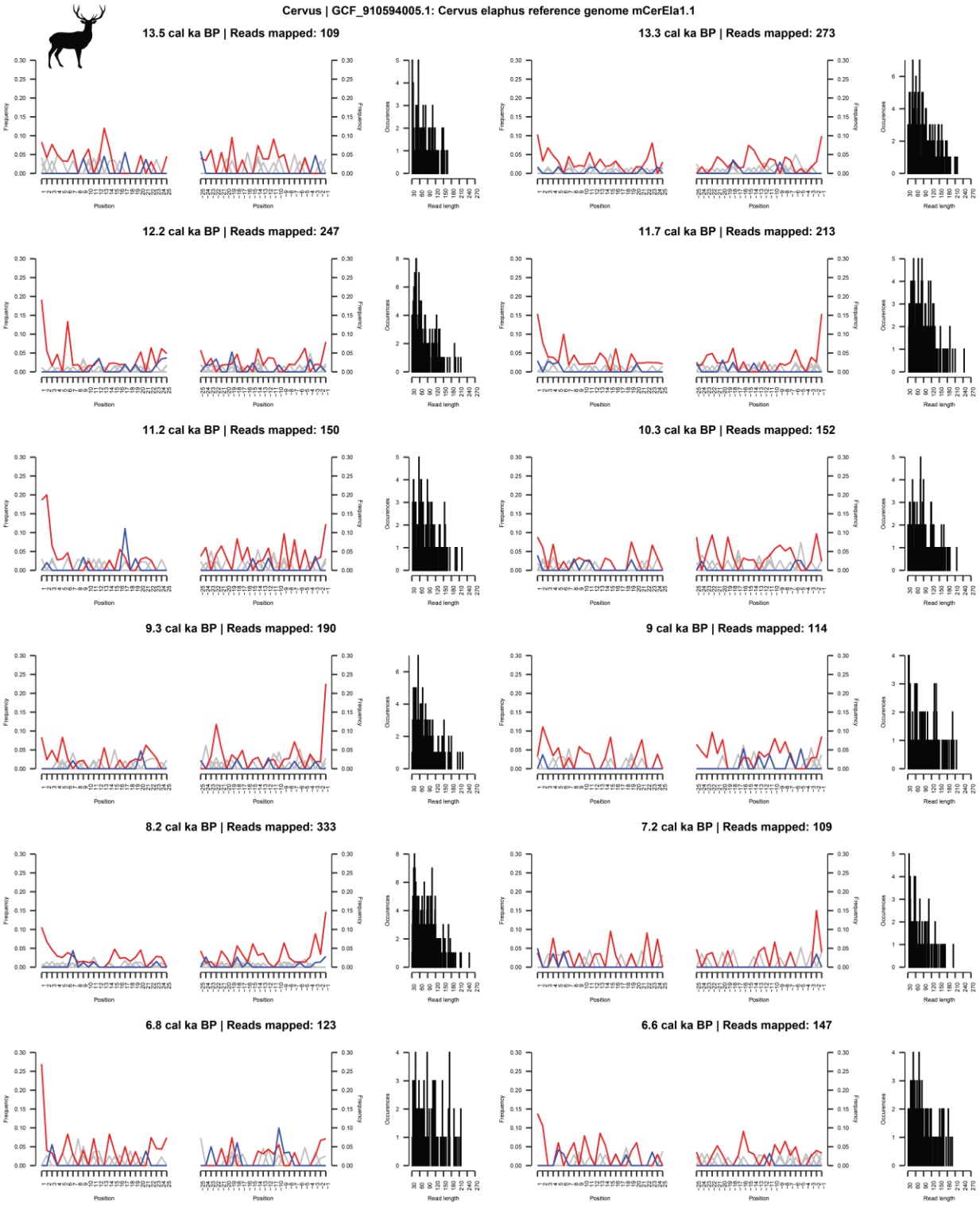
Cervus | GCF_910594005.1: Cervus elaphus reference genome mCerEla1.1
13.5 cal ka BP | Reads mapped: 109
13.3 cal ka BP | Reads mapped: 273
12.2 cal ka BP | Reads mapped: 247
11.7 cal ka BP | Reads mapped: 213
11.2 cal ka BP | Reads mapped: 150
10.3 cal ka BP | Reads mapped: 152
9.3 cal ka BP | Reads mapped: 190
9 cal ka BP | Reads mapped: 114
8.2 cal ka BP | Reads mapped: 333
7.2 cal ka BP | Reads mapped: 109
6.8 cal ka BP | Reads mapped: 123
6.6 cal ka BP | Reads mapped: 147
Frequency
Position
Occurences
Read length

Continued

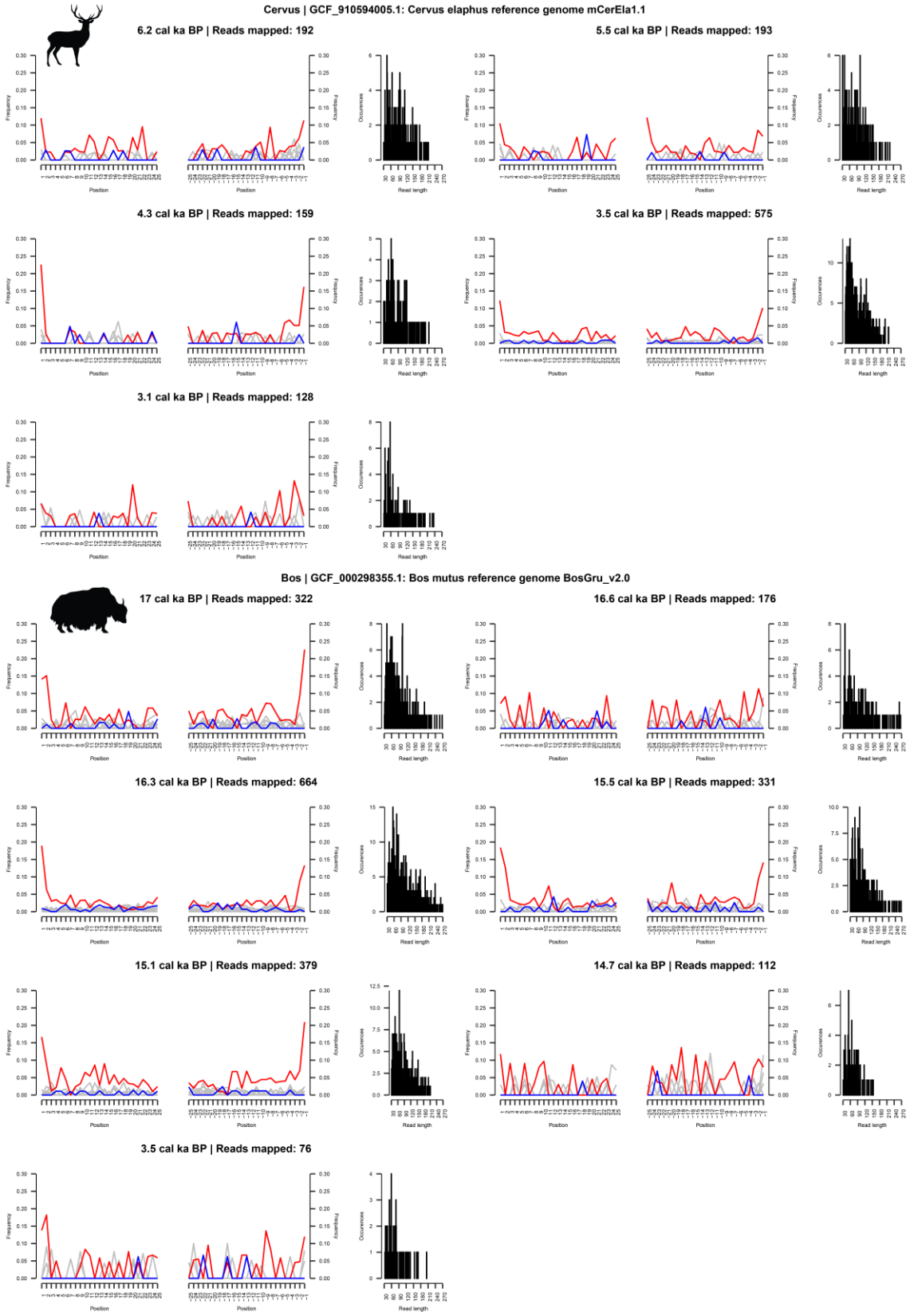
Cervus | GCF_910594005.1: Cervus elaphus reference genome mCerEla1.1
6.2 cal ka BP | Reads mapped: 192
5.5 cal ka BP | Reads mapped: 193
4.3 cal ka BP | Reads mapped: 159
3.5 cal ka BP | Reads mapped: 575
3.1 cal ka BP | Reads mapped: 128
Bos | GCF_000298355.1: Bos mutus reference genome BosGru_v2.0
17 cal ka BP | Reads mapped: 322
16.6 cal ka BP | Reads mapped: 176
16.3 cal ka BP | Reads mapped: 664
15.5 cal ka BP | Reads mapped: 331
15.1 cal ka BP | Reads mapped: 379
14.7 cal ka BP | Reads mapped: 112
3.5 cal ka BP | Reads mapped: 76
Frequency
Position
Occurences
Read length

Continued

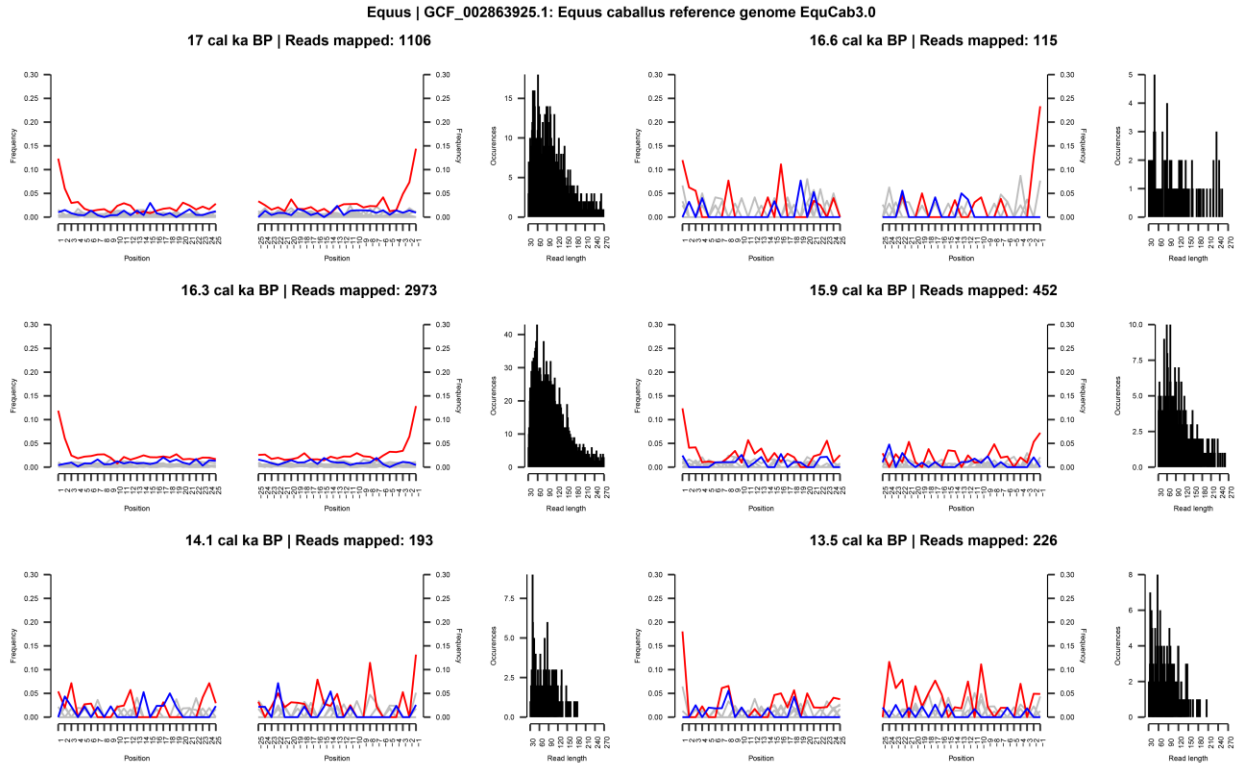
Equus | GCF_002863925.1: Equus caballus reference genome EquCab3.0
17 cal ka BP | Reads mapped: 1106
16.6 cal ka BP | Reads mapped: 115
16.3 cal ka BP | Reads mapped: 2973
15.9 cal ka BP | Reads mapped: 452
14.1 cal ka BP | Reads mapped: 193
13.5 cal ka BP | Reads mapped: 226
Frequency
Position
Occurences
Read length

Continued

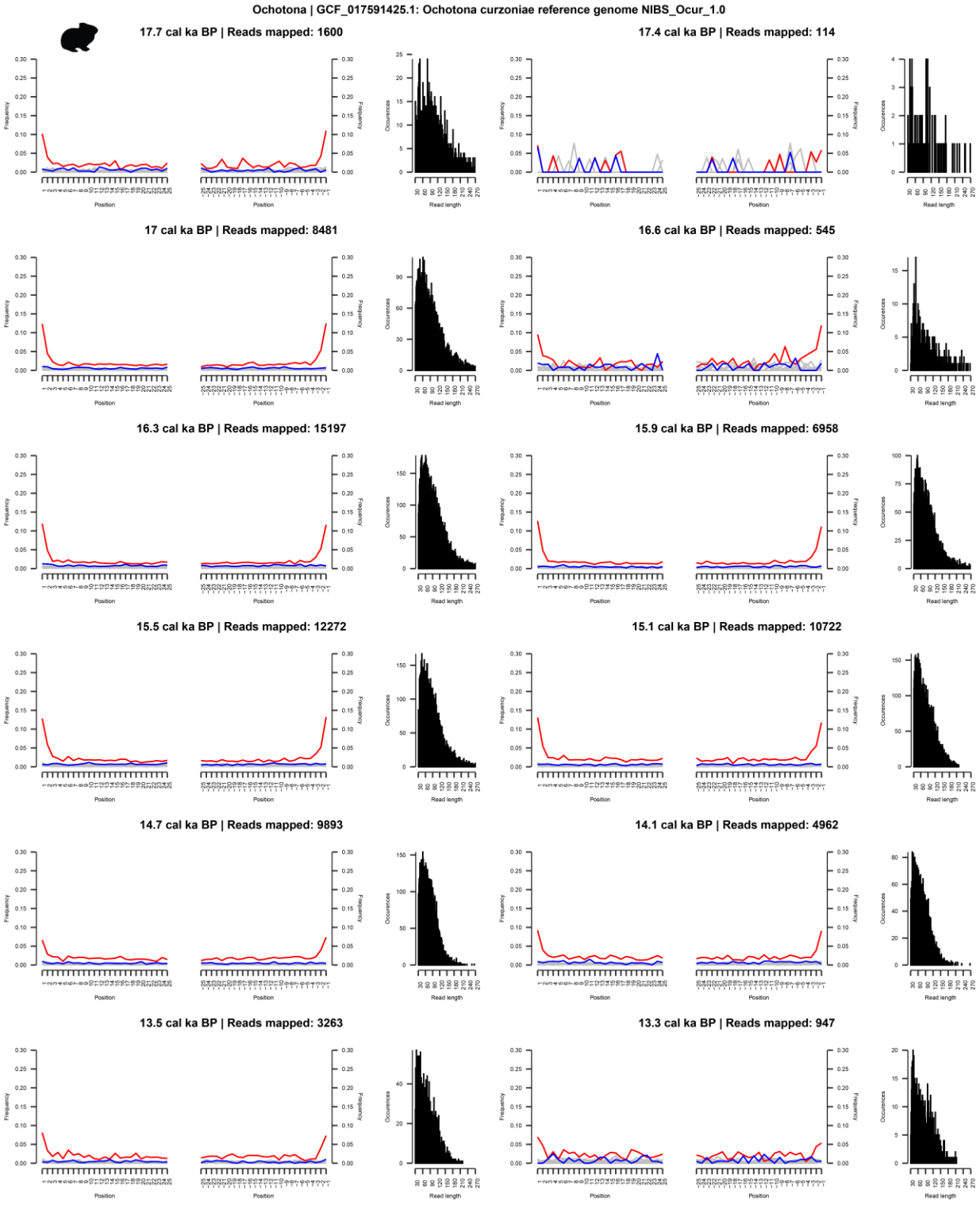
Ochotona | GCF_017591425.1: Ochotona curzoniae reference genome NIBS_Ocur_1.0
17.7 cal ka BP | Reads mapped: 1600
17.4 cal ka BP | Reads mapped: 114
17 cal ka BP | Reads mapped: 8481
16.6 cal ka BP | Reads mapped: 545
16.3 cal ka BP | Reads mapped: 15197
15.9 cal ka BP | Reads mapped: 6958
15.5 cal ka BP | Reads mapped: 12272
15.1 cal ka BP | Reads mapped: 10722
14.7 cal ka BP | Reads mapped: 9893
14.1 cal ka BP | Reads mapped: 4962
13.5 cal ka BP | Reads mapped: 3263
13.3 cal ka BP | Reads mapped: 947
Frequency
Position
Occurences
Read length

Continued

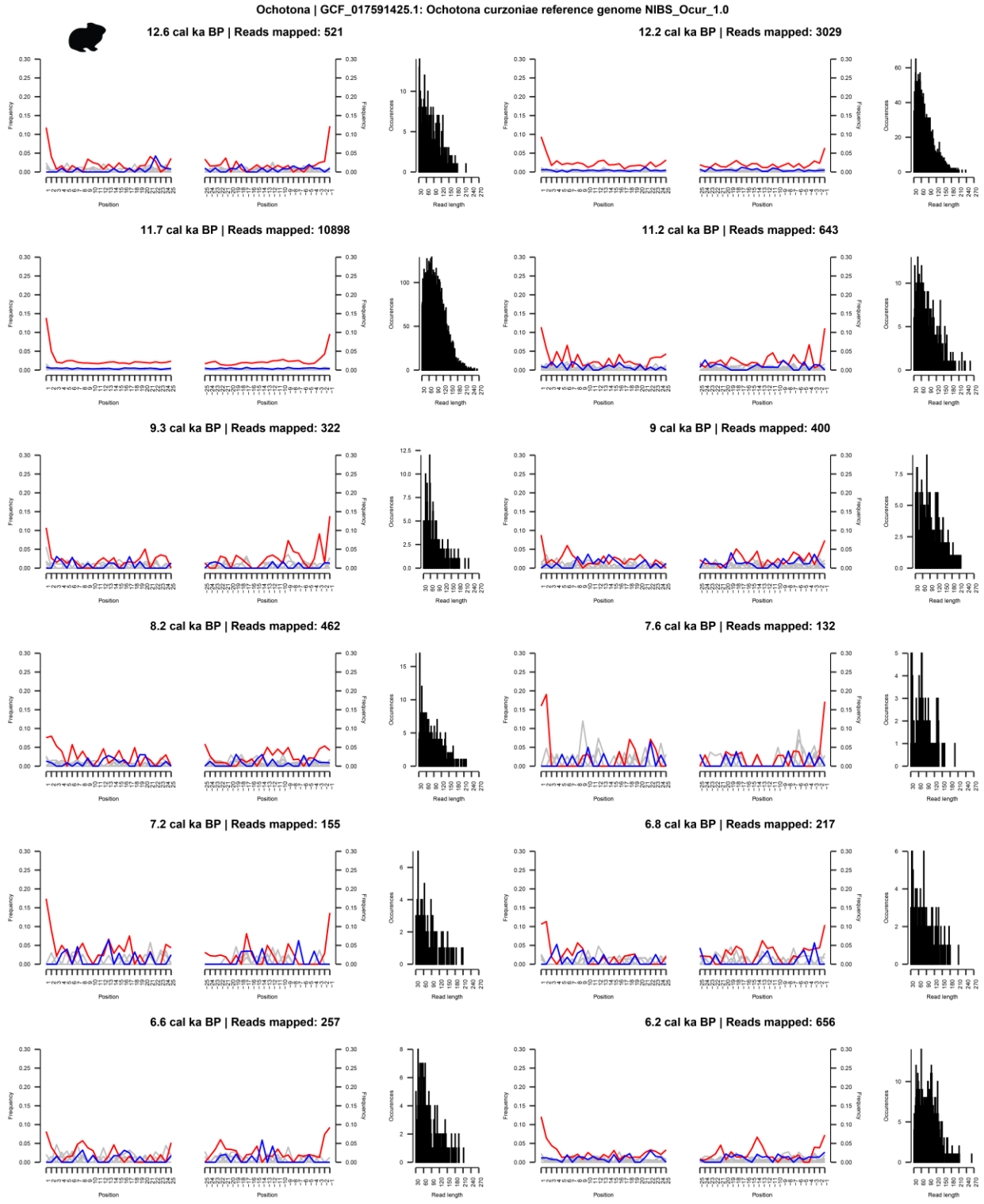
Ochotona | GCF_017591425.1: Ochotona curzoniae reference genome NIBS_Ocur_1.0
12.6 cal ka BP | Reads mapped: 521
12.2 cal ka BP | Reads mapped: 3029
11.7 cal ka BP | Reads mapped: 10898
11.2 cal ka BP | Reads mapped: 643
9.3 cal ka BP | Reads mapped: 322
9 cal ka BP | Reads mapped: 400
8.2 cal ka BP | Reads mapped: 462
7.6 cal ka BP | Reads mapped: 132
7.2 cal ka BP | Reads mapped: 155
6.8 cal ka BP | Reads mapped: 217
6.6 cal ka BP | Reads mapped: 257
6.2 cal ka BP | Reads mapped: 656
Frequency
Position
Occurences
Read length

Continued

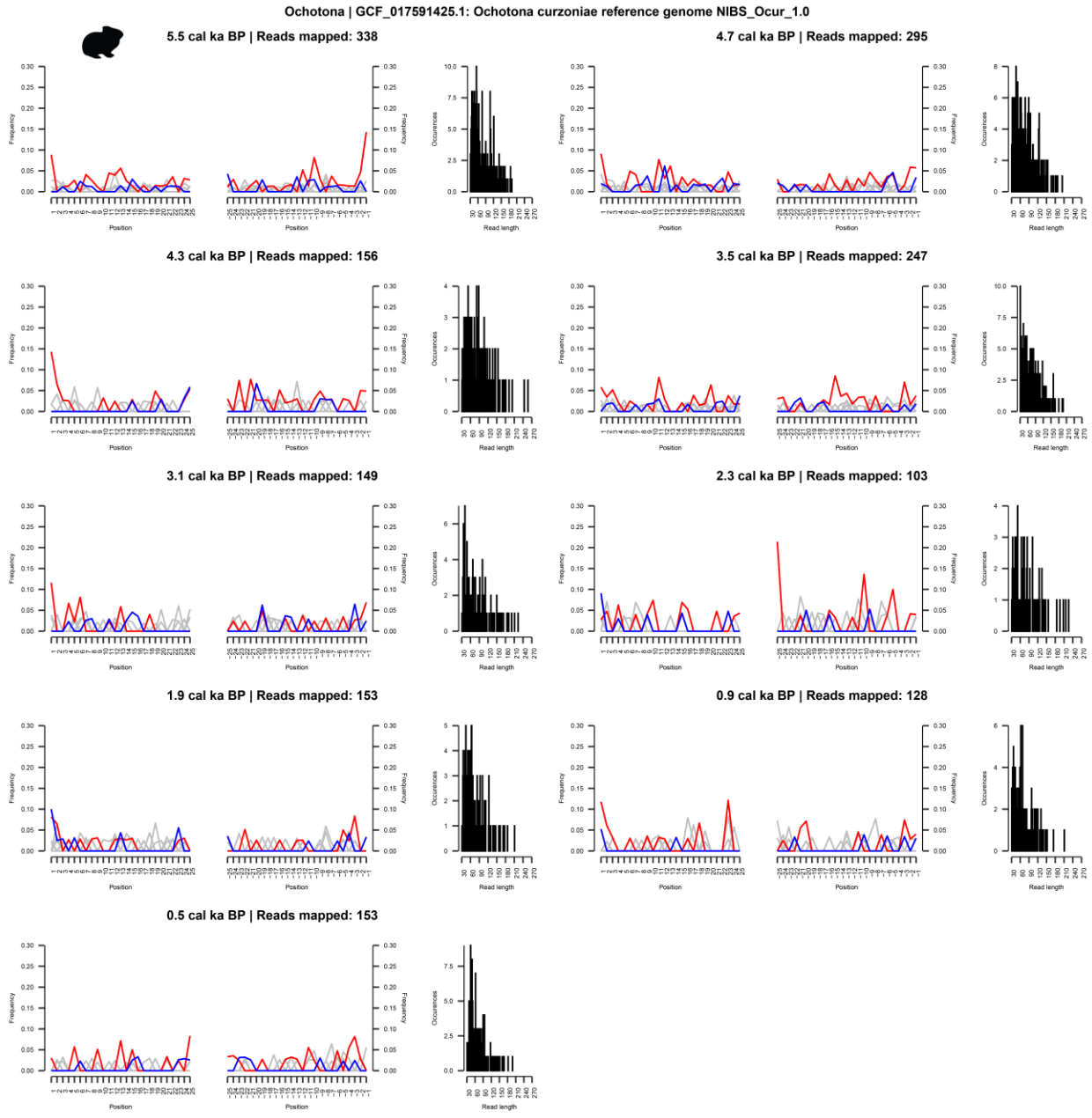
Ochotona | GCF_017591425.1: Ochotona curzoniae reference genome NIBS_Ocur_1.0
5.5 cal ka BP | Reads mapped: 338
4.7 cal ka BP | Reads mapped: 295
4.3 cal ka BP | Reads mapped: 156
3.5 cal ka BP | Reads mapped: 247
3.1 cal ka BP | Reads mapped: 149
2.3 cal ka BP | Reads mapped: 103
1.9 cal ka BP | Reads mapped: 153
0.9 cal ka BP | Reads mapped: 128
0.5 cal ka BP | Reads mapped: 153
Frequency
Position
Occurences
Read length

Continued

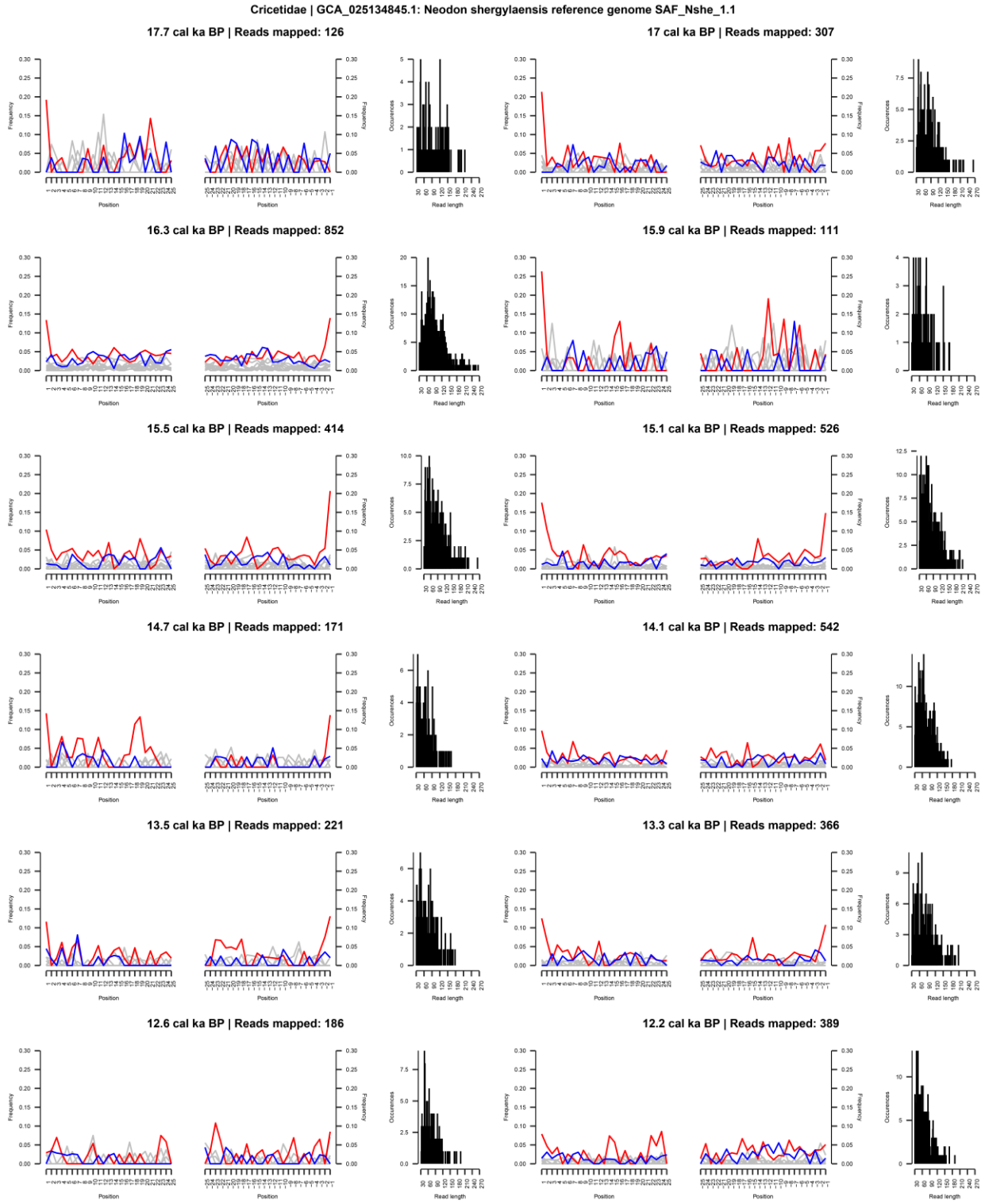
Cricetidae | GCA_025134845.1: Neodon shergylaensis reference genome SAF_Nshe_1.1
17.7 cal ka BP | Reads mapped: 126
17 cal ka BP | Reads mapped: 307
16.3 cal ka BP | Reads mapped: 852
15.9 cal ka BP | Reads mapped: 111
15.5 cal ka BP | Reads mapped: 414
15.1 cal ka BP | Reads mapped: 526
14.7 cal ka BP | Reads mapped: 171
14.1 cal ka BP | Reads mapped: 542
13.5 cal ka BP | Reads mapped: 221
13.3 cal ka BP | Reads mapped: 366
12.6 cal ka BP | Reads mapped: 186
12.2 cal ka BP | Reads mapped: 389
Frequency
Position
Occurences
Read length

Continued

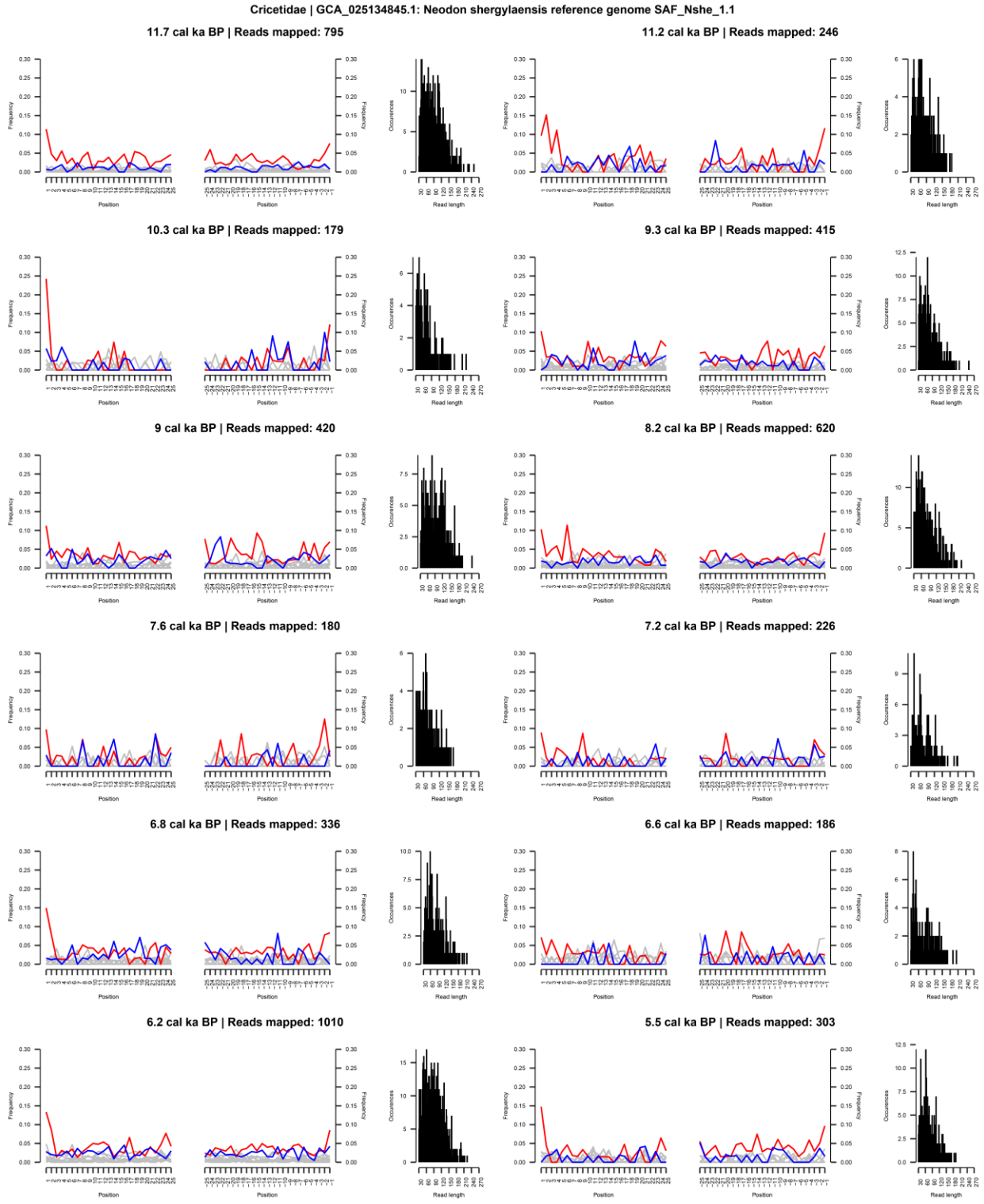
Cricetidae | GCA_025134845.1: Neodon shergylaensis reference genome SAF_Nshe_1.1
11.7 cal ka BP | Reads mapped: 795
11.2 cal ka BP | Reads mapped: 246
10.3 cal ka BP | Reads mapped: 179
9.3 cal ka BP | Reads mapped: 415
9 cal ka BP | Reads mapped: 420
8.2 cal ka BP | Reads mapped: 620
7.6 cal ka BP | Reads mapped: 180
7.2 cal ka BP | Reads mapped: 226
6.8 cal ka BP | Reads mapped: 336
6.6 cal ka BP | Reads mapped: 186
6.2 cal ka BP | Reads mapped: 1010
5.5 cal ka BP | Reads mapped: 303
Frequency
Occurences
Position
Read length

Continued

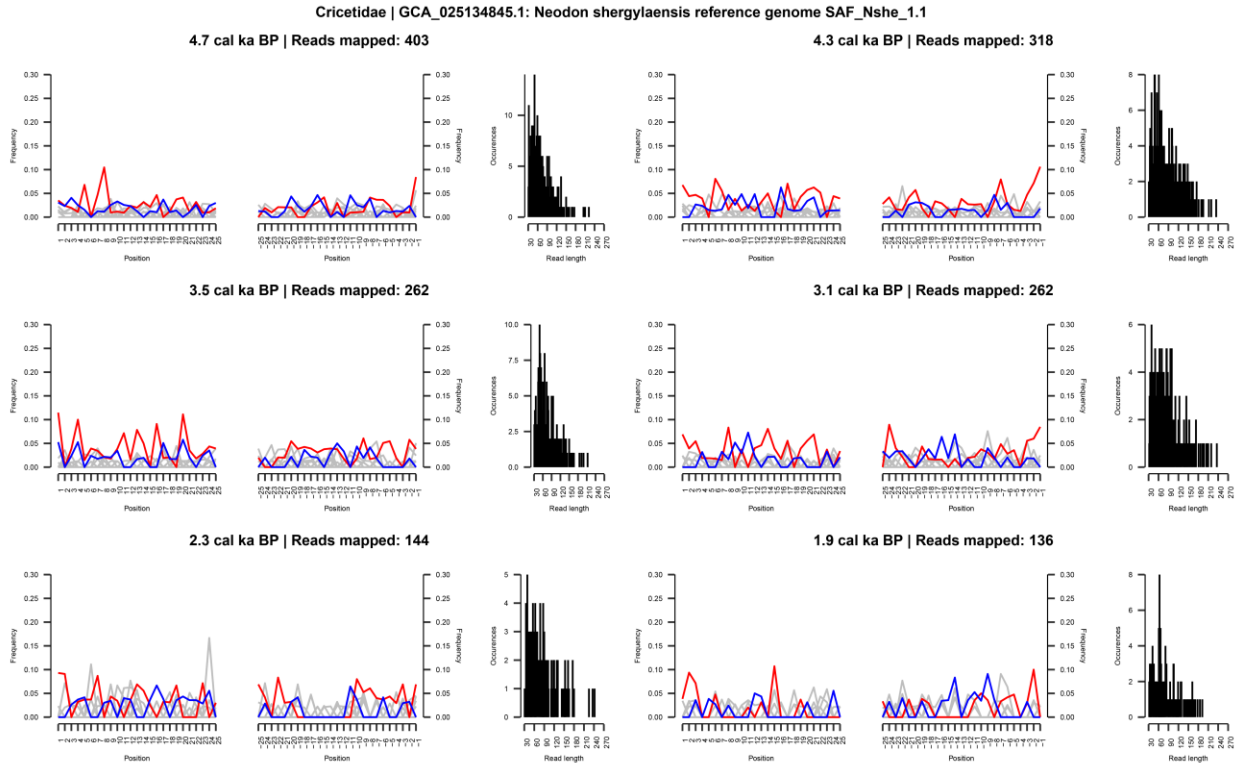
Cricetidae | GCA_025134845.1: Neodon shergylaensis reference genome SAF_Nshe_1.1
4.7 cal ka BP | Reads mapped: 403
4.3 cal ka BP | Reads mapped: 318
3.5 cal ka BP | Reads mapped: 262
3.1 cal ka BP | Reads mapped: 262
2.3 cal ka BP | Reads mapped: 144
1.9 cal ka BP | Reads mapped: 136
Frequency
Position
Occurences
Read length

Continued

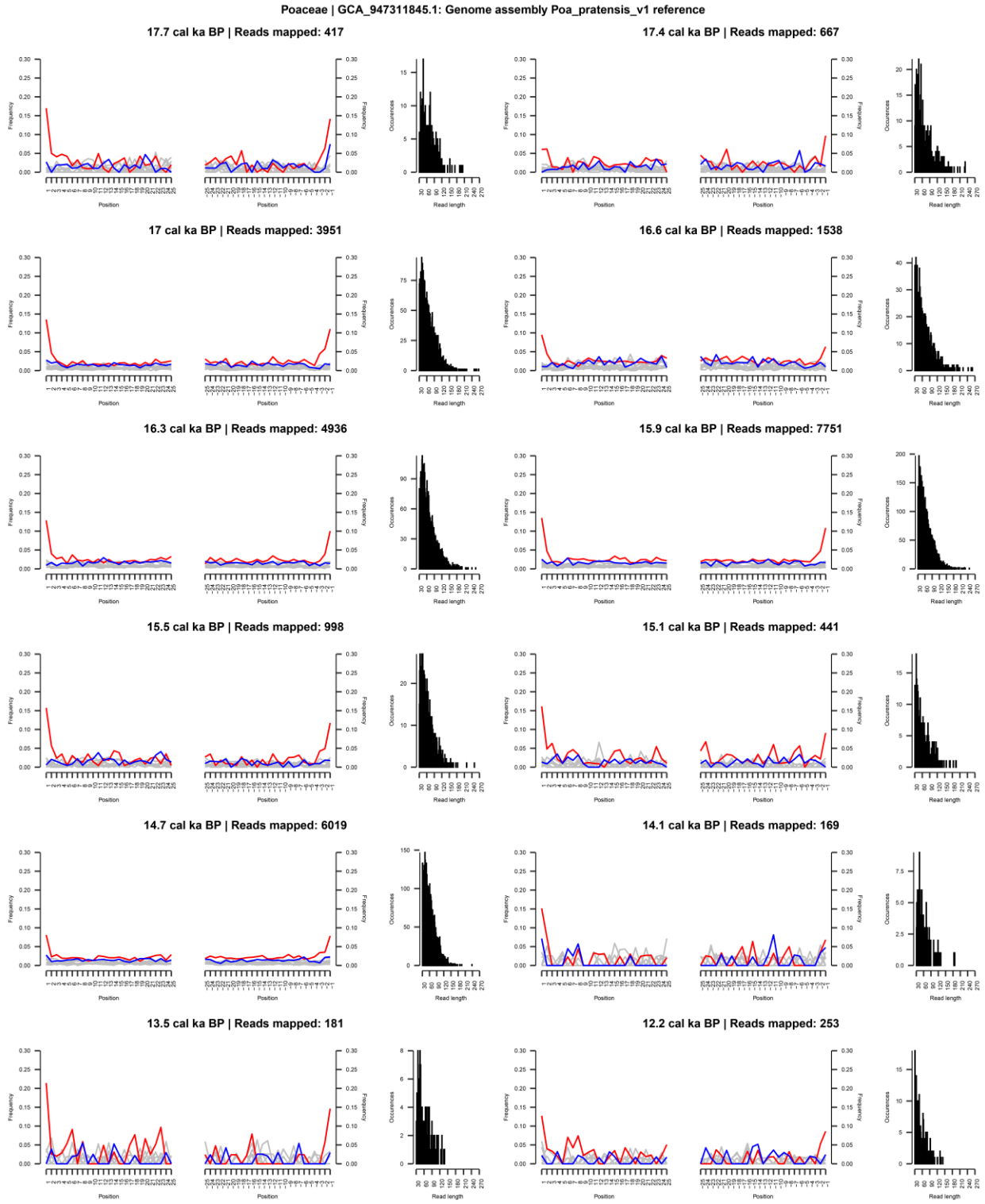
Poaceae | GCA_947311845.1: Genome assembly Poa_pratensis_v1 reference
17.7 cal ka BP | Reads mapped: 417
17.4 cal ka BP | Reads mapped: 667
17 cal ka BP | Reads mapped: 3951
16.6 cal ka BP | Reads mapped: 1538
16.3 cal ka BP | Reads mapped: 4936
15.9 cal ka BP | Reads mapped: 7751
15.5 cal ka BP | Reads mapped: 998
15.1 cal ka BP | Reads mapped: 441
14.7 cal ka BP | Reads mapped: 6019
14.1 cal ka BP | Reads mapped: 169
13.5 cal ka BP | Reads mapped: 181
12.2 cal ka BP | Reads mapped: 253
Frequency
Position
Occurences
Read length

Continued

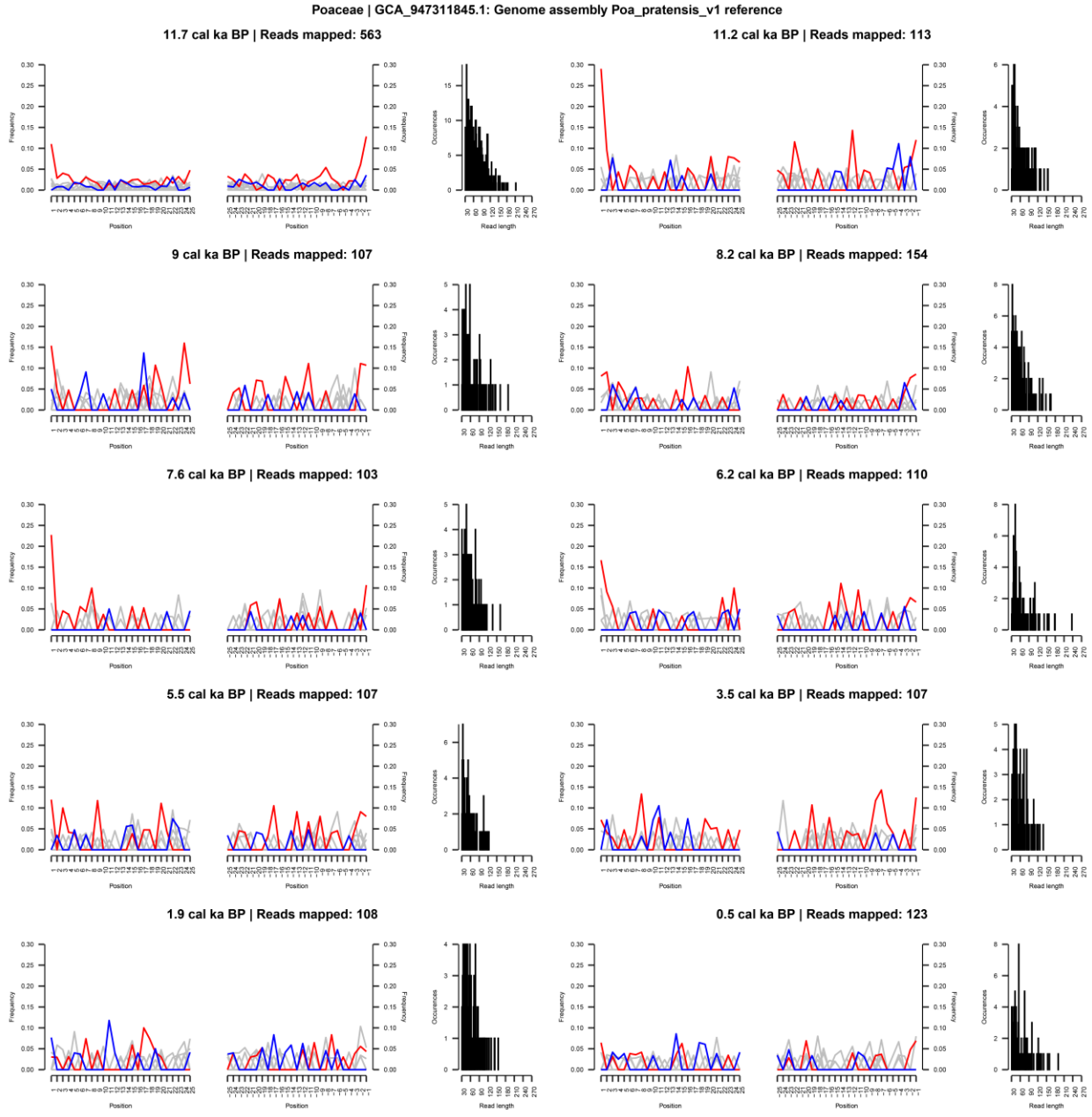
Poaceae | GCA_947311845.1: Genome assembly Poa_pratensis_v1 reference
11.7 cal ka BP | Reads mapped: 563
11.2 cal ka BP | Reads mapped: 113
9 cal ka BP | Reads mapped: 107
8.2 cal ka BP | Reads mapped: 154
7.6 cal ka BP | Reads mapped: 103
6.2 cal ka BP | Reads mapped: 110
5.5 cal ka BP | Reads mapped: 107
3.5 cal ka BP | Reads mapped: 107
1.9 cal ka BP | Reads mapped: 108
0.5 cal ka BP | Reads mapped: 123
Frequency
Position
Occurences
Read length

Continued

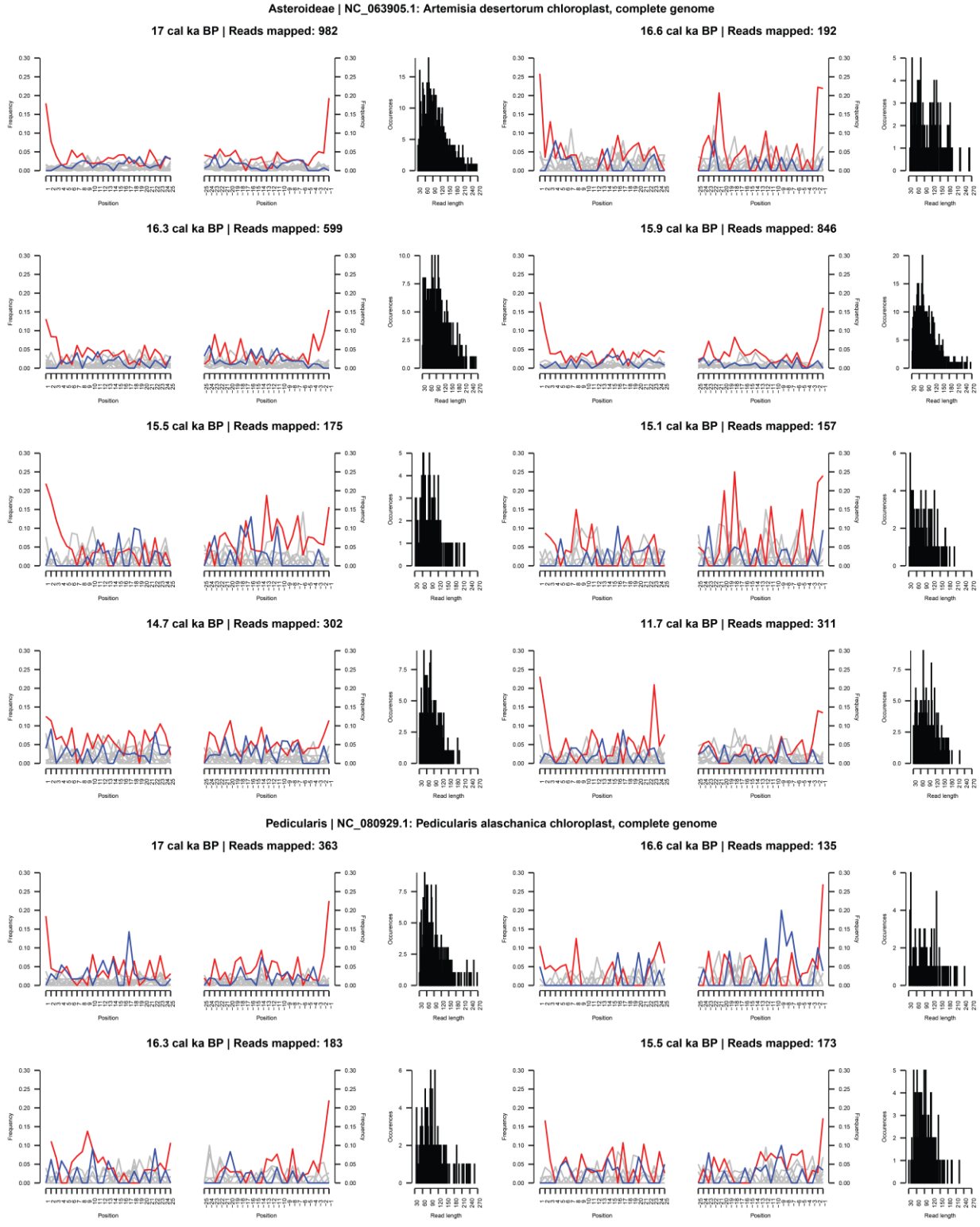
Asteroideae | NC_063905.1: Artemisia desertorum chloroplast, complete genome
17 cal ka BP | Reads mapped: 982
16.6 cal ka BP | Reads mapped: 192
16.3 cal ka BP | Reads mapped: 599
15.9 cal ka BP | Reads mapped: 846
15.5 cal ka BP | Reads mapped: 175
15.1 cal ka BP | Reads mapped: 157
14.7 cal ka BP | Reads mapped: 302
11.7 cal ka BP | Reads mapped: 311
Pedicularis | NC_080929.1: Pedicularis alaschanica chloroplast, complete genome
17 cal ka BP | Reads mapped: 363
16.6 cal ka BP | Reads mapped: 135
16.3 cal ka BP | Reads mapped: 183
15.5 cal ka BP | Reads mapped: 173
Frequency
Occurences
Position
Read length

Continued

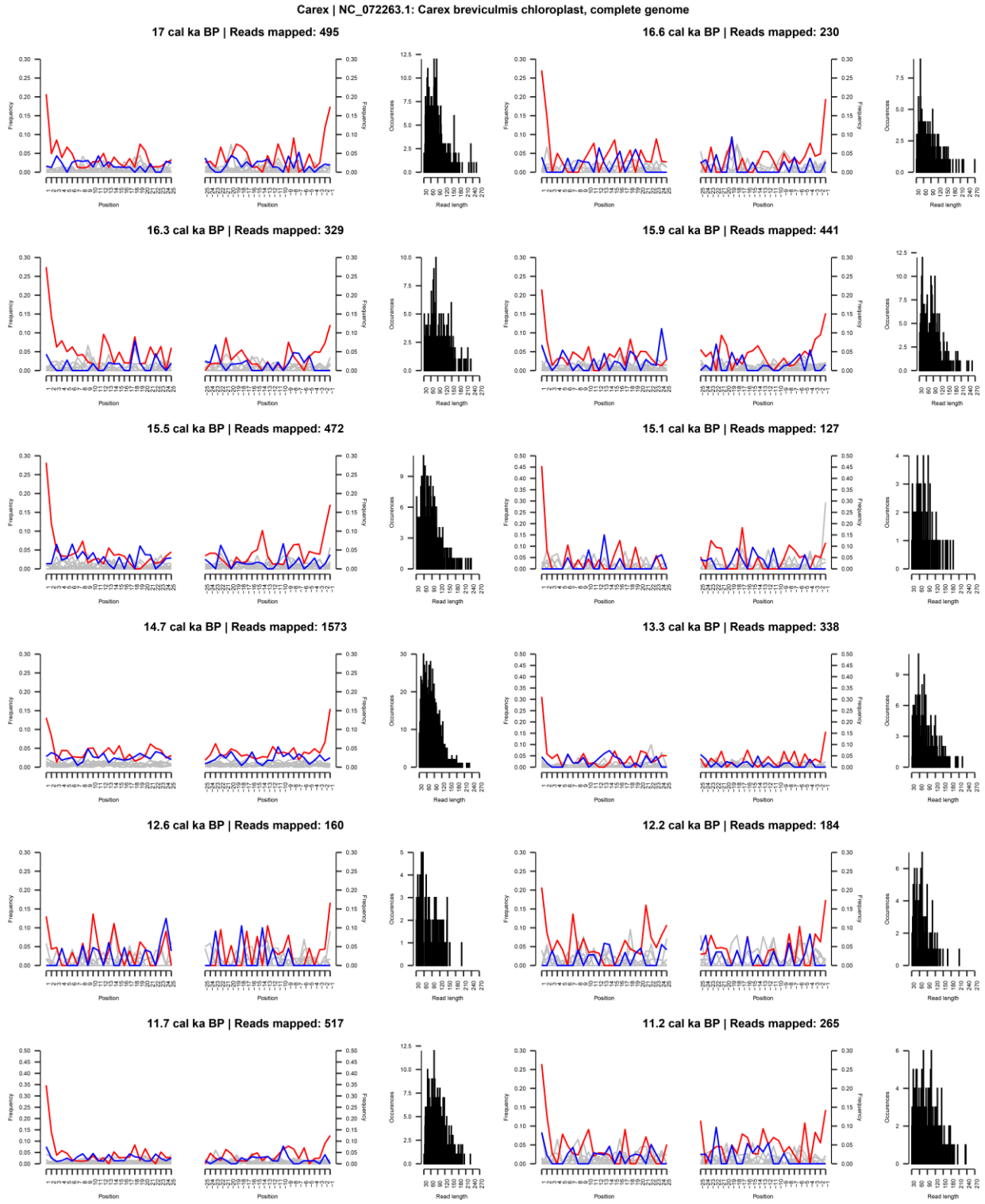
Carex | NC_072263.1: Carex breviculmis chloroplast, complete genome
17 cal ka BP | Reads mapped: 495
16.6 cal ka BP | Reads mapped: 230
16.3 cal ka BP | Reads mapped: 329
15.9 cal ka BP | Reads mapped: 441
15.5 cal ka BP | Reads mapped: 472
15.1 cal ka BP | Reads mapped: 127
14.7 cal ka BP | Reads mapped: 1573
13.3 cal ka BP | Reads mapped: 338
12.6 cal ka BP | Reads mapped: 160
12.2 cal ka BP | Reads mapped: 184
11.7 cal ka BP | Reads mapped: 517
11.2 cal ka BP | Reads mapped: 265
Frequency
Position
Occurences
Read length

Continued

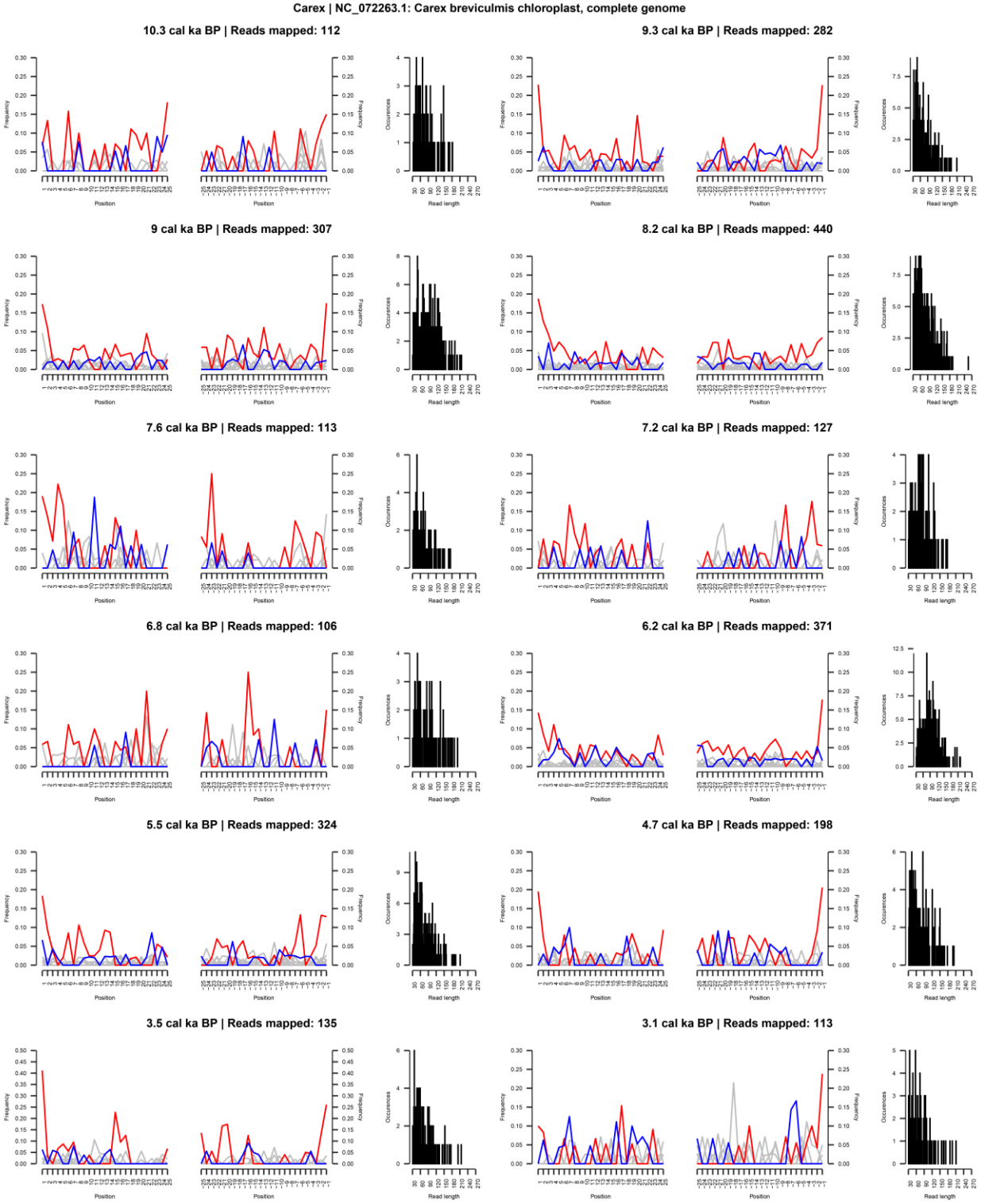
Carex | NC_072263.1: Carex breviculmis chloroplast, complete genome
10.3 cal ka BP | Reads mapped: 112
9.3 cal ka BP | Reads mapped: 282
9 cal ka BP | Reads mapped: 307
8.2 cal ka BP | Reads mapped: 440
7.6 cal ka BP | Reads mapped: 113
7.2 cal ka BP | Reads mapped: 127
6.8 cal ka BP | Reads mapped: 106
6.2 cal ka BP | Reads mapped: 371
5.5 cal ka BP | Reads mapped: 324
4.7 cal ka BP | Reads mapped: 198
3.5 cal ka BP | Reads mapped: 135
3.1 cal ka BP | Reads mapped: 113
Frequency
Occurences
Position
Read length

Continued

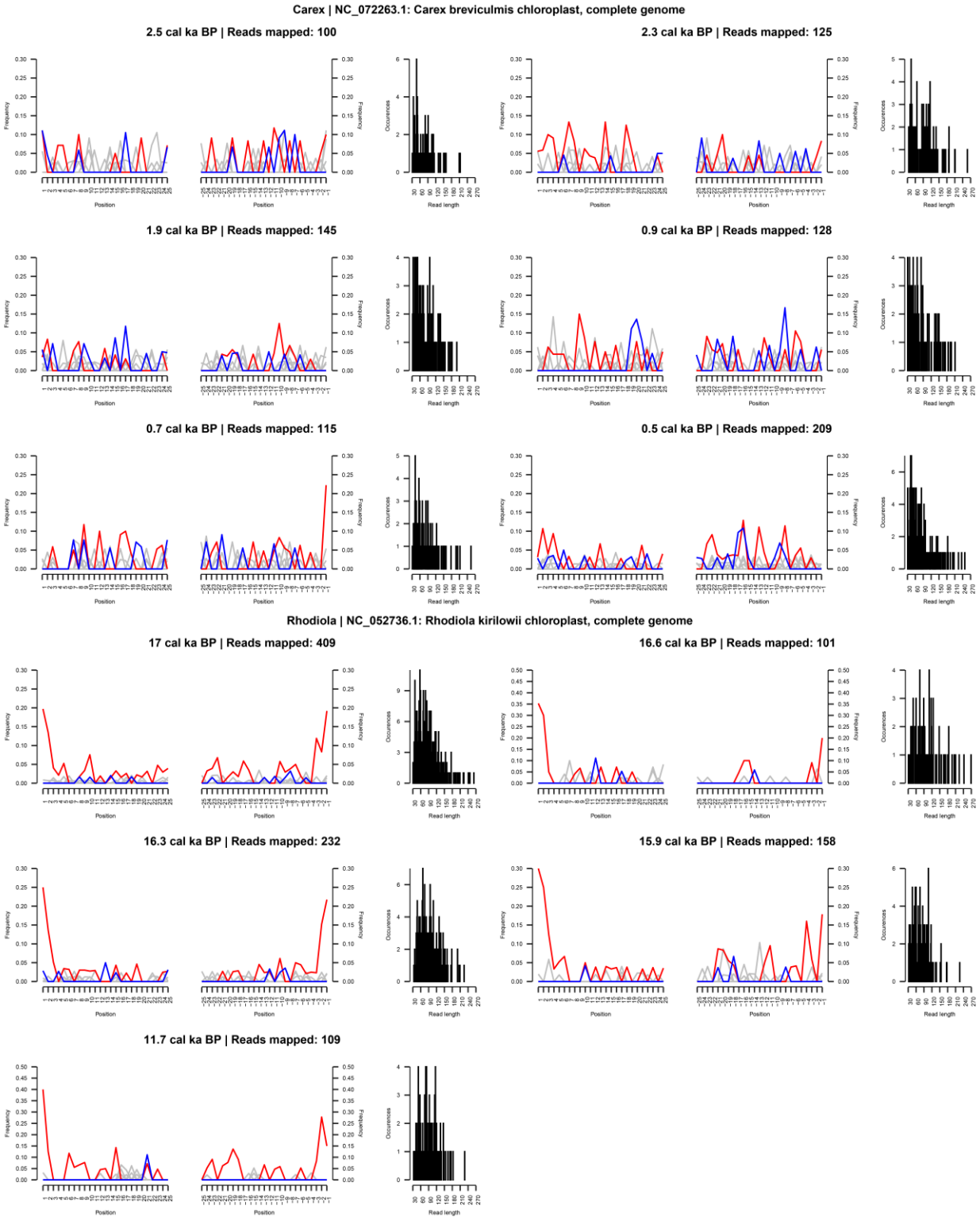
Carex | NC_072263.1: Carex breviculmis chloroplast, complete genome
2.5 cal ka BP | Reads mapped: 100
2.3 cal ka BP | Reads mapped: 125
1.9 cal ka BP | Reads mapped: 145
0.9 cal ka BP | Reads mapped: 128
0.7 cal ka BP | Reads mapped: 115
0.5 cal ka BP | Reads mapped: 209
Rhodiola | NC_052736.1: Rhodiola kirilowii chloroplast, complete genome
17 cal ka BP | Reads mapped: 409
16.6 cal ka BP | Reads mapped: 101
16.3 cal ka BP | Reads mapped: 232
15.9 cal ka BP | Reads mapped: 158
11.7 cal ka BP | Reads mapped: 109
Frequency
Occurences
Position
Read length

Continued

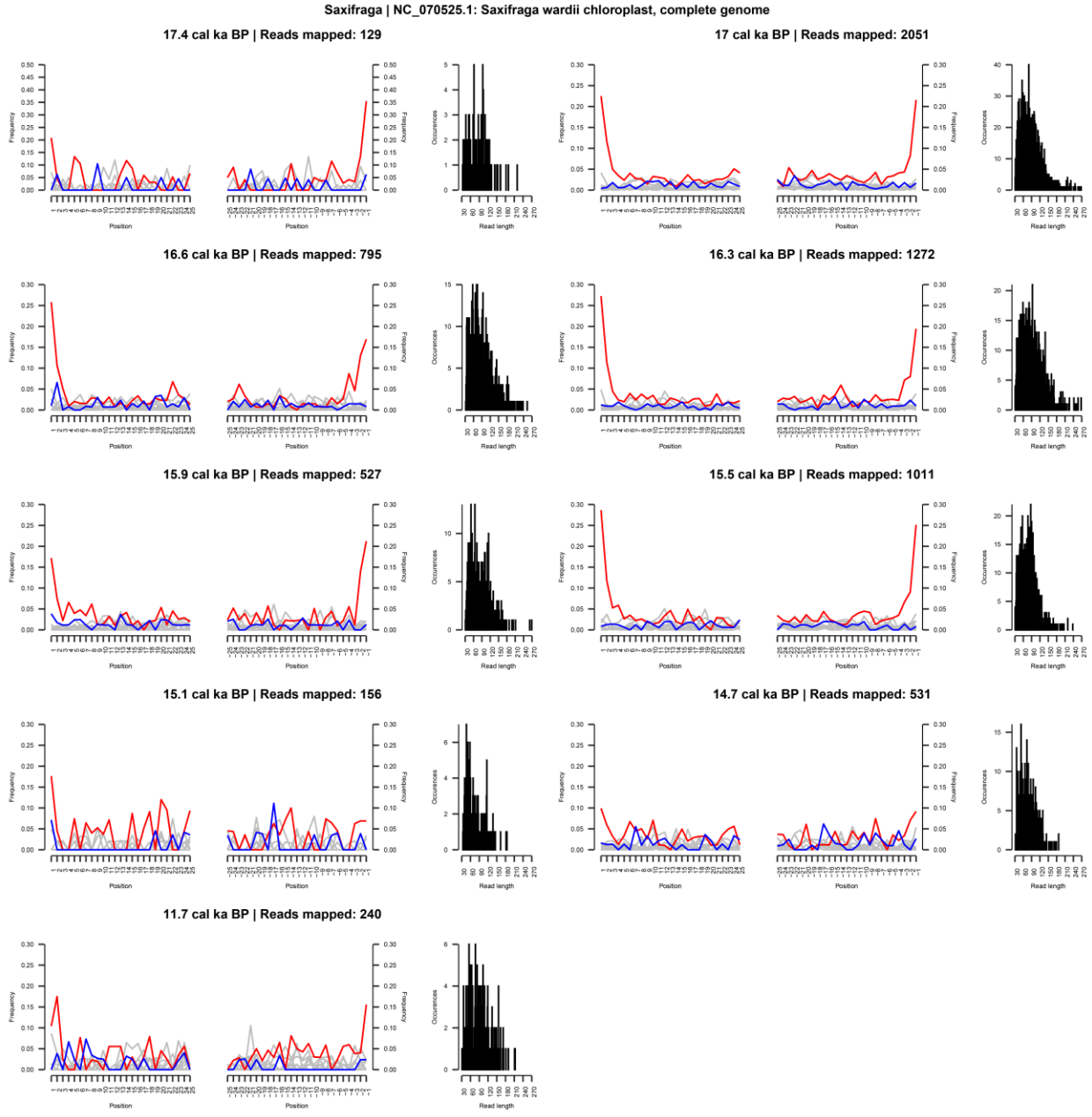
Saxifraga | NC_070525.1: Saxifraga wardii chloroplast, complete genome
17.4 cal ka BP | Reads mapped: 129
17 cal ka BP | Reads mapped: 2051
16.6 cal ka BP | Reads mapped: 795
16.3 cal ka BP | Reads mapped: 1272
15.9 cal ka BP | Reads mapped: 527
15.5 cal ka BP | Reads mapped: 1011
15.1 cal ka BP | Reads mapped: 156
14.7 cal ka BP | Reads mapped: 531
11.7 cal ka BP | Reads mapped: 240
Frequency
Position
Occurences
Read length

Continued

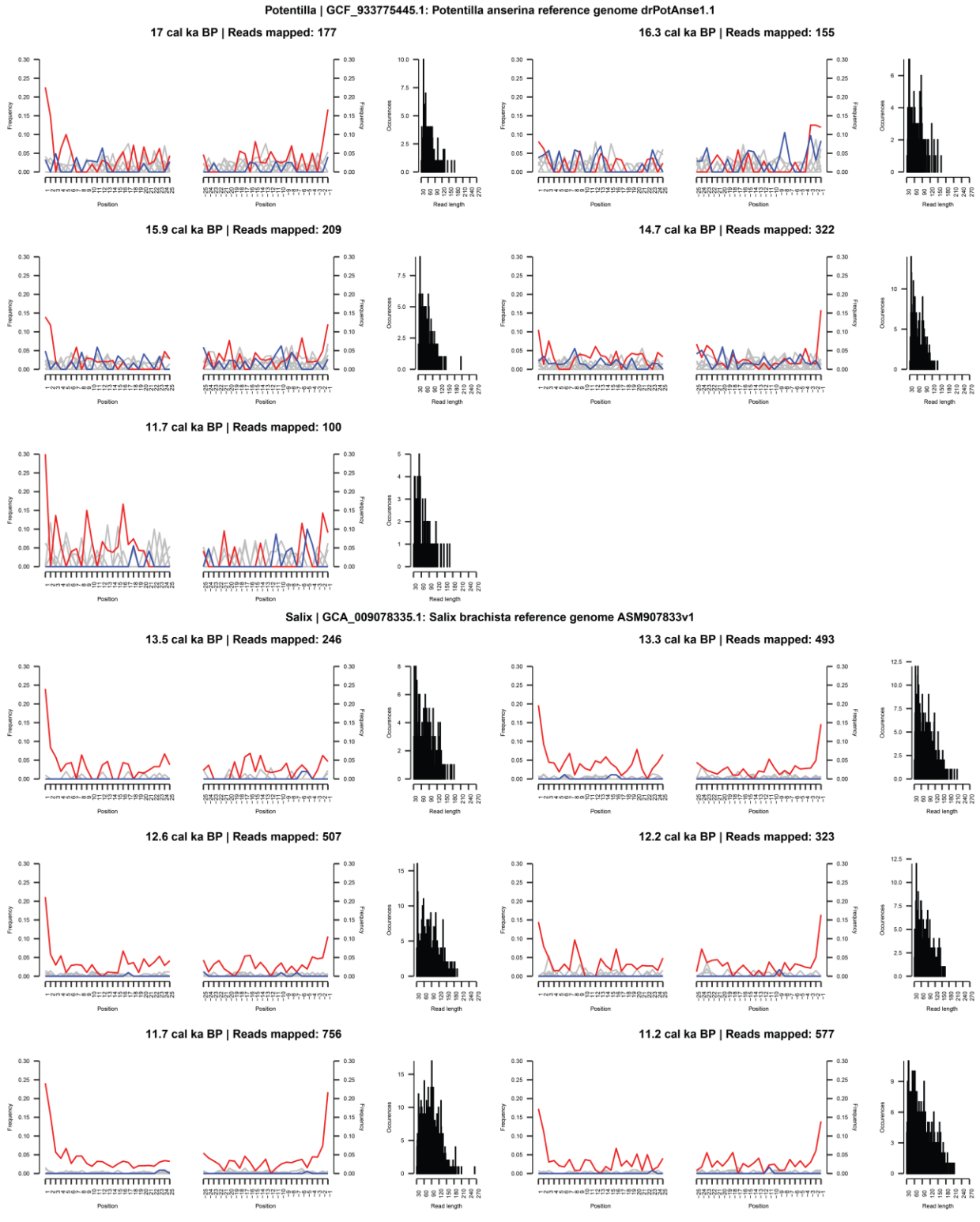
Potentilla | GCF_933775445.1: Potentilla anserina reference genome drPotAnse1.1
17 cal ka BP | Reads mapped: 177
16.3 cal ka BP | Reads mapped: 155
15.9 cal ka BP | Reads mapped: 209
14.7 cal ka BP | Reads mapped: 322
11.7 cal ka BP | Reads mapped: 100
Salix | GCA_009078335.1: Salix brachista reference genome ASM907833v1
13.5 cal ka BP | Reads mapped: 246
13.3 cal ka BP | Reads mapped: 493
12.6 cal ka BP | Reads mapped: 507
12.2 cal ka BP | Reads mapped: 323
11.7 cal ka BP | Reads mapped: 756
11.2 cal ka BP | Reads mapped: 577
Frequency
Position
Occurences
Read length

Continued

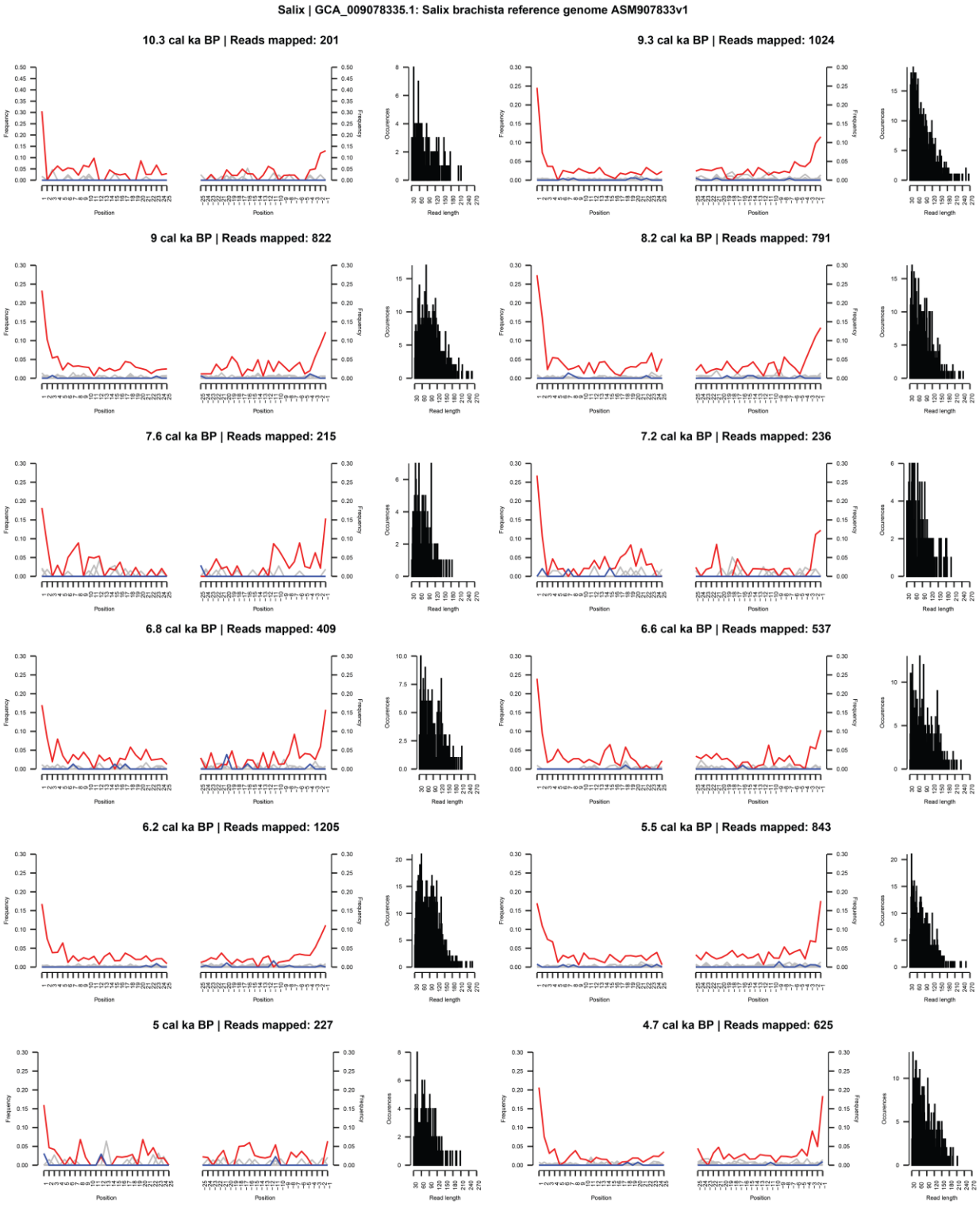
Salix | GCA_009078335.1: Salix brachista reference genome ASM907833v1
10.3 cal ka BP | Reads mapped: 201
9.3 cal ka BP | Reads mapped: 1024
9 cal ka BP | Reads mapped: 822
8.2 cal ka BP | Reads mapped: 791
7.6 cal ka BP | Reads mapped: 215
7.2 cal ka BP | Reads mapped: 236
6.8 cal ka BP | Reads mapped: 409
6.6 cal ka BP | Reads mapped: 537
6.2 cal ka BP | Reads mapped: 1205
5.5 cal ka BP | Reads mapped: 843
5 cal ka BP | Reads mapped: 227
4.7 cal ka BP | Reads mapped: 625
Frequency
Position
Occurences
Read length

Continued

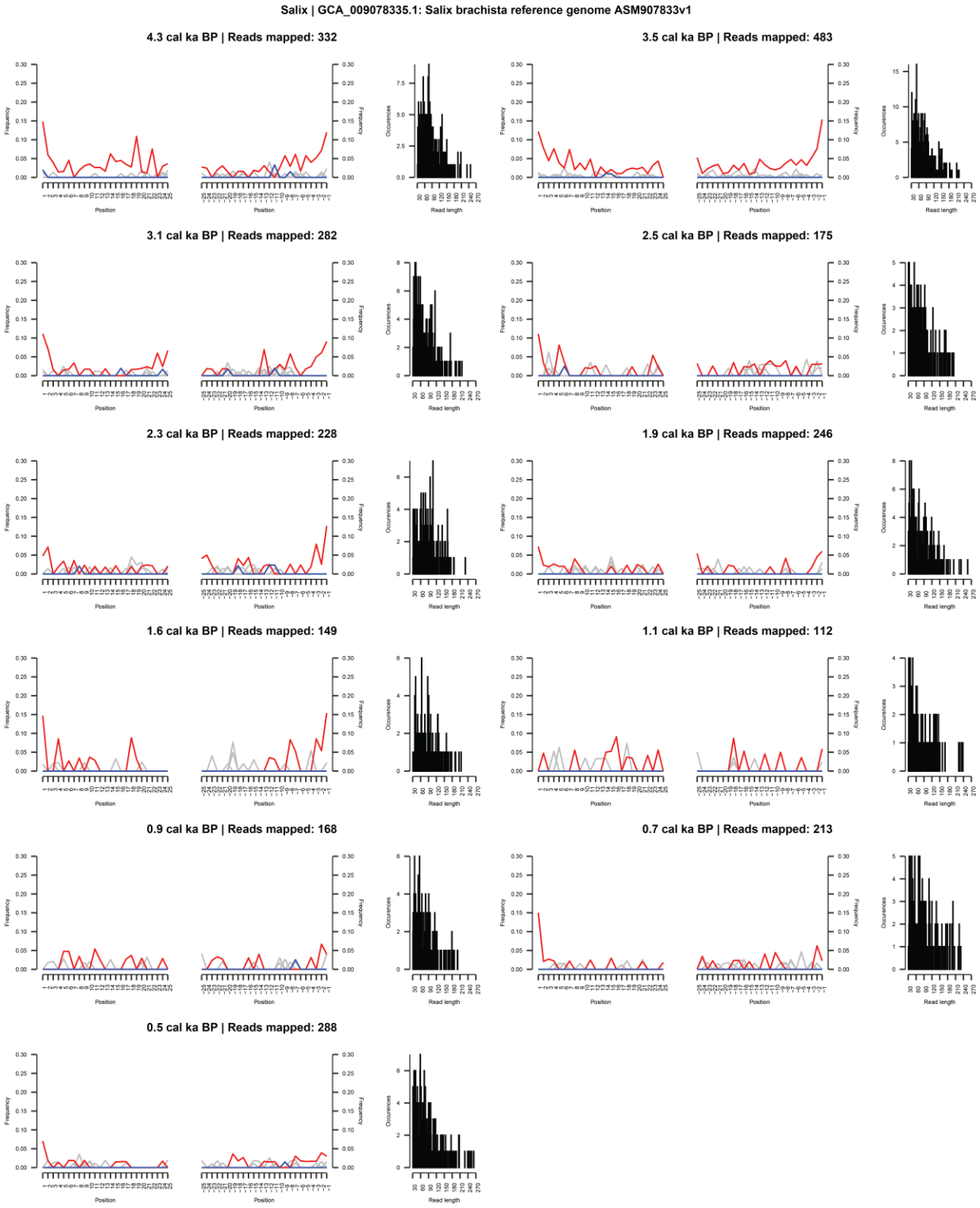
Salix | GCA_009078335.1: Salix brachista reference genome ASM907833v1
4.3 cal ka BP | Reads mapped: 332
3.5 cal ka BP | Reads mapped: 483
3.1 cal ka BP | Reads mapped: 282
2.5 cal ka BP | Reads mapped: 175
2.3 cal ka BP | Reads mapped: 228
1.9 cal ka BP | Reads mapped: 246
1.6 cal ka BP | Reads mapped: 149
1.1 cal ka BP | Reads mapped: 112
0.9 cal ka BP | Reads mapped: 168
0.7 cal ka BP | Reads mapped: 213
0.5 cal ka BP | Reads mapped: 288
Frequency
Position
Occurences
Read length

Continued

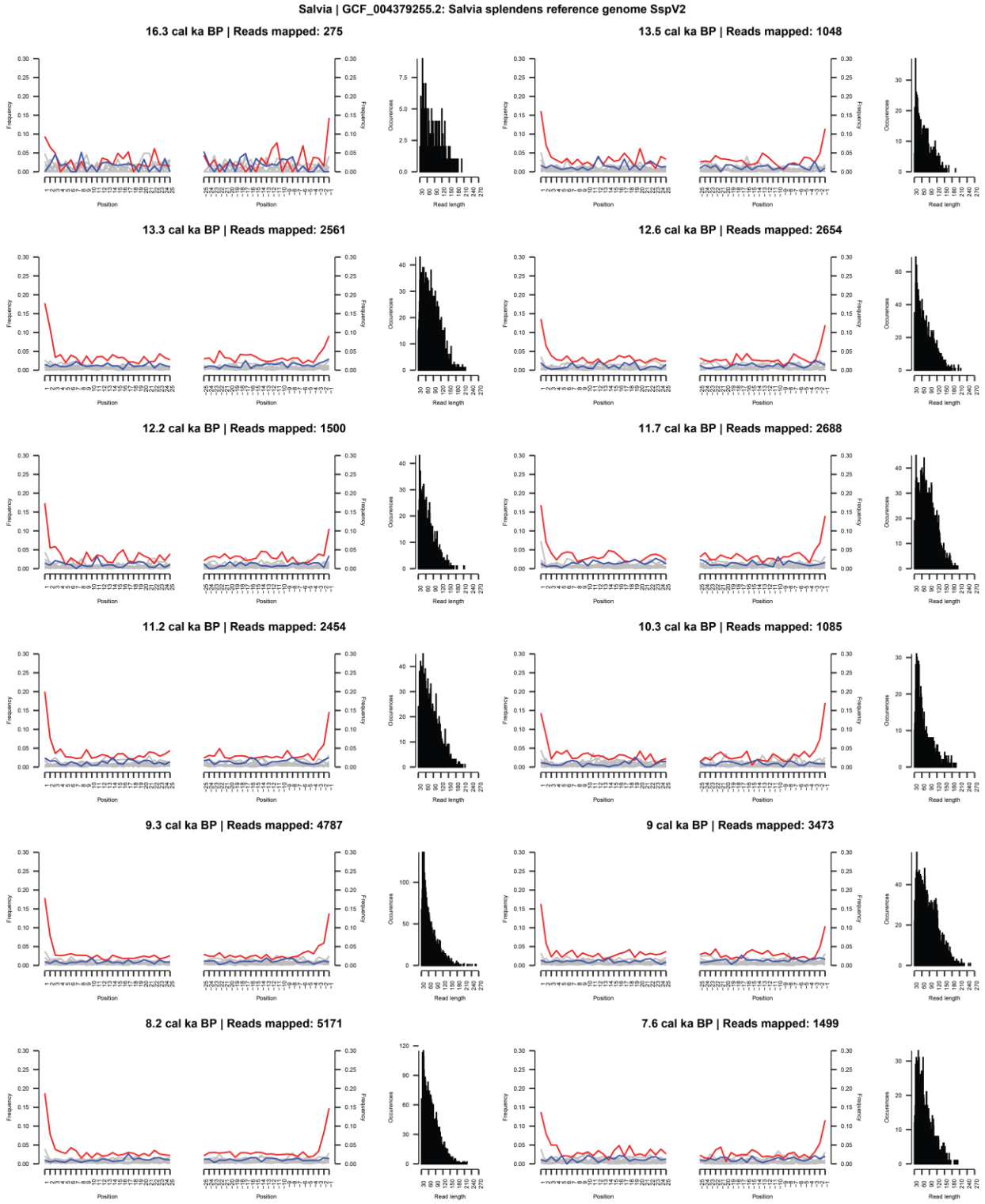
Salvia | GCF_004379255.2: Salvia splendens reference genome SspV2
16.3 cal ka BP | Reads mapped: 275
13.5 cal ka BP | Reads mapped: 1048
13.3 cal ka BP | Reads mapped: 2561
12.6 cal ka BP | Reads mapped: 2654
12.2 cal ka BP | Reads mapped: 1500
11.7 cal ka BP | Reads mapped: 2688
11.2 cal ka BP | Reads mapped: 2454
10.3 cal ka BP | Reads mapped: 1085
9.3 cal ka BP | Reads mapped: 4787
9 cal ka BP | Reads mapped: 3473
8.2 cal ka BP | Reads mapped: 5171
7.6 cal ka BP | Reads mapped: 1499
Frequency
Position
Occurences
Read length

Continued

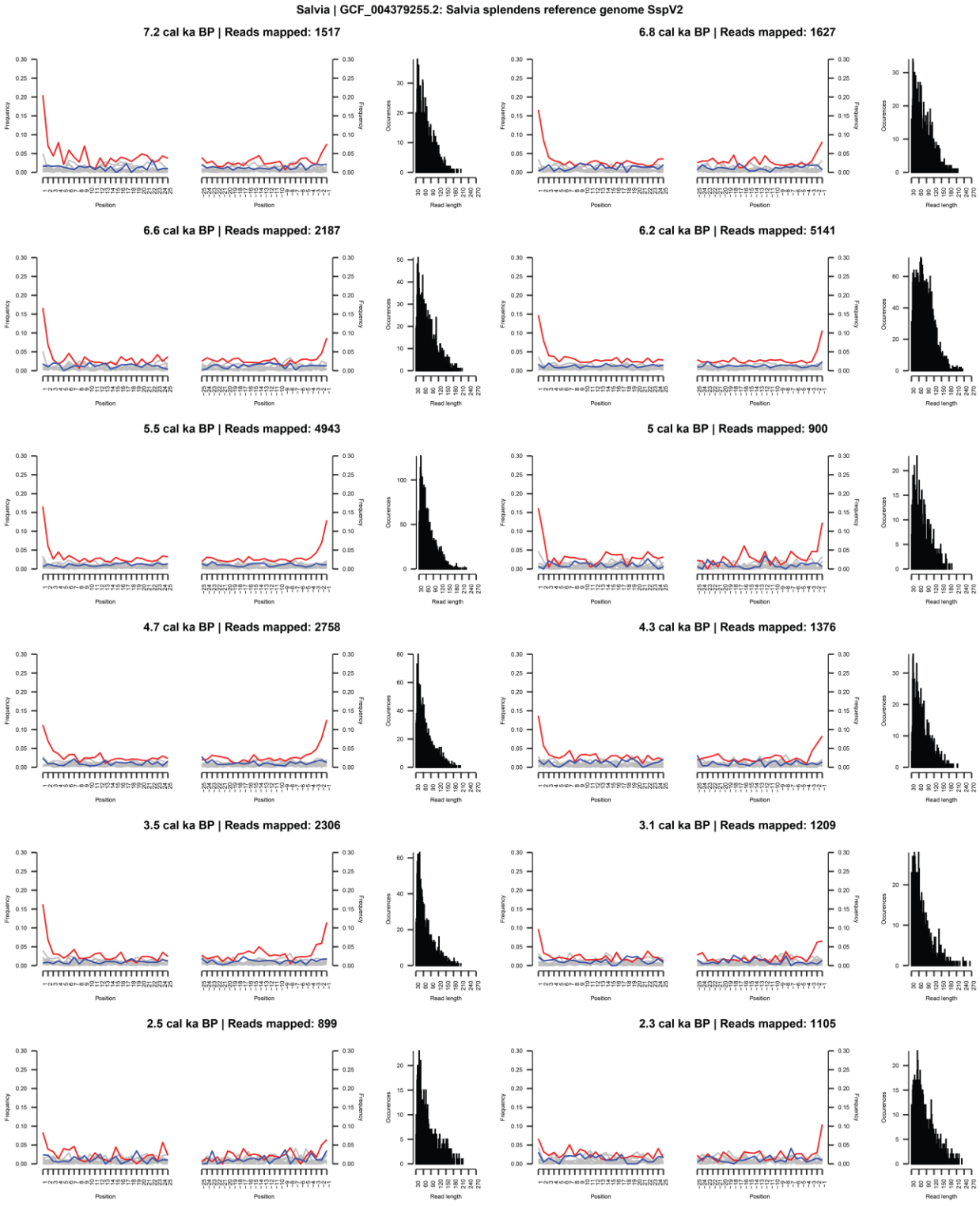
Salvia | GCF_004379255.2: Salvia splendens reference genome SspV2
7.2 cal ka BP | Reads mapped: 1517
6.8 cal ka BP | Reads mapped: 1627
6.6 cal ka BP | Reads mapped: 2187
6.2 cal ka BP | Reads mapped: 5141
5.5 cal ka BP | Reads mapped: 4943
5 cal ka BP | Reads mapped: 900
4.7 cal ka BP | Reads mapped: 2758
4.3 cal ka BP | Reads mapped: 1376
3.5 cal ka BP | Reads mapped: 2306
3.1 cal ka BP | Reads mapped: 1209
2.5 cal ka BP | Reads mapped: 899
2.3 cal ka BP | Reads mapped: 1105
Frequency
Position
Occurences
Read length

Continued

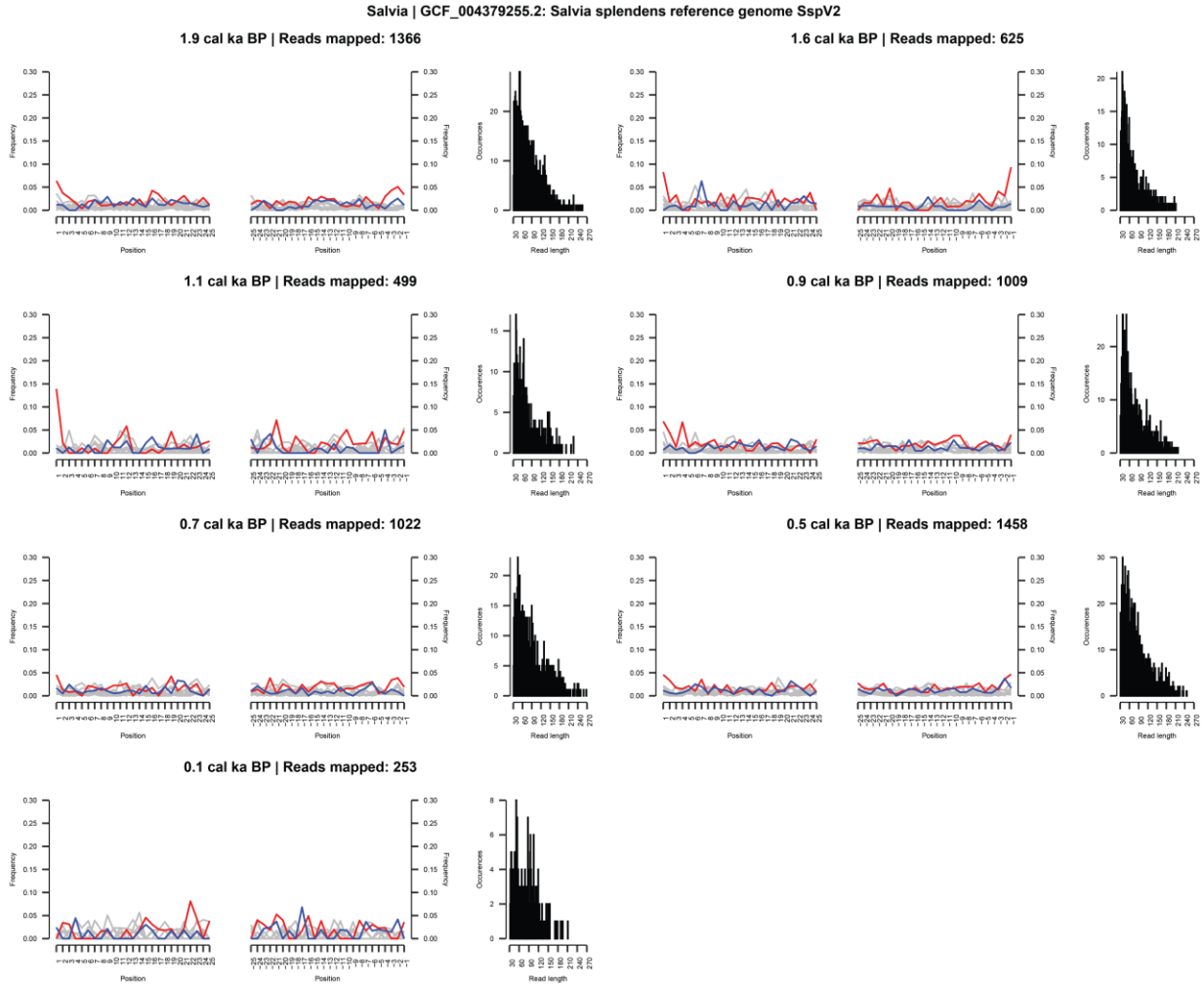
Salvia | GCF_004379255.2: Salvia splendens reference genome SspV2
1.9 cal ka BP | Reads mapped: 1366
1.6 cal ka BP | Reads mapped: 625
1.1 cal ka BP | Reads mapped: 499
0.9 cal ka BP | Reads mapped: 1009
0.7 cal ka BP | Reads mapped: 1022
0.5 cal ka BP | Reads mapped: 1458
0.1 cal ka BP | Reads mapped: 253
Frequency
Position
Occurences
Read length

Continued

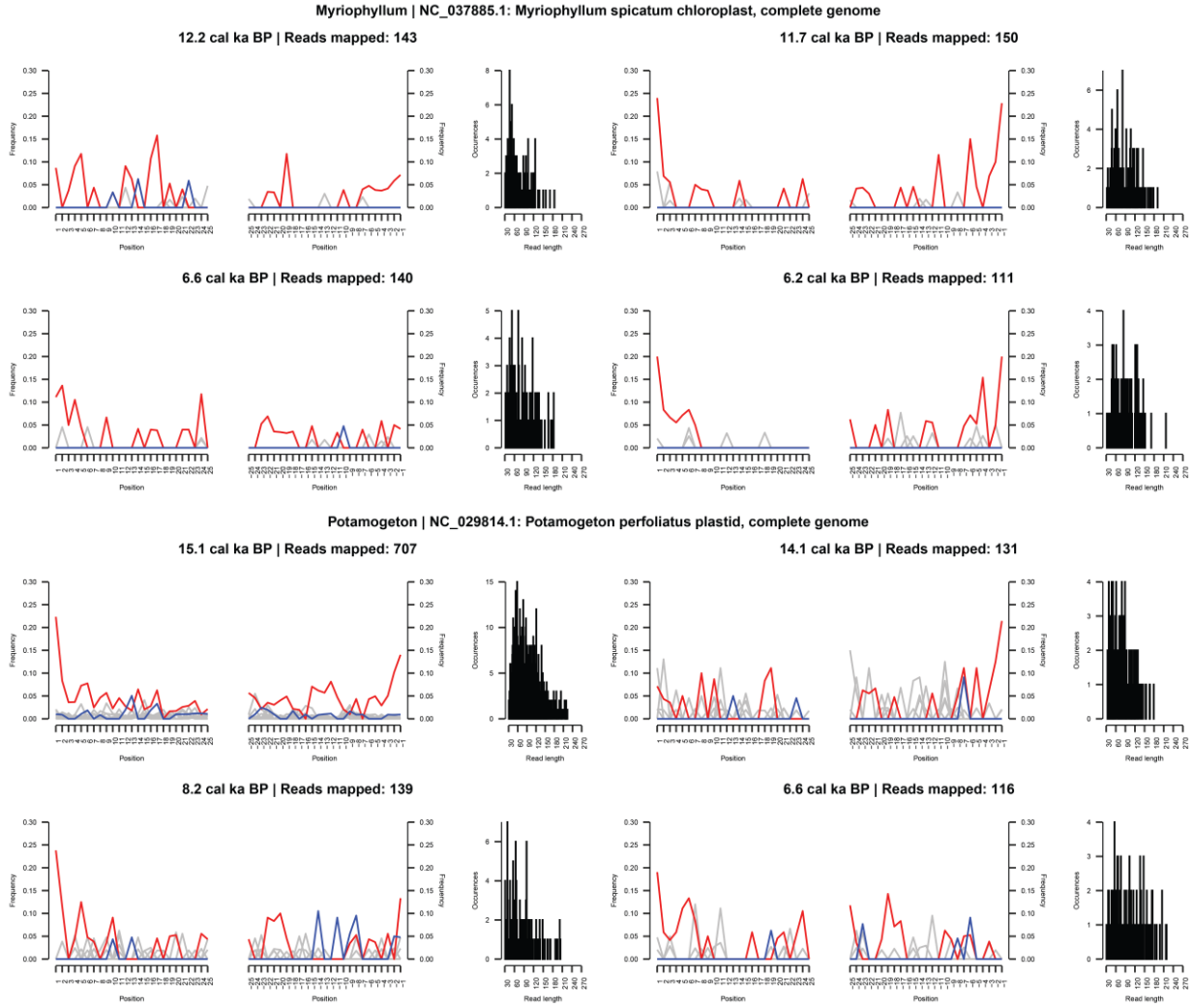
Myriophyllum | NC_037885.1: Myriophyllum spicatum chloroplast, complete genome
12.2 cal ka BP | Reads mapped: 143
11.7 cal ka BP | Reads mapped: 150
6.6 cal ka BP | Reads mapped: 140
6.2 cal ka BP | Reads mapped: 111
Potamogeton | NC_029814.1: Potamogeton perfoliatus plastid, complete genome
15.1 cal ka BP | Reads mapped: 707
14.1 cal ka BP | Reads mapped: 131
8.2 cal ka BP | Reads mapped: 139
6.6 cal ka BP | Reads mapped: 116
Position
Frequency
Occurences
Read length

Continued

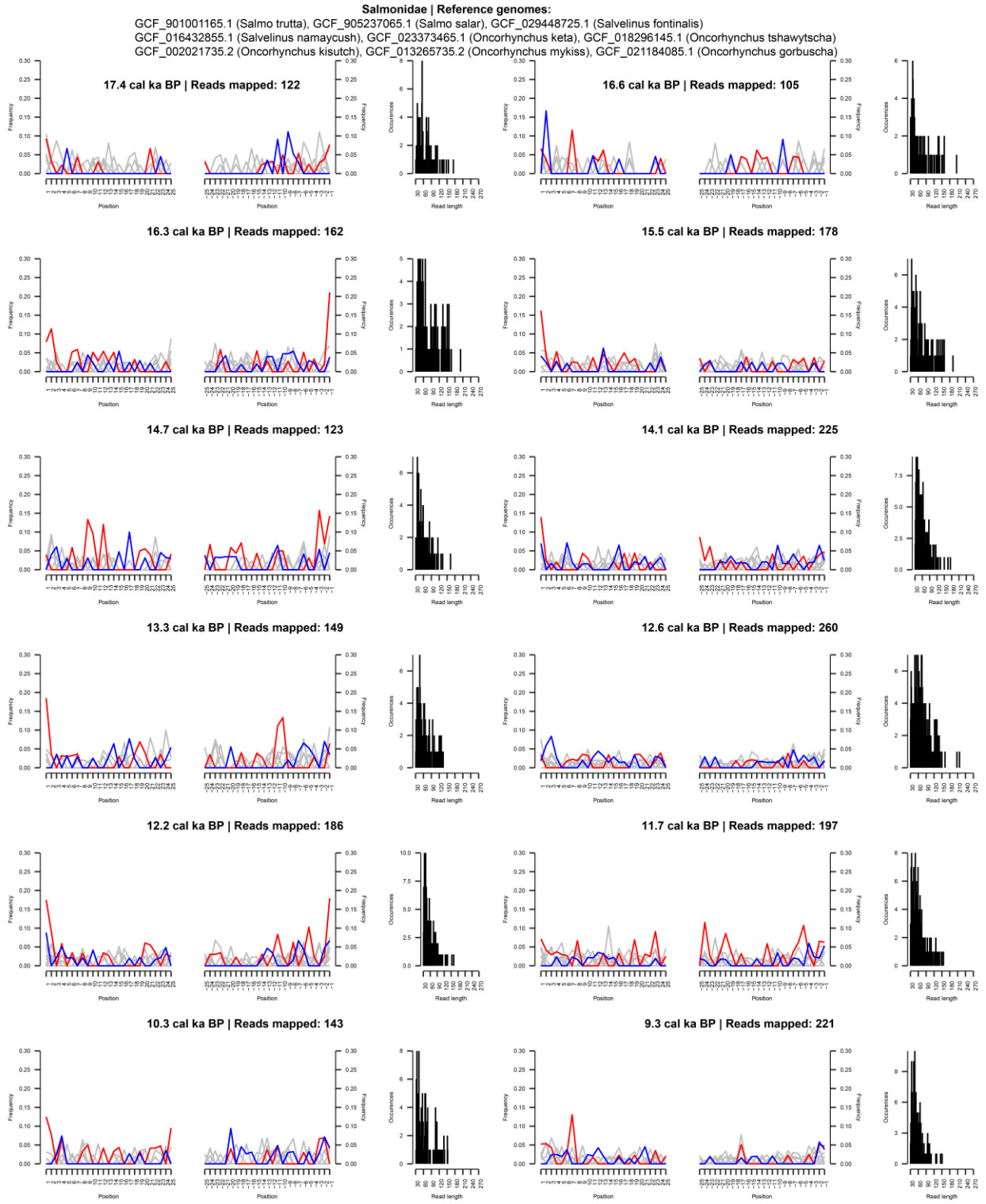
Salmonidae | Reference genomes:
GCF_901001165.1 (Salmo trutta), GCF_905237065.1 (Salmo salar), GCF_029448725.1 (Salvelinus fontinalis)
GCF_016432855.1 (Salvelinus namaycush), GCF_023373465.1 (Oncorhynchus keta), GCF_018296145.1 (Oncorhynchus tshawytscha)
GCF_002021735.2 (Oncorhynchus kisutch), GCF_013265735.2 (Oncorhynchus mykiss), GCF_021184085.1 (Oncorhynchus gorbuscha)
17.4 cal ka BP | Reads mapped: 122
16.6 cal ka BP | Reads mapped: 105
16.3 cal ka BP | Reads mapped: 162
15.5 cal ka BP | Reads mapped: 178
14.7 cal ka BP | Reads mapped: 123
14.1 cal ka BP | Reads mapped: 225
13.3 cal ka BP | Reads mapped: 149
12.6 cal ka BP | Reads mapped: 260
12.2 cal ka BP | Reads mapped: 186
11.7 cal ka BP | Reads mapped: 197
10.3 cal ka BP | Reads mapped: 143
9.3 cal ka BP | Reads mapped: 221
Frequency
Position
Occurences
Read length

Continued

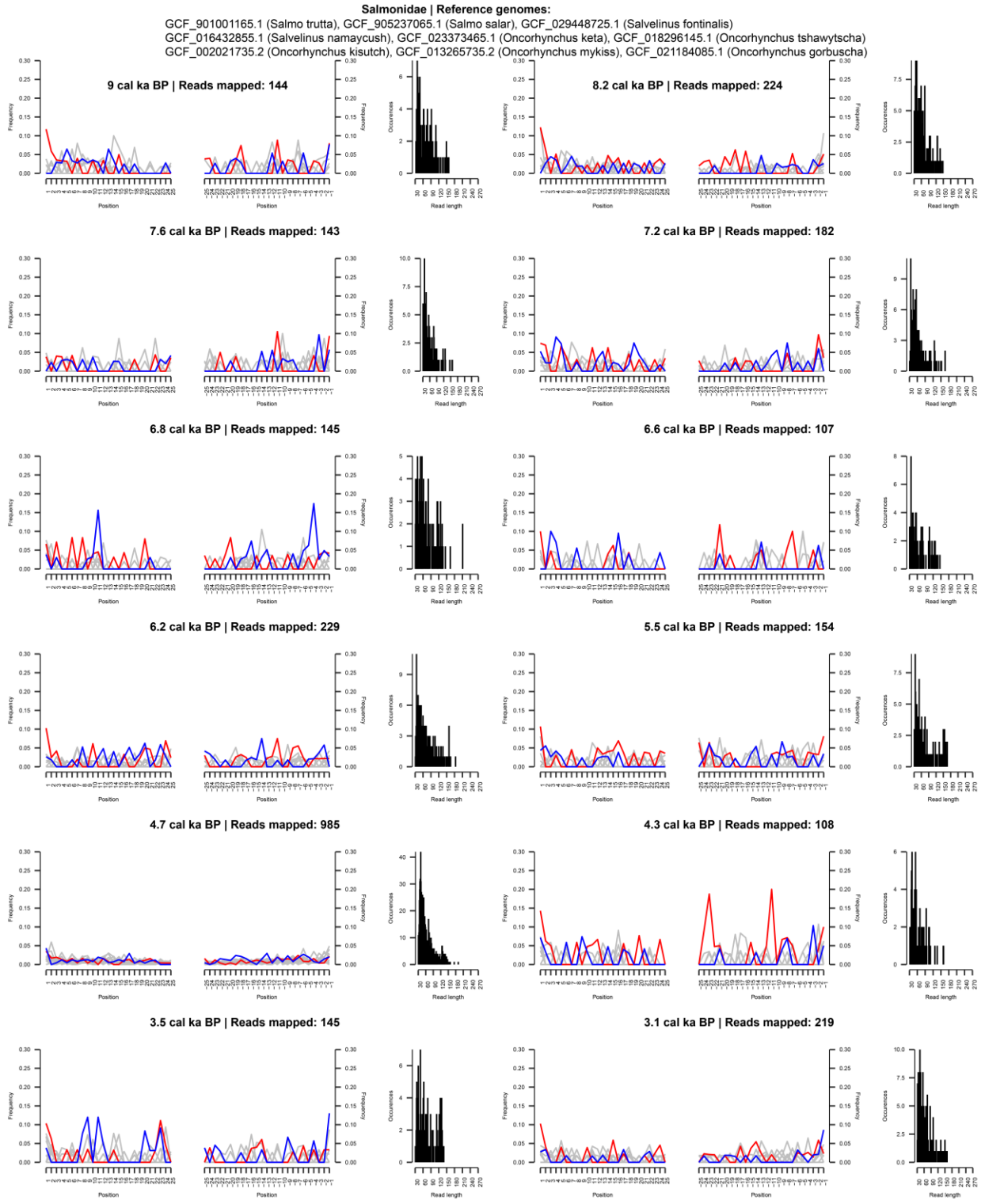
Salmonidae | Reference genomes:
GCF_901001165.1 (Salmo trutta), GCF_905237065.1 (Salmo salar), GCF_029448725.1 (Salvelinus fontinalis)
GCF_016432855.1 (Salvelinus namaycush), GCF_023373465.1 (Oncorhynchus keta), GCF_018296145.1 (Oncorhynchus tshawytscha)
GCF_002021735.2 (Oncorhynchus kisutch), GCF_013265735.2 (Oncorhynchus mykiss), GCF_021184085.1 (Oncorhynchus gorbuscha)
9 cal ka BP | Reads mapped: 144
8.2 cal ka BP | Reads mapped: 224
7.6 cal ka BP | Reads mapped: 143
7.2 cal ka BP | Reads mapped: 182
6.8 cal ka BP | Reads mapped: 145
6.6 cal ka BP | Reads mapped: 107
6.2 cal ka BP | Reads mapped: 229
5.5 cal ka BP | Reads mapped: 154
4.7 cal ka BP | Reads mapped: 985
4.3 cal ka BP | Reads mapped: 108
3.5 cal ka BP | Reads mapped: 145
3.1 cal ka BP | Reads mapped: 219
Frequency
Position
Occurences
Read length

Continued

Salmonidae | Referene genomes:

GCF_901001165.1 (Salmo trutta), GCF_905237065.1 (Salmo salar), GCF_029448725.1 (Salvelinus fontinalis)
GCF_016432855.1 (Salvelinus namaycush), GCF_023373465.1 (Oncorhynchus keta), GCF_018296145.1 (Oncorhynchus tshawytscha)
GCF_002021735.2 (Oncorhynchus kisutch), GCF_013265735.2 (Oncorhynchus mykiss), GCF_021184085.1 (Oncorhynchus gorbuscha)

2.3 cal ka BP | Reads mapped: 112

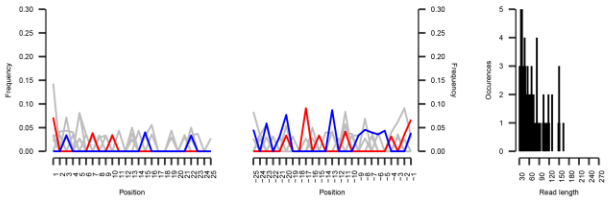

1.1 cal ka BP | Reads mapped: 147

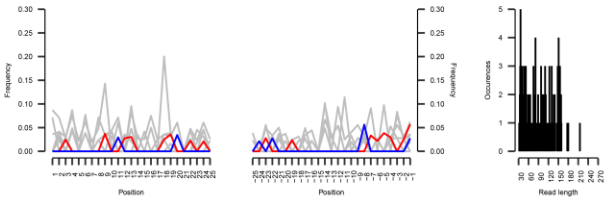

0.5 cal ka BP | Reads mapped: 105

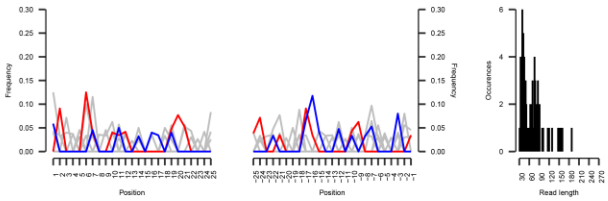

Cyprinidae | GCF_001515625.1: Sinocyclocheilus rhinocerous Reference genome SAMN03320098_v1.1

16.3 cal ka BP | Reads mapped: 219

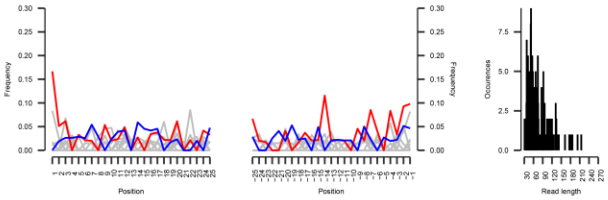

Continued

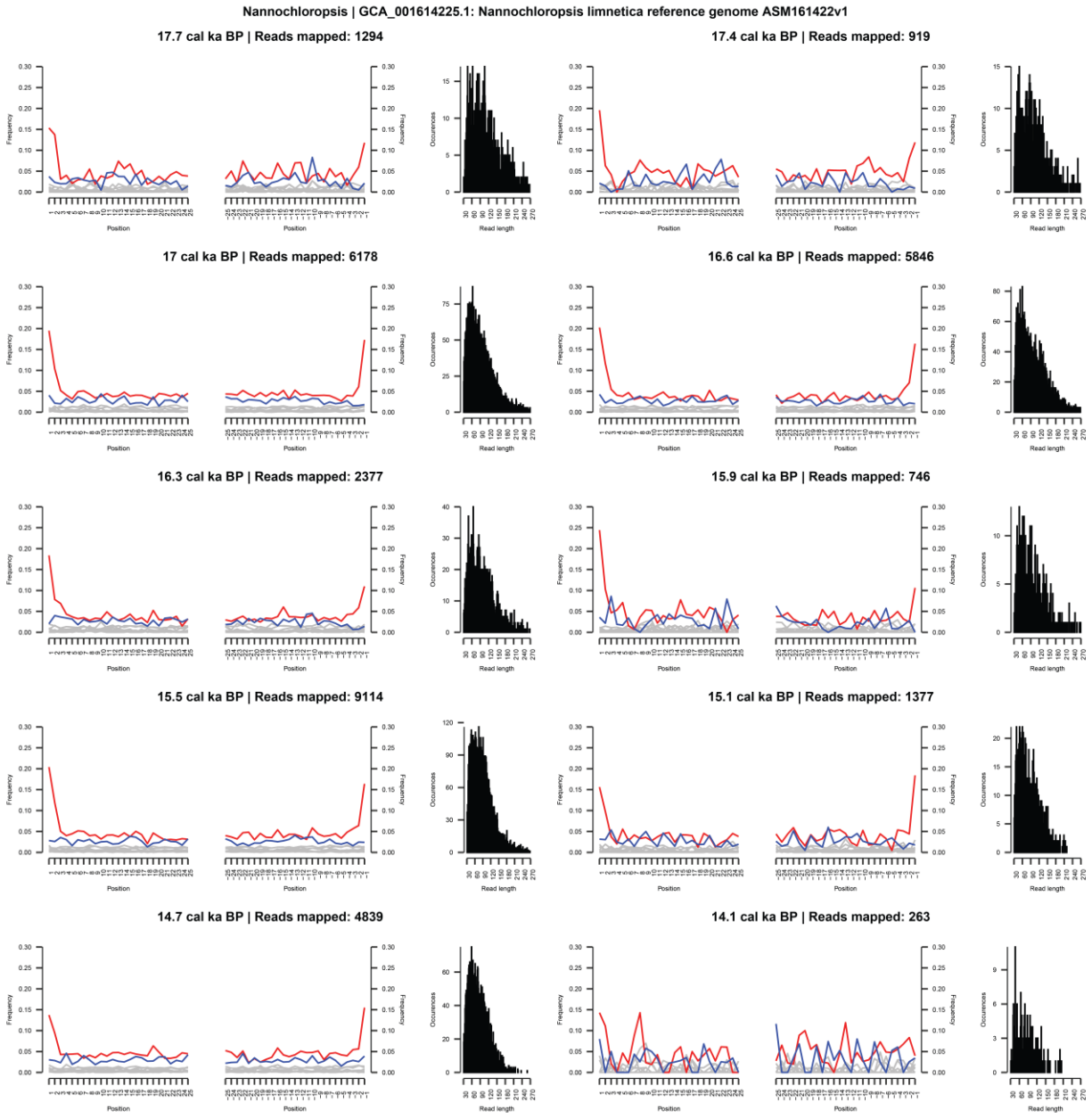
Nannochloropsis | GCA_001614225.1: Nannochloropsis limnetica reference genome ASM161422v1
17.7 cal ka BP | Reads mapped: 1294
17.4 cal ka BP | Reads mapped: 919
17 cal ka BP | Reads mapped: 6178
16.6 cal ka BP | Reads mapped: 5846
16.3 cal ka BP | Reads mapped: 2377
15.9 cal ka BP | Reads mapped: 746
15.5 cal ka BP | Reads mapped: 9114
15.1 cal ka BP | Reads mapped: 1377
14.7 cal ka BP | Reads mapped: 4839
14.1 cal ka BP | Reads mapped: 263
Frequency
Position
Occurrences
Read length

Continued

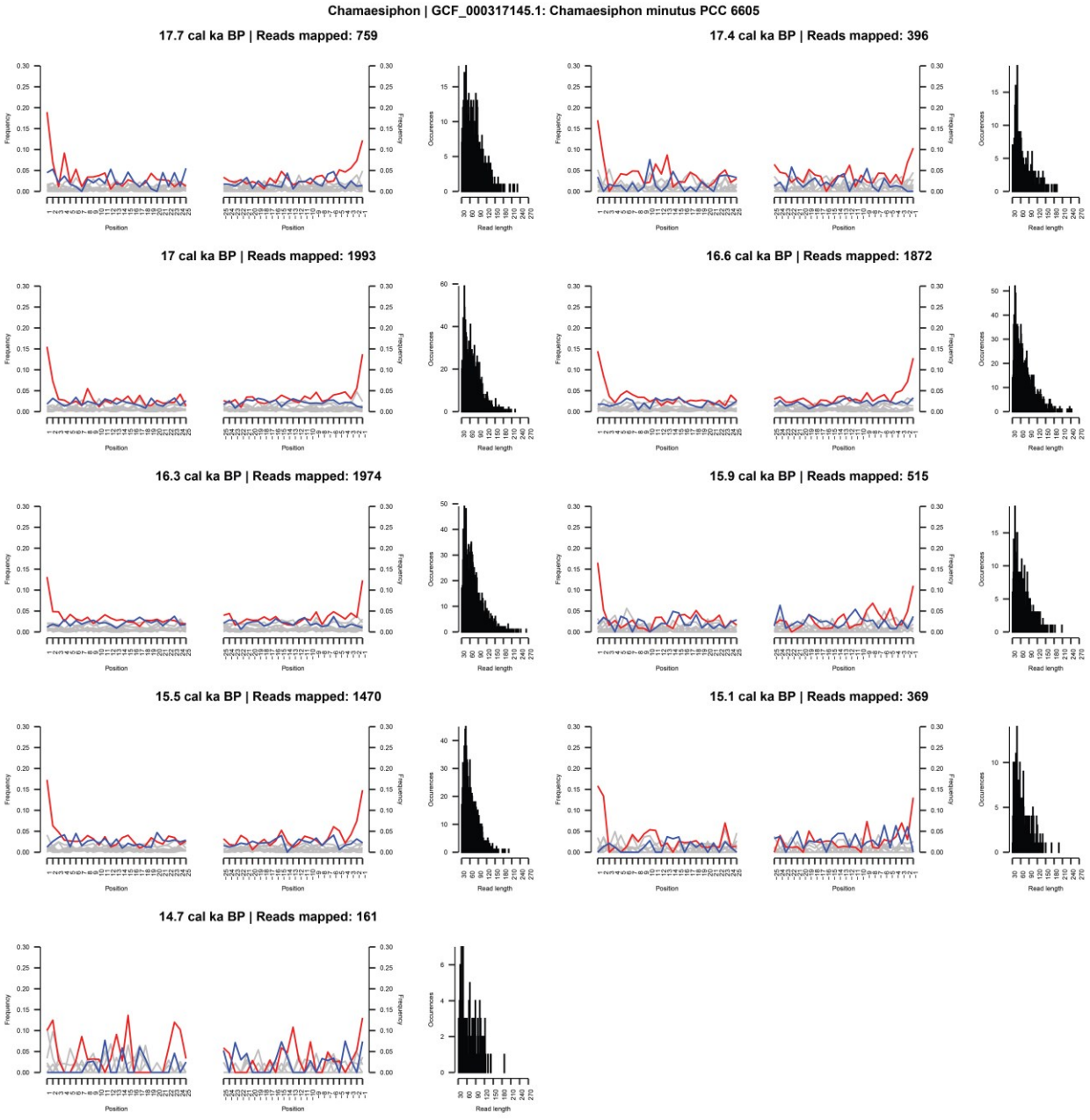
Chamaesiphon | GCF_000317145.1: Chamaesiphon minutus PCC 6605
17.7 cal ka BP | Reads mapped: 759
17.4 cal ka BP | Reads mapped: 396
17 cal ka BP | Reads mapped: 1993
16.6 cal ka BP | Reads mapped: 1872
16.3 cal ka BP | Reads mapped: 1974
15.9 cal ka BP | Reads mapped: 515
15.5 cal ka BP | Reads mapped: 1470
15.1 cal ka BP | Reads mapped: 369
14.7 cal ka BP | Reads mapped: 161
Frequency
Position
Occurrences
Read length

Continued

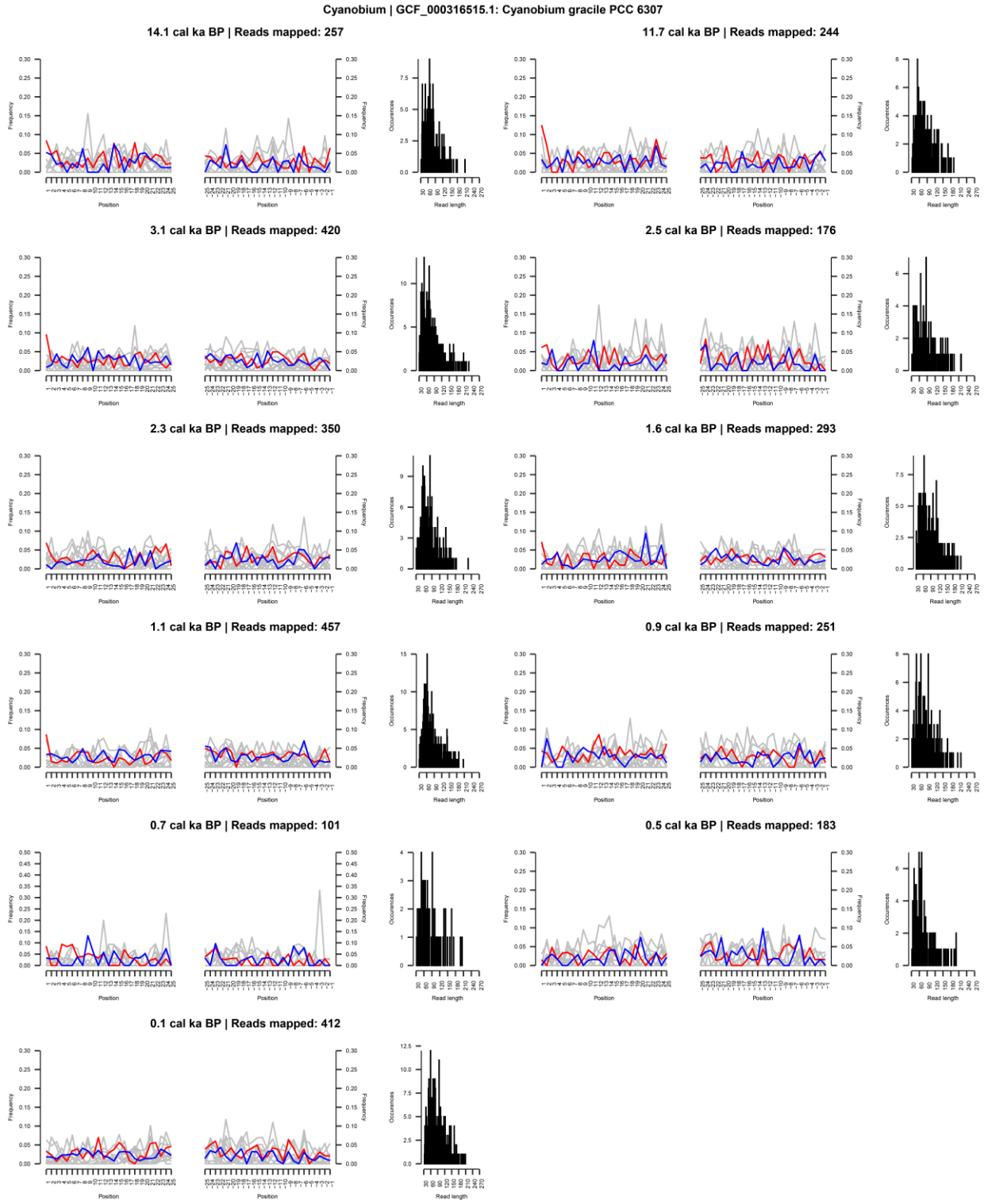
Cyanobium | GCF_000316515.1: Cyanobium gracile PCC 6307
14.1 cal ka BP | Reads mapped: 257
11.7 cal ka BP | Reads mapped: 244
3.1 cal ka BP | Reads mapped: 420
2.5 cal ka BP | Reads mapped: 176
2.3 cal ka BP | Reads mapped: 350
1.6 cal ka BP | Reads mapped: 293
1.1 cal ka BP | Reads mapped: 457
0.9 cal ka BP | Reads mapped: 251
0.7 cal ka BP | Reads mapped: 101
0.5 cal ka BP | Reads mapped: 183
0.1 cal ka BP | Reads mapped: 412
Frequency
Position
Occurences
Read length

Continued

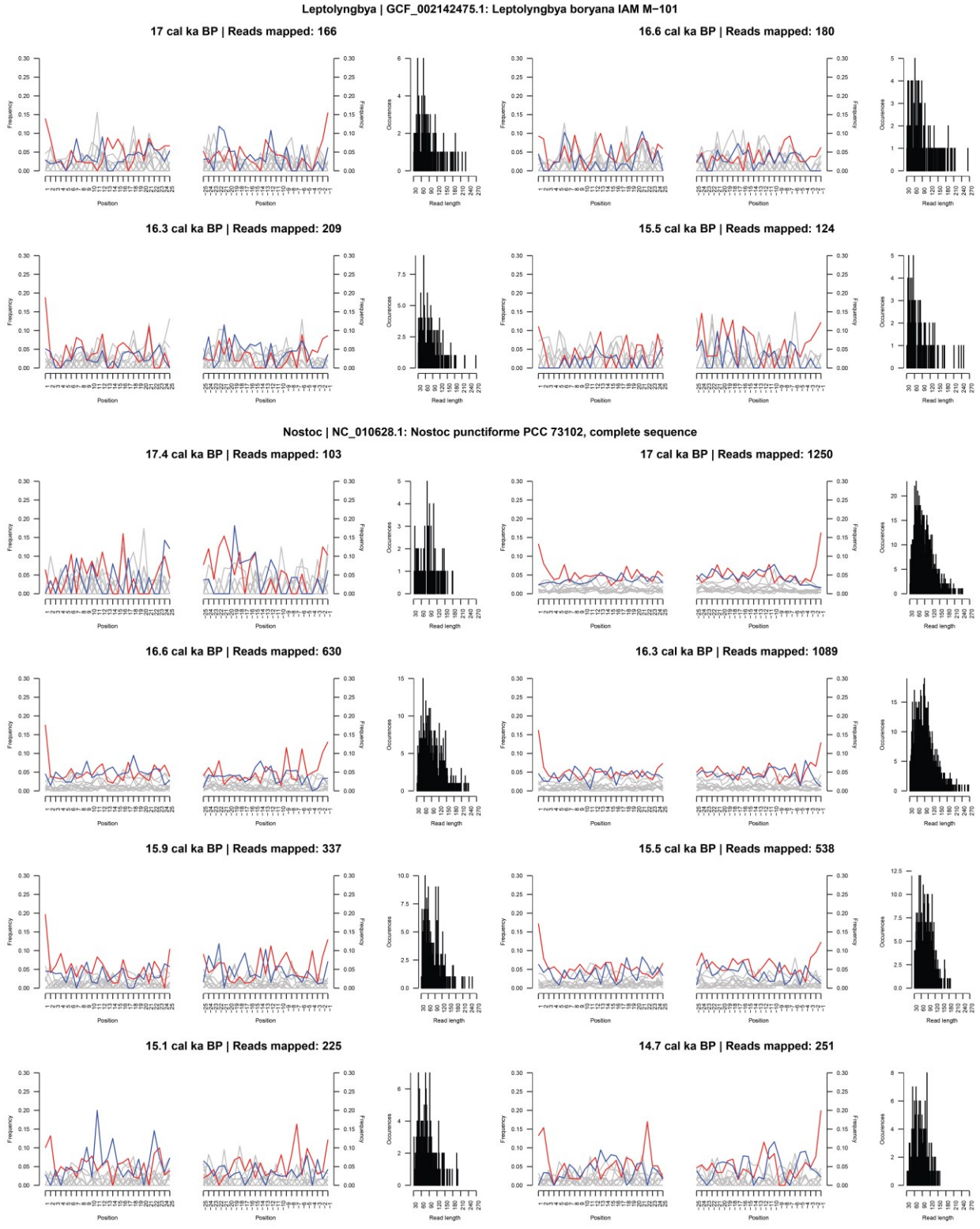
Leptolyngbya | GCF_002142475.1: Leptolyngbya boryana IAM M−101
17 cal ka BP | Reads mapped: 166
16.6 cal ka BP | Reads mapped: 180
16.3 cal ka BP | Reads mapped: 209
15.5 cal ka BP | Reads mapped: 124
Nostoc | NC_010628.1: Nostoc punctiforme PCC 73102, complete sequence
17.4 cal ka BP | Reads mapped: 103
17 cal ka BP | Reads mapped: 1250
16.6 cal ka BP | Reads mapped: 630
16.3 cal ka BP | Reads mapped: 1089
15.9 cal ka BP | Reads mapped: 337
15.5 cal ka BP | Reads mapped: 538
15.1 cal ka BP | Reads mapped: 225
14.7 cal ka BP | Reads mapped: 251
Frequency
Position
Occurences
Read length

Continued

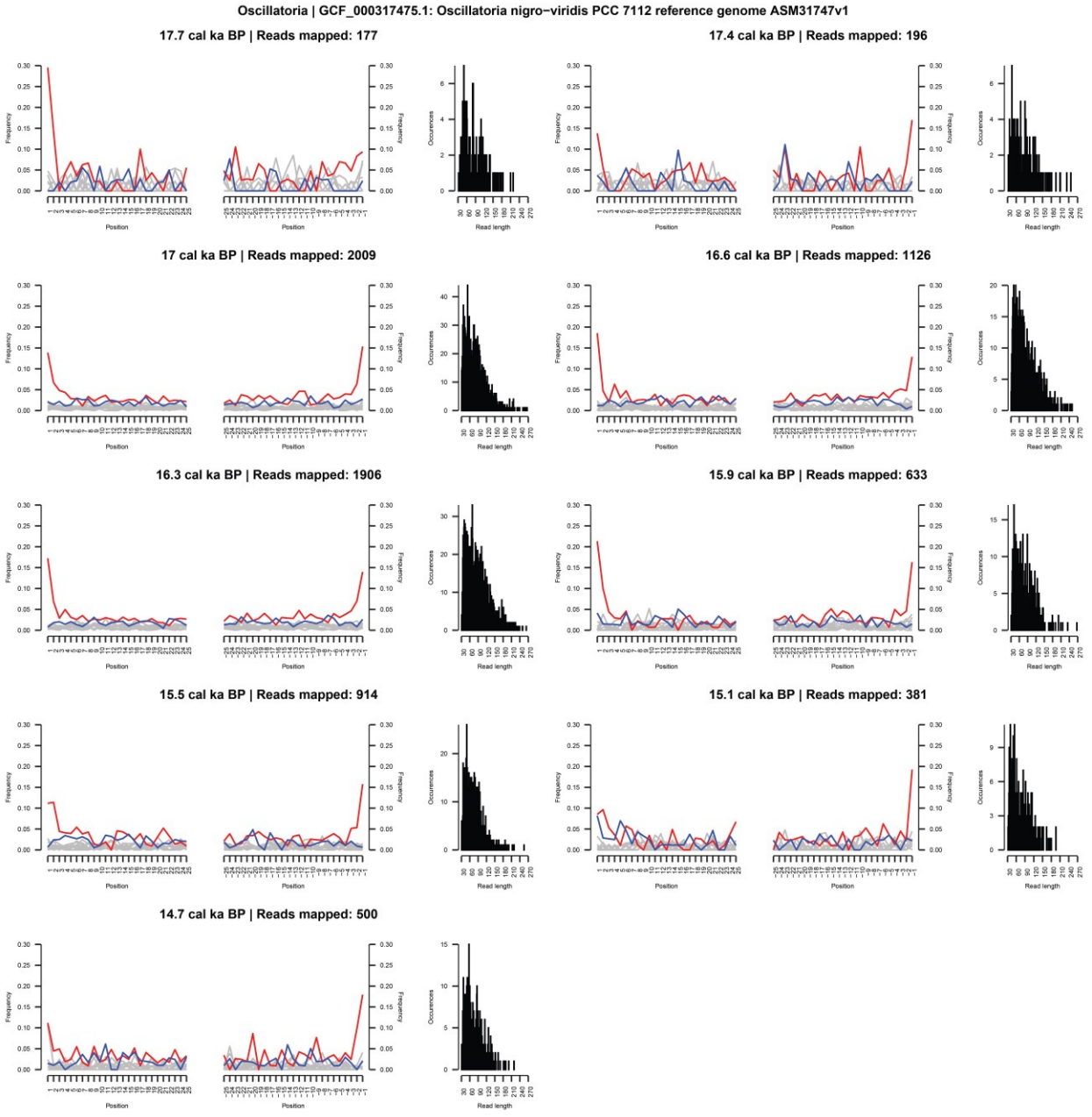
Oscillatoria | GCF_000317475.1: Oscillatoria nigro−viridis PCC 7112 reference genome ASM31747v1
17.7 cal ka BP | Reads mapped: 177
17.4 cal ka BP | Reads mapped: 196
17 cal ka BP | Reads mapped: 2009
16.6 cal ka BP | Reads mapped: 1126
16.3 cal ka BP | Reads mapped: 1906
15.9 cal ka BP | Reads mapped: 633
15.5 cal ka BP | Reads mapped: 914
15.1 cal ka BP | Reads mapped: 381
14.7 cal ka BP | Reads mapped: 500
Position
Frequency
Read length
Occurrences

Continued

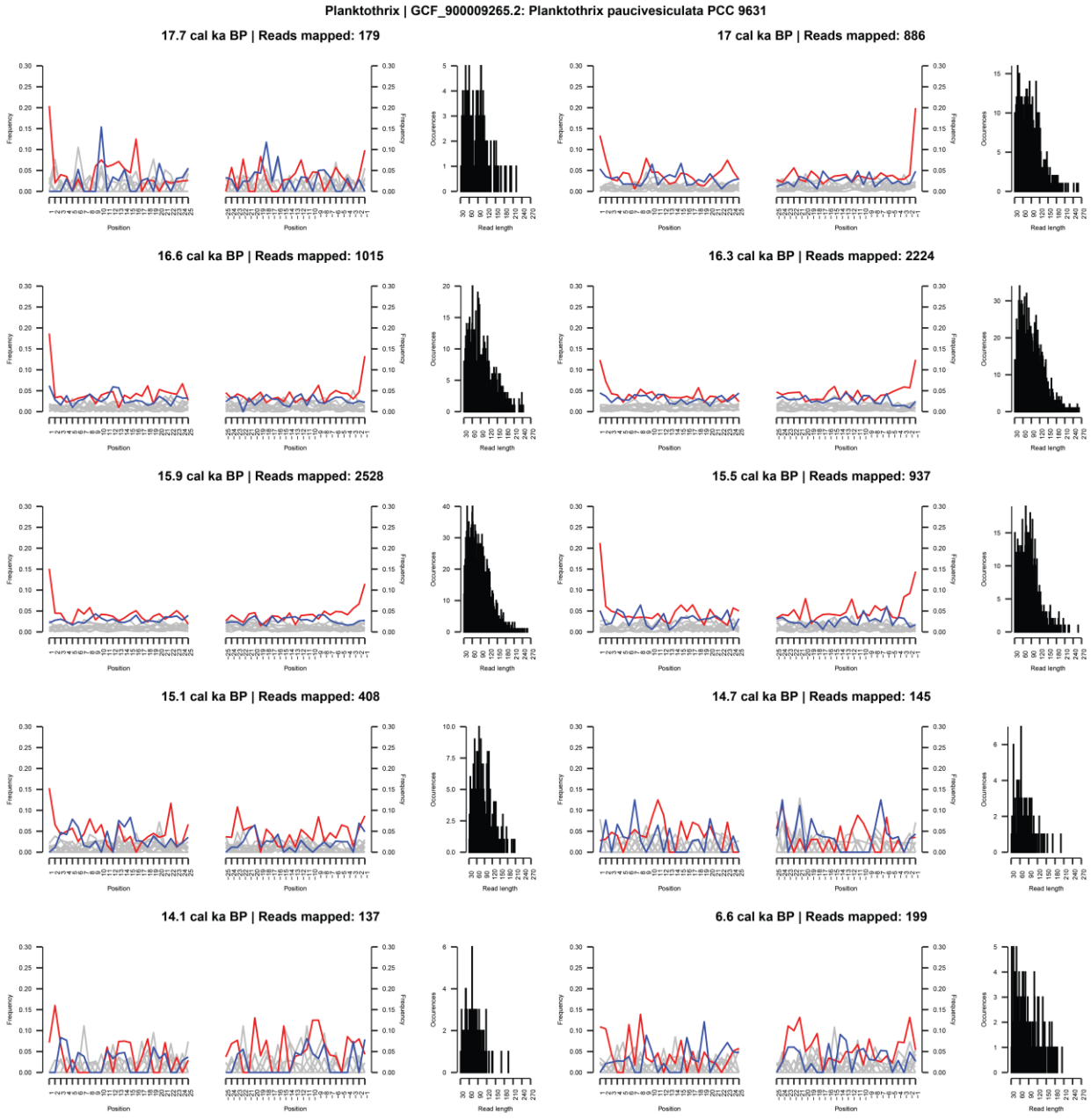
Planktothrix | GCF_900009265.2: Planktothrix paucivesiculata PCC 9631
17.7 cal ka BP | Reads mapped: 179
17 cal ka BP | Reads mapped: 886
16.6 cal ka BP | Reads mapped: 1015
16.3 cal ka BP | Reads mapped: 2224
15.9 cal ka BP | Reads mapped: 2528
15.5 cal ka BP | Reads mapped: 937
15.1 cal ka BP | Reads mapped: 408
14.7 cal ka BP | Reads mapped: 145
14.1 cal ka BP | Reads mapped: 137
6.6 cal ka BP | Reads mapped: 199
Frequency
Occurrences
Position
Read length

Continued

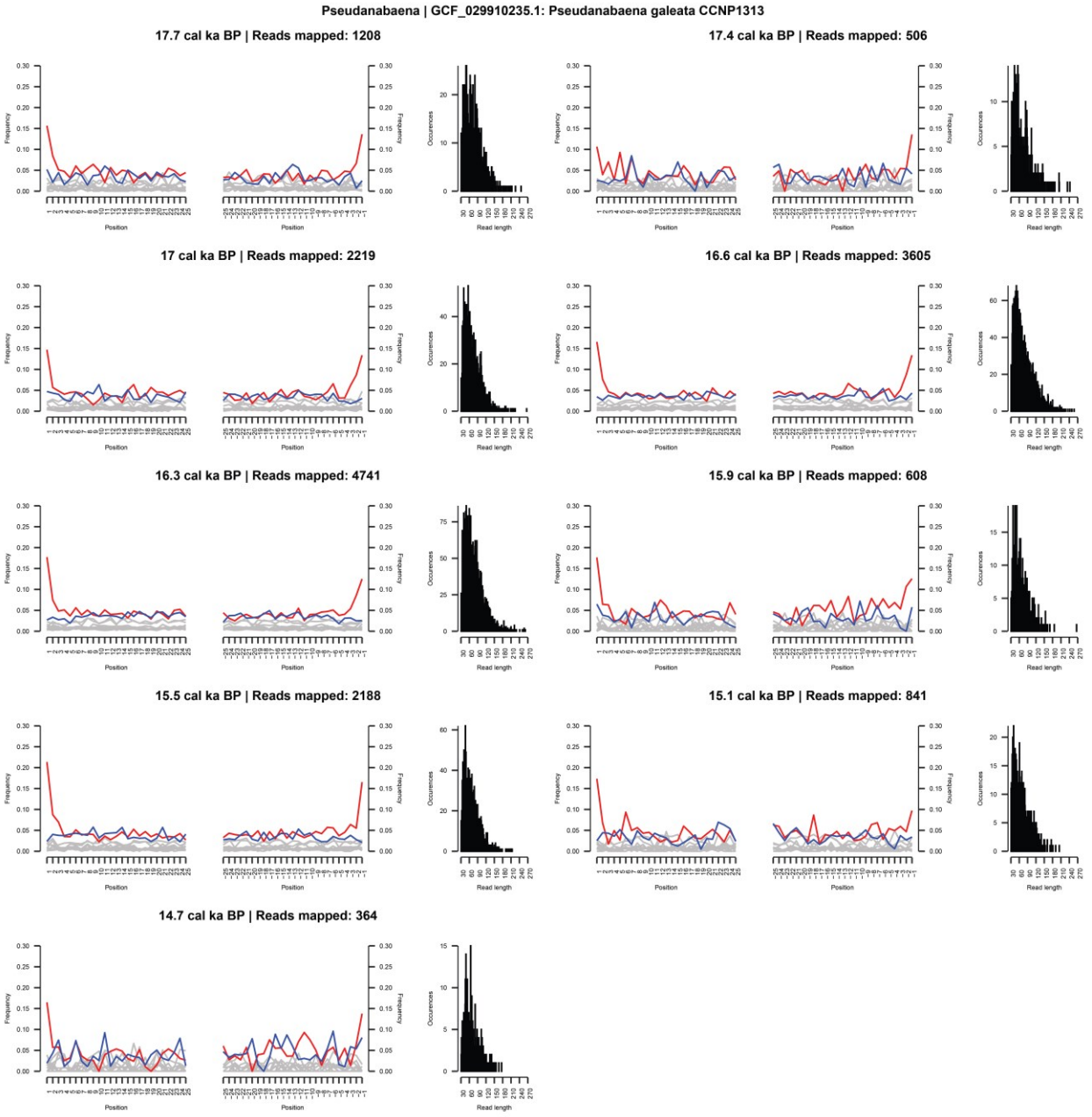

Fig. S3. Ancient damage patterns for 26 common taxa in terrestrial and aquatic ecosystems through time. Authentication of taxa at each time point was performed using mapDamage v.2.2.1 (*108*) with the settings '--rescale --single-stranded,' employing corresponding classified reads. The ancient origin of reads was evaluated using the miscoding lesion pattern (left plots, red: C to T substitutions, blue: G to A substitutions, gray: all other substitutions, y-axis is frequency on a scale of 0−0.3 and x-axis is position) and length distribution (right plot, y-axis is occurrence on a varying scale and x-axis is read length from 30 to 270 bp). The highest deamination rates, observed at the 5' and 3’ end, confirm that the identified terrestrial and aquatic taxa DNA is of ancient origin.

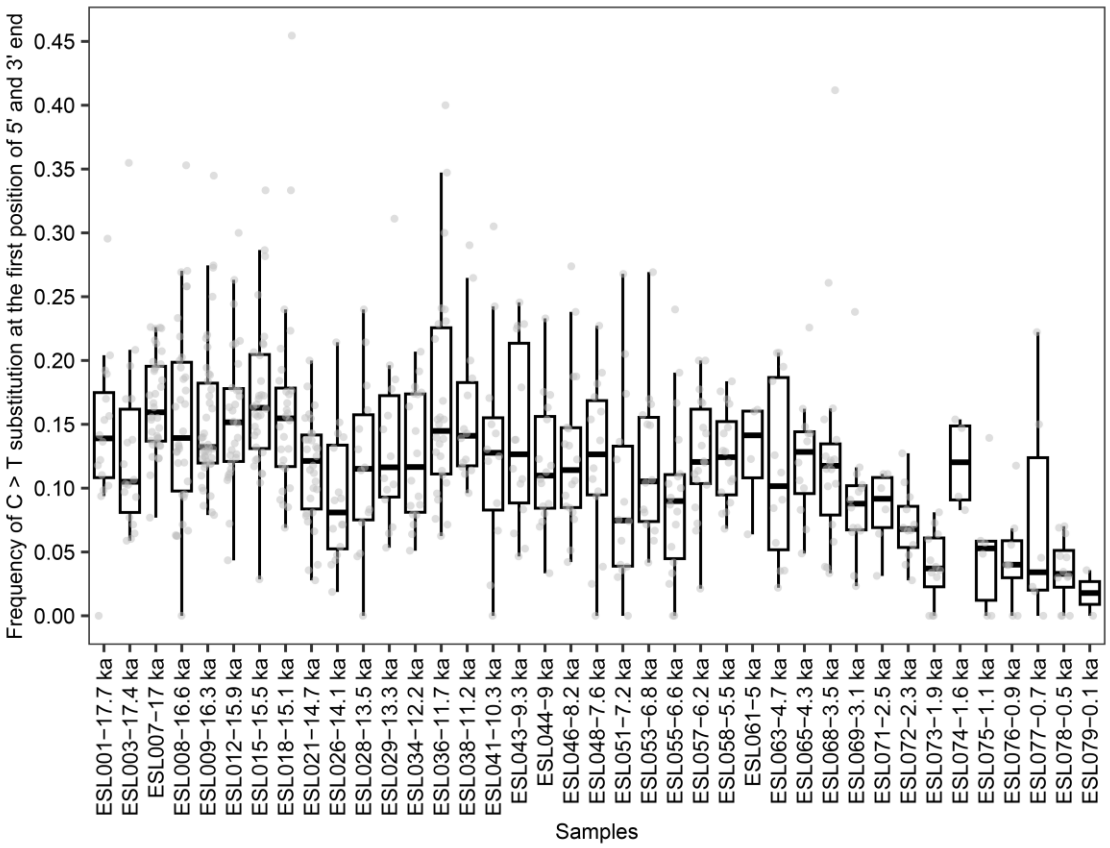

Fig. S4. Ancient damage patterns across time intervals show a clear increase in the substitution rate with age, suggesting that metagenomic DNA is ancient in origin and well-preserved in Lake Naleng. The observation of clay mineral-rich fine fractions in sediment over time (*96*) provides further evidence of good preservation conditions (*155*).

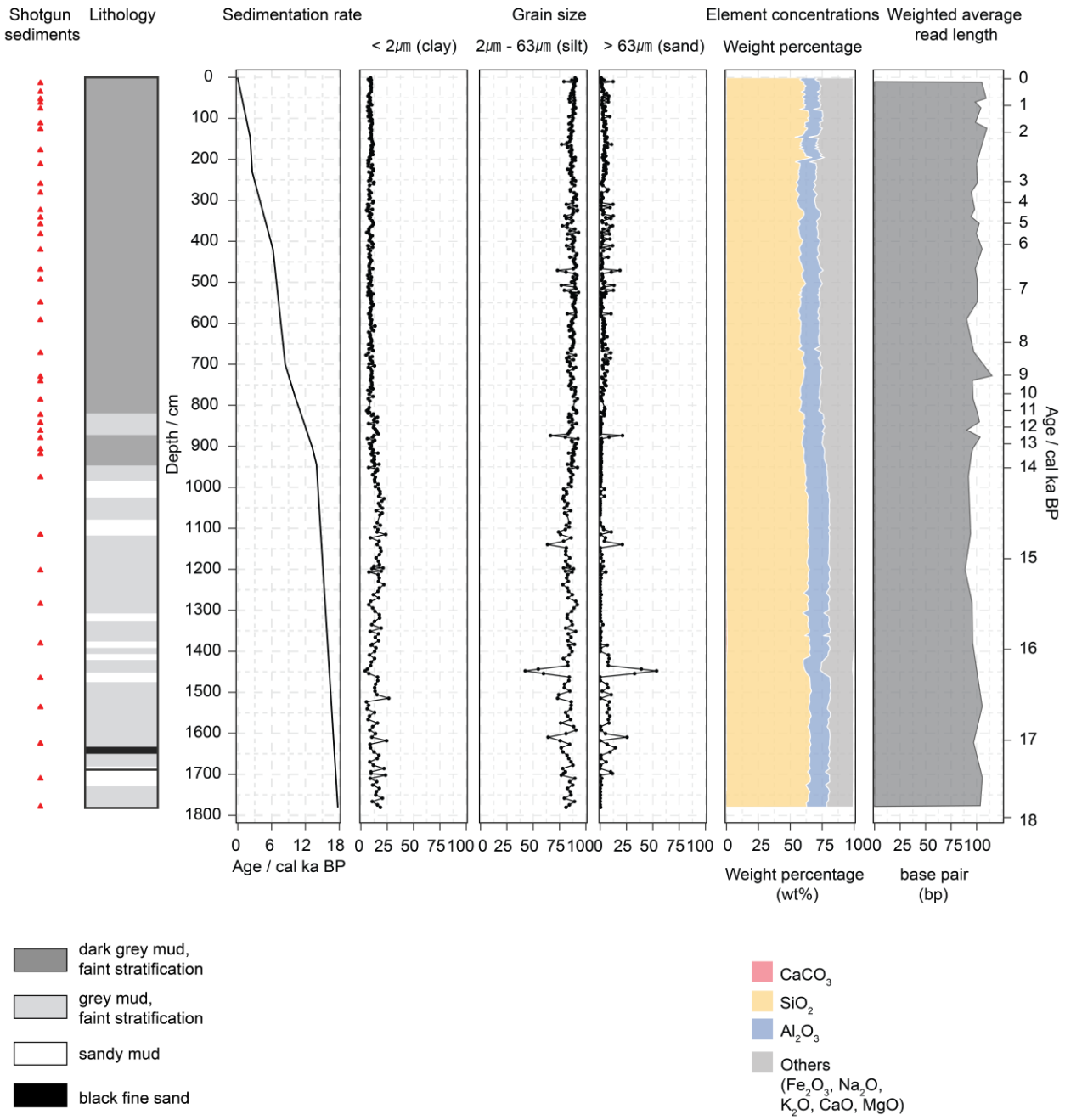

Fig. S5. Overview of the Lake Naleng sediment core and weighted average read length of Lake Naleng's shotgun data. Sediments designated for shotgun sequencing are highlighted in red. The majority of these sediments are collected from lake mud, with two additional samples obtained from sandy mud to enhance temporal resolution. The basic lithostratigraphy is established through visual inspection. The sedimentation rate in the lower section of the core (between 1780 and 950 cm) is relatively higher than in the upper part, primarily due to the enhanced accumulation of sediments derived from glacial erosion. Grain-size fractions and concentrations of major elements exhibit consistent patterns throughout the core, with higher variations observed in grain-size fractions below 950 cm. The presence of CaO is assumed to be attributed to silicates, as Lake Naleng lacks calcareous rocks in its catchment area, and the lake sediments have a low carbonate content (< 1%). The source data are derived from (*96*). The merged reads are applied to calculate the average read length, which is weighted by read count, considering it as a proxy for read fragmentation.

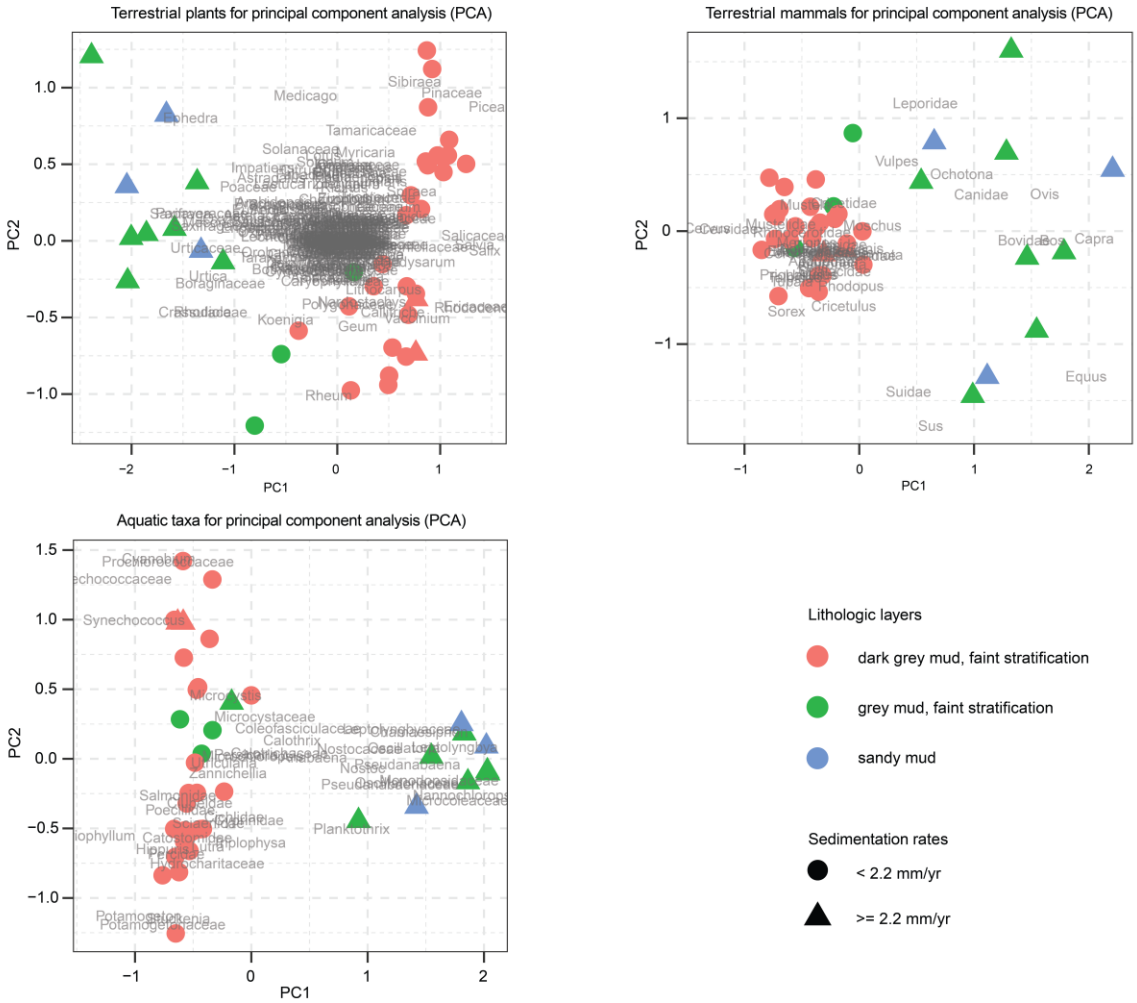

Fig. S6. Principal component analysis (PCA) of terrestrial plants, terrestrial mammals, and aquatic communities. Samples are not clustered by sediment type. No specific samples or taxa exhibit extremely large values that notably skew the PCA plots. Instead, the covariance structure of the three communities directly corresponds to past environmental changes.

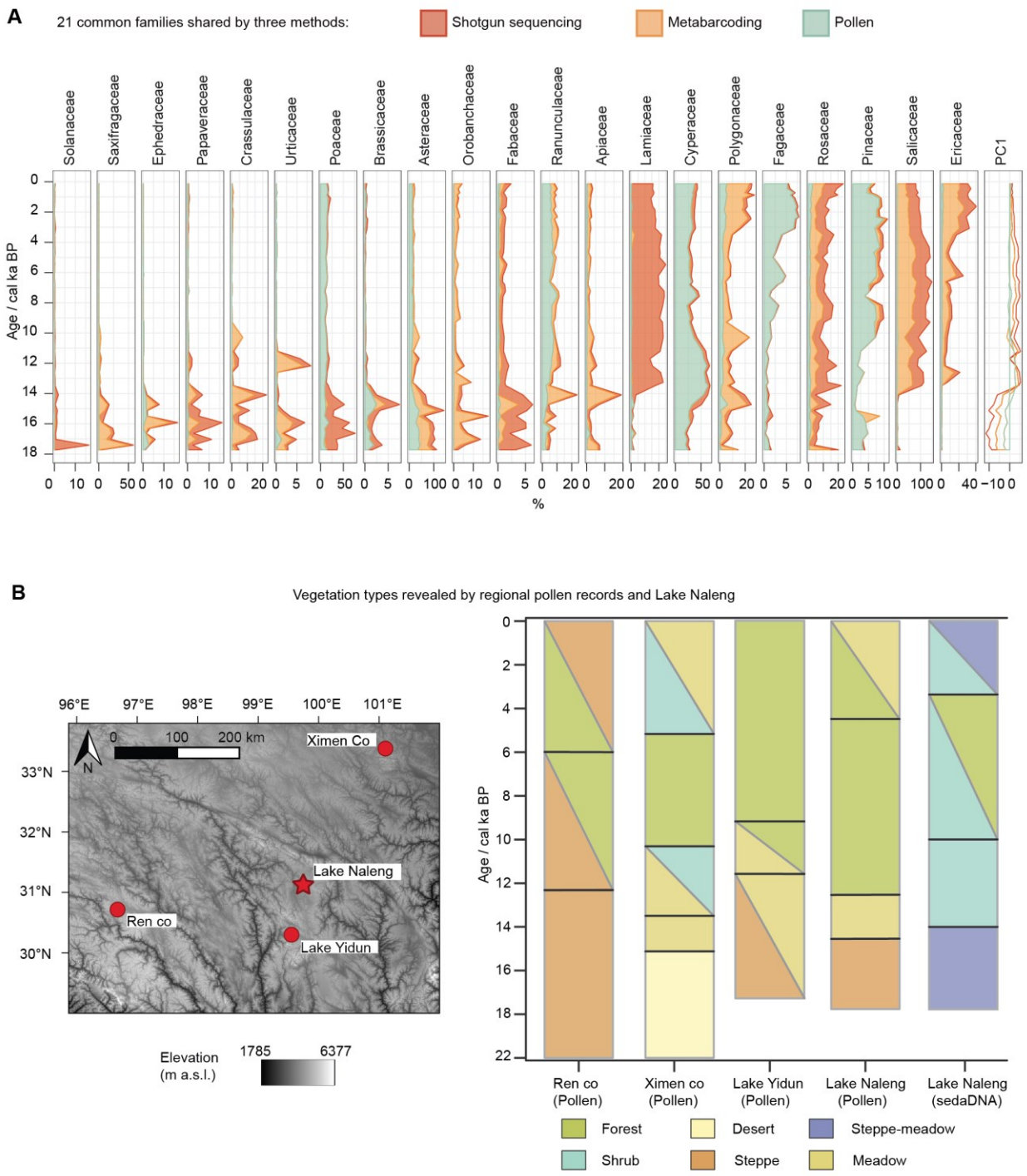

Fig. S7. Proxy records of vegetation changes archived in Lake Naleng sediments and of comparisons with surrounding lake sediment cores. (A) After comparing the relative abundance and PC1 of metagenomics/shotgun sequencing, metabarcoding, and pollen analysis, we focused on 21 common families retrieved by all three methods. (B) We compared these proxy-based vegetation types to pollen-based ones from the closest lake cores that were dated to at least the late glacial period. The synthesis of multiple proxies confirms a cold-adapted vegetation in the late glacial which turns to warm-adapted woodland in the Holocene. Plot B is modified from (*15*).

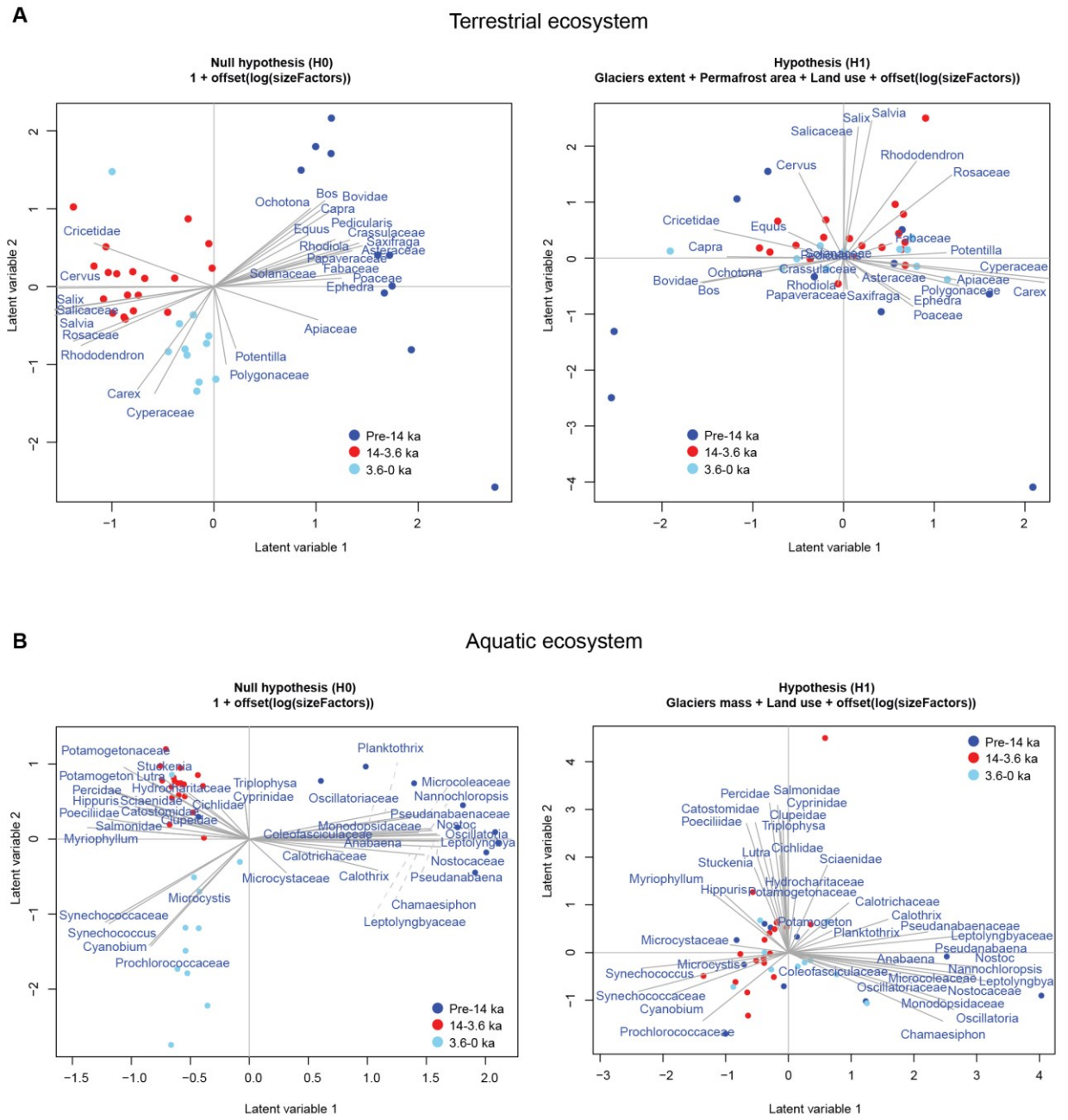

Fig. S8. Results of latent factor analysis via Gaussian copula graphical models (GCGMs) with unconstrained (left plot) and constrained latent variables (right plot) for terrestrial (A) and aquatic ecosystems (B). Three clusters of samples in terms of these covariates are in the null model (H0), while these patterns are absent after controlling for co-variance of environmental factors (H1). These shifts indicate that the co-occurrence patterns revealed by H1 are mainly generated by biotic interactions rather than shared responses to environmental covariates. The effect of sequencing depth (sampling effort) is excluded from models by taking the log of size factor.

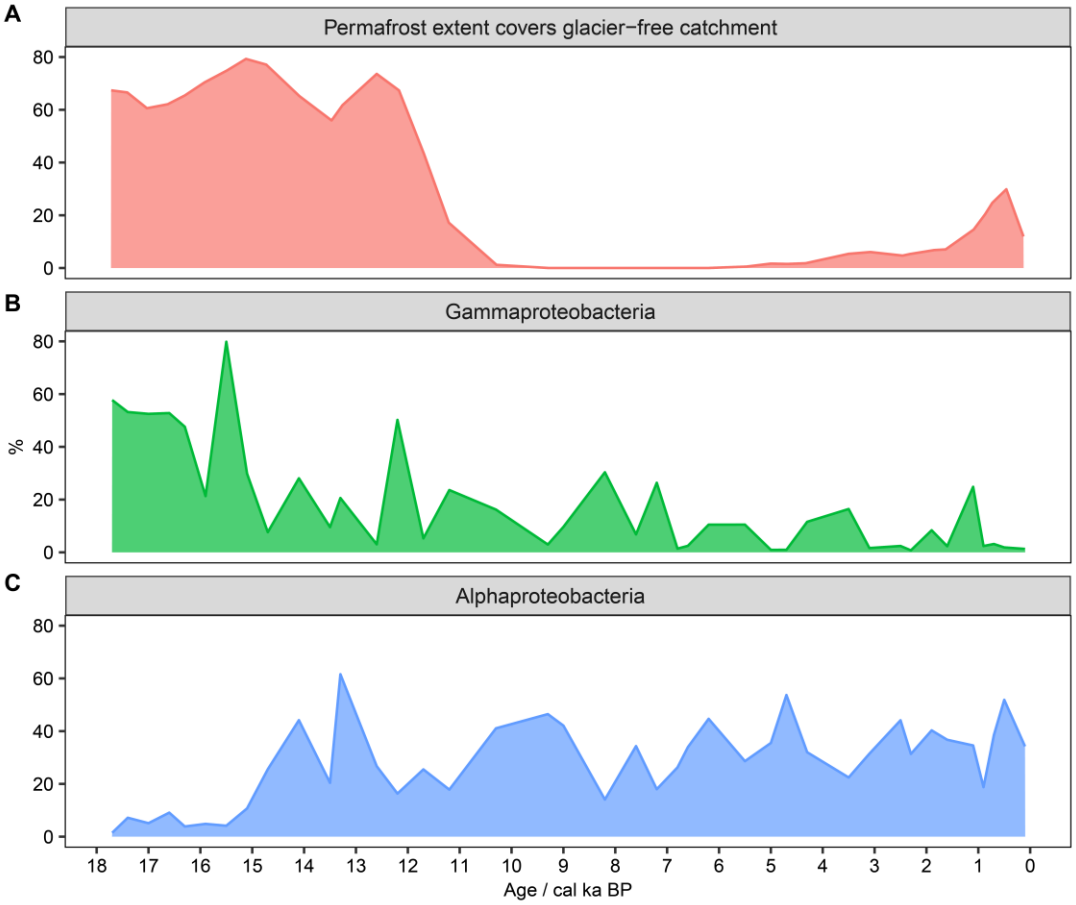

Fig. S9. Shotgun-data-based authentication of the simulated permafrost extent. (A) The simulated permafrost extent accounted for the glacier-free catchment. (B) The relative abundance of Gammaproteobacteria against Bacteria. (C) The relative abundance of Alphaproteobacteria against Bacteria. Both Proteobacteria dominate in the permafrost soils and active layers on the Tibetan Plateau, respectively (*148*). The simulated percentages of permafrost extent with 500-year intervals are linearly interpolated to the same temporal resolution as lake sediments.

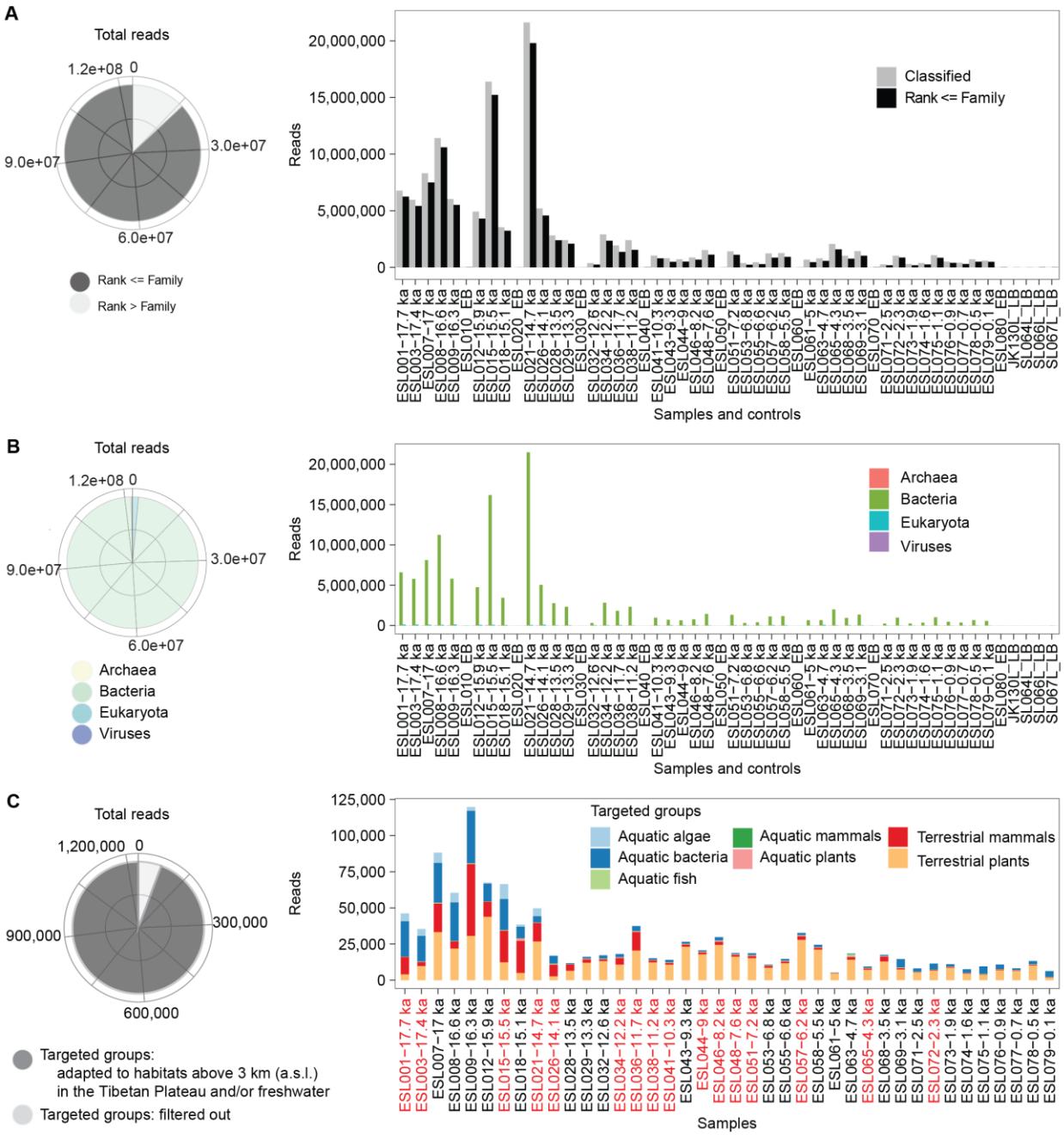

Fig. S10. Data overview. (A) Total reads of classified cellular organisms and taxa with taxonomic rank ≤ Family (left plot) as well as their distribution across samples and controls (right plot). (B) The total reads of superkingdoms (left plot) and their distribution across samples and controls (right plot). (C) The total reads of targeted groups that can adapt to habitats above 3000 m a.s.l. on the Tibetan Plateau and/or in freshwater (left plot), along with their distribution across samples (right plot). Those sediments having a library with deep sequencing are marked in red once to avoid excessive coloration.

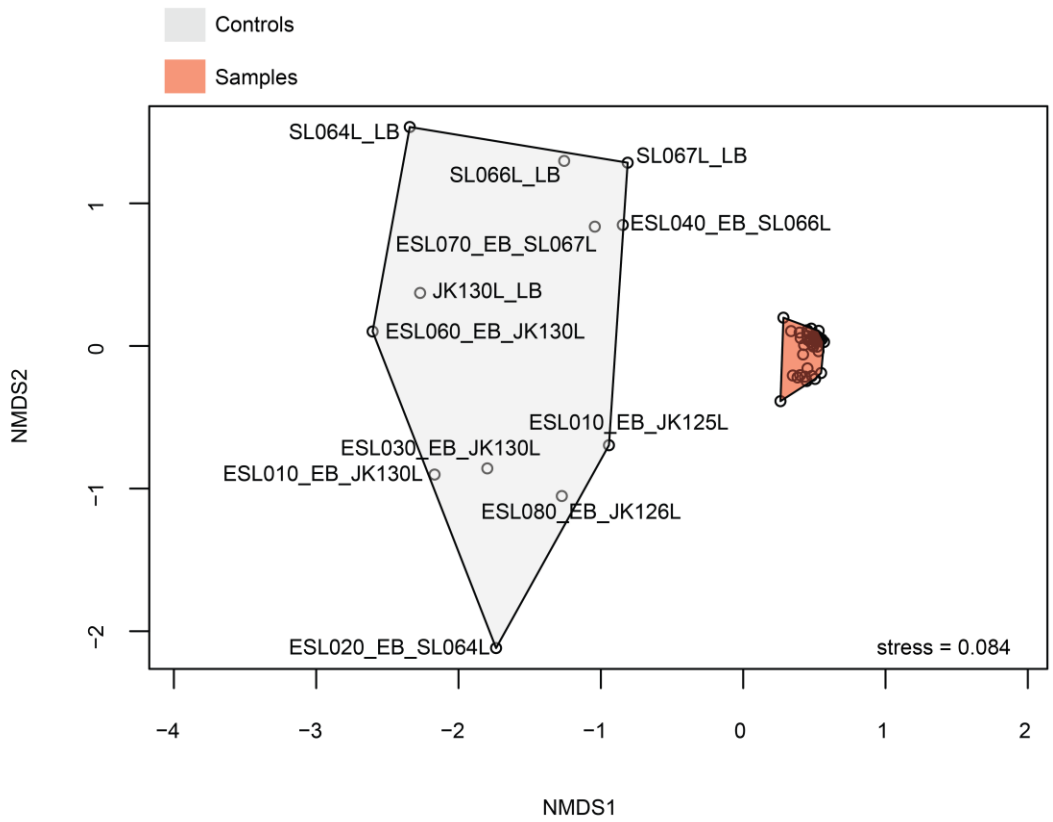

Fig. S11. Non-metric multidimensional scaling (NMDS) results indicate the notable dissimilarity of community composition between controls and samples.

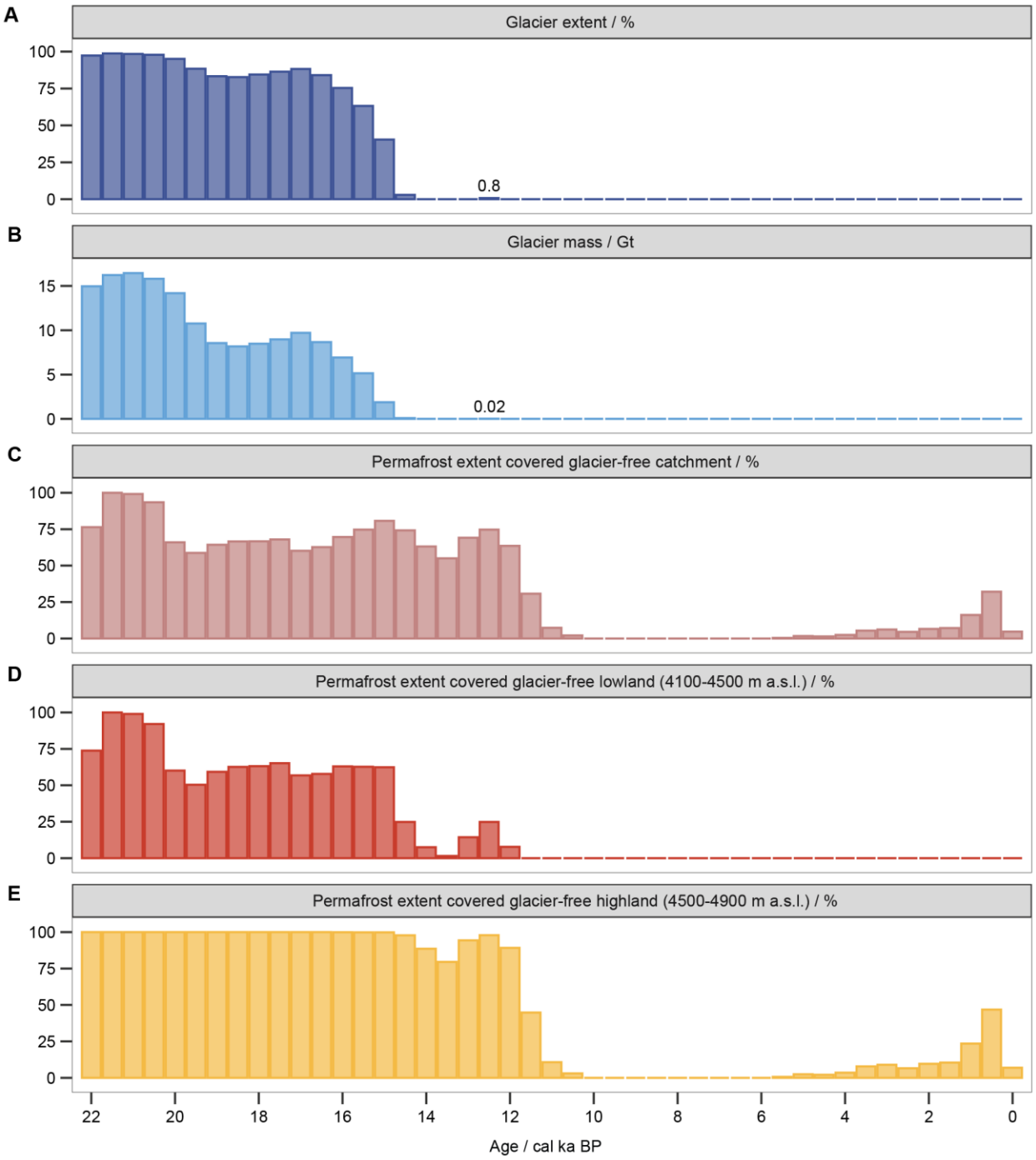

Fig. S12. Simulated past cryosphere changes are represented by the percentage of simulated glacier extent (A), glacier mass (B), and permafrost extent (C-E) within Lake Naleng's catchment from 22 to 0 ka. The simulated glacier extent was extracted from ref. (*45*).

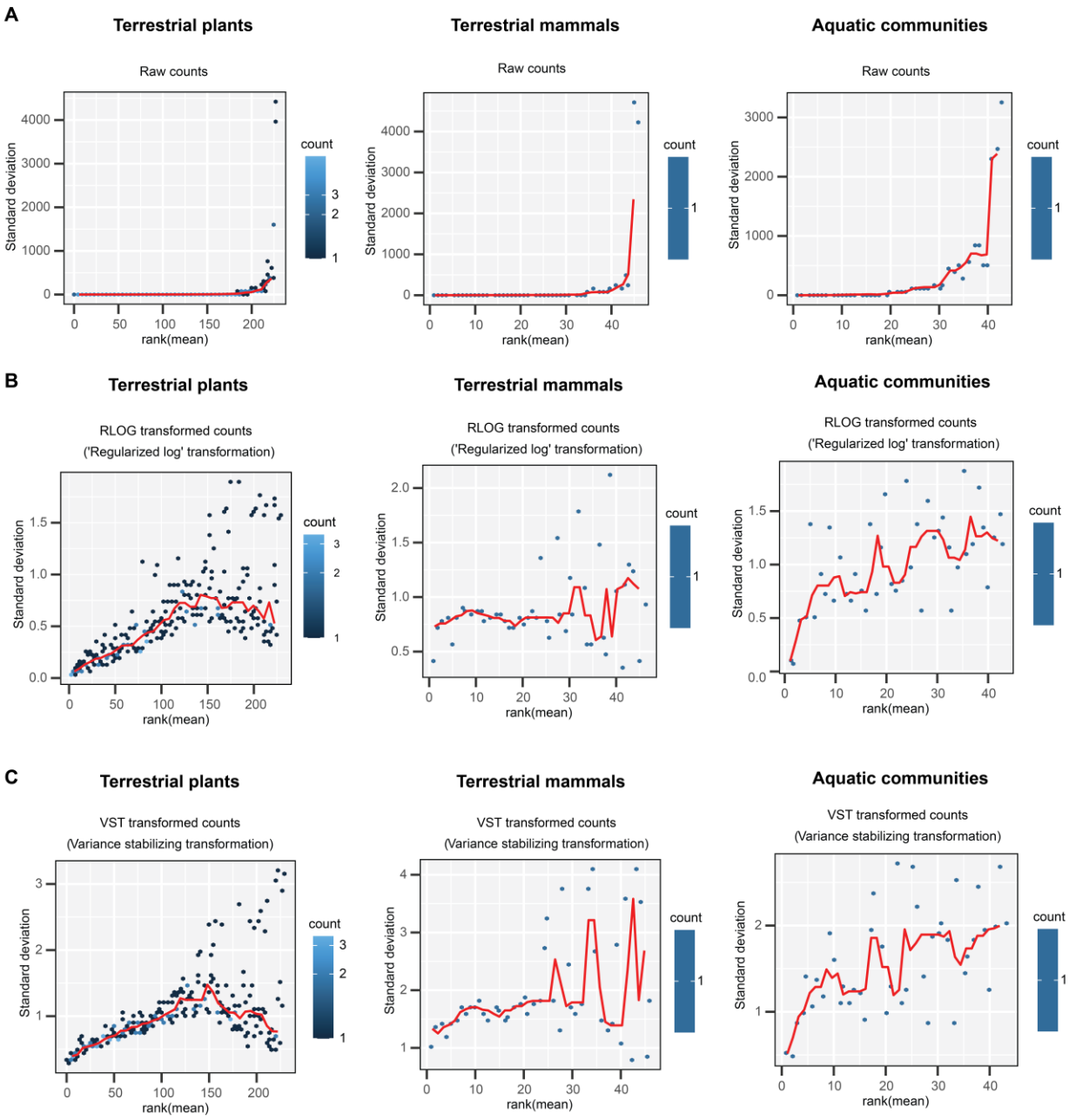

Fig. S13. Mean-variance relationship for raw counts (A), 'regularized log' (RLOG) transformed (B), and variance stabilizing transformed (VST) counts (C) of terrestrial plants, terrestrial mammals, and aquatic communities. Heteroscedasticity is clearly observed in the mean-variance relationship based on raw counts as standard deviation varies over several orders of magnitude. Both transformation approaches significantly stabilize variance across samples. RLOG transformed counts are used for ordination analysis due to their lower standard deviation. The transformation ensures that the variance and co-variance of taxa composition turnover over time are primarily influenced by predictor variables (e.g., environmental factors) rather than sampling effort or sequencing depth.

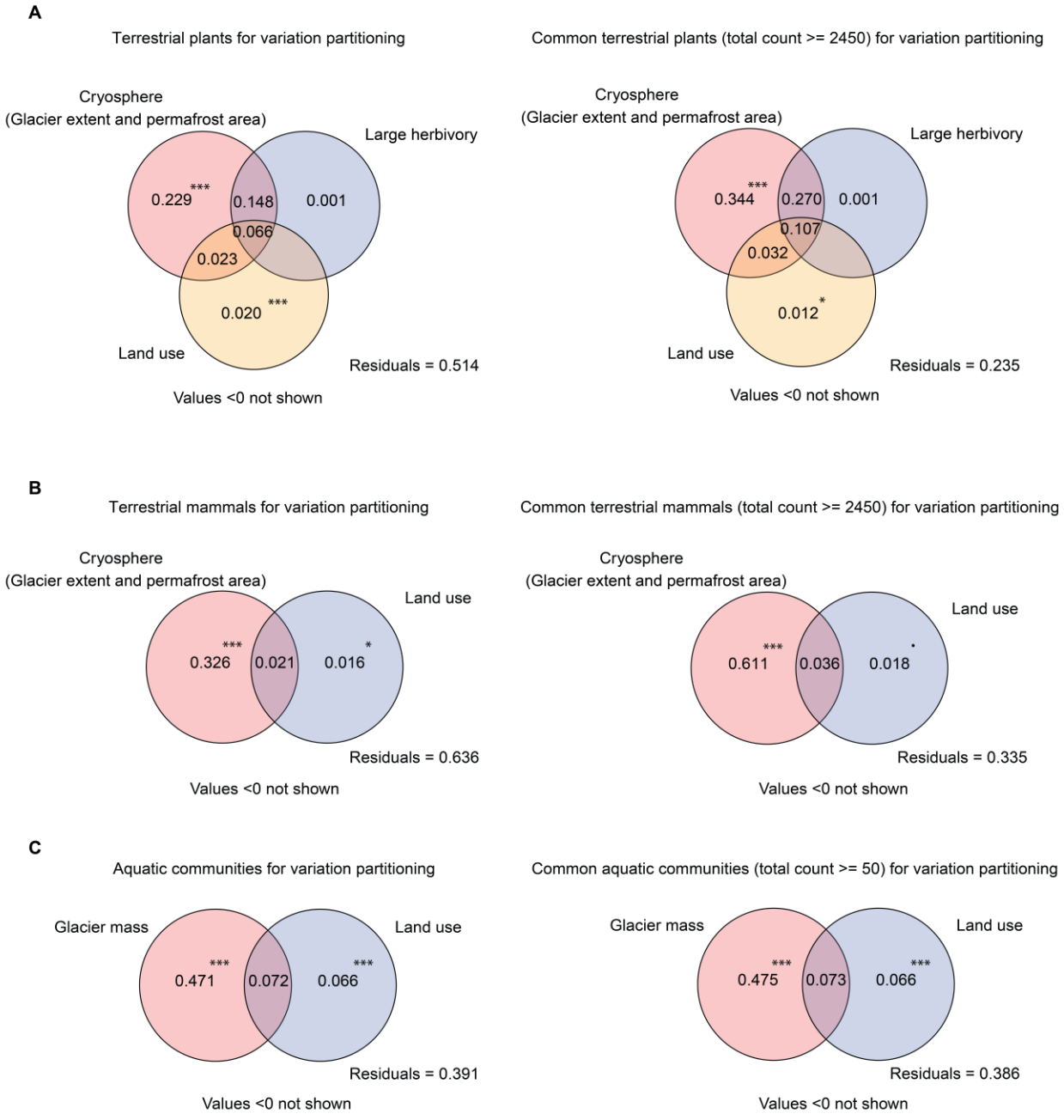

Fig. S14. Variation partitioning analysis for terrestrial plants (A), terrestrial mammals (B), and aquatic communities (C). The results based on composition of common taxa align coherently with the results for the whole composition. Significance codes of F-test with 999 permutations: '***' 0.001, '**' 0.01, '*' 0.05, '.' 0.1

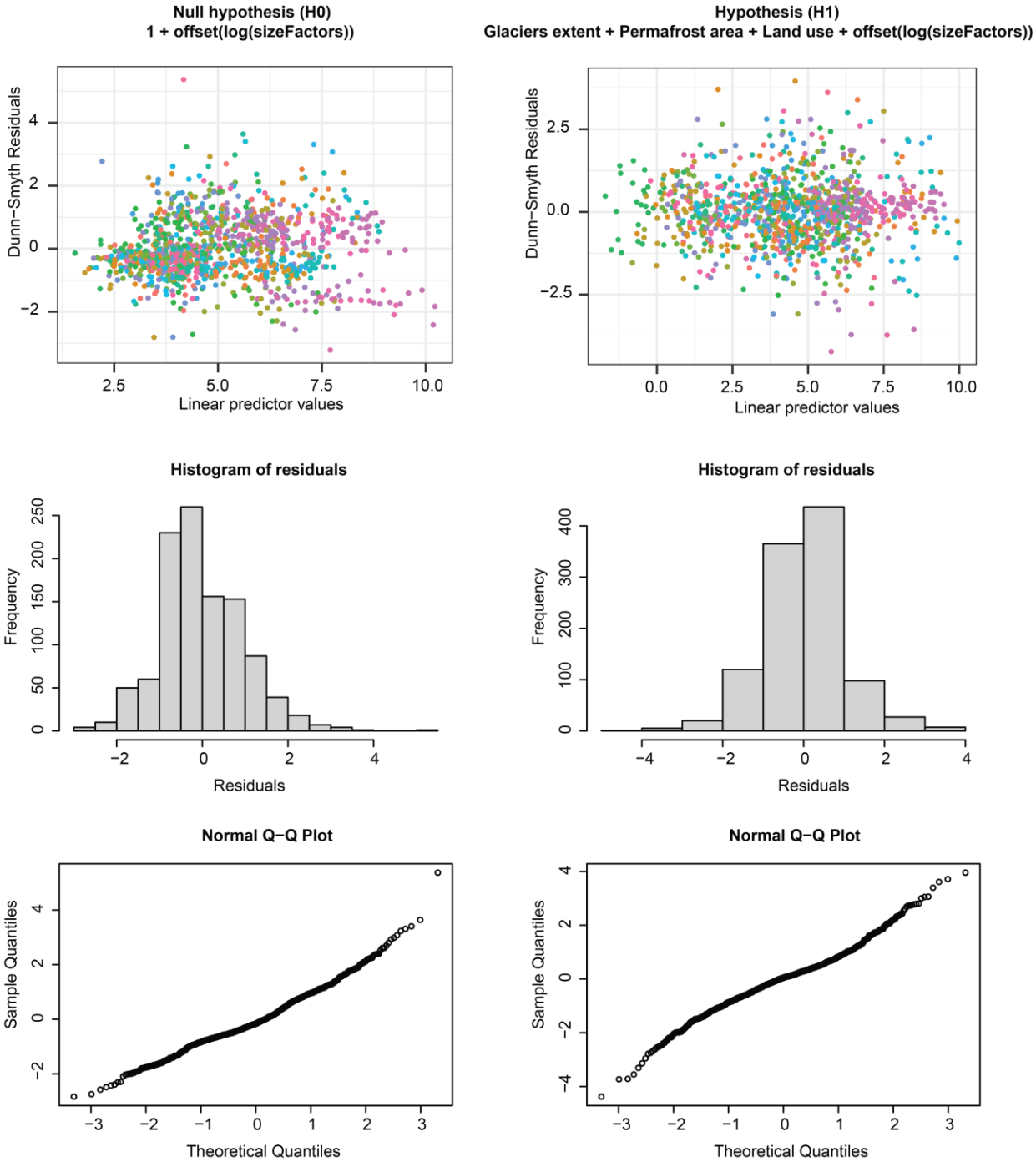

Fig. S15. Diagnostics of marginal regression models of latent factor analysis and Gaussian copula graphical network for the terrestrial ecosystem. Both the null model (left panel) and the hypothesis model (right panel) exhibit no discernible patterns in the plot of residuals against linear predictor values (top row), show no significant outliers in the histogram (middle row), and strong skewness in the Q-Q plot (bottom row). These characteristics suggest that the marginal modes adhere to the basic assumptions of the Gaussian copula graphical model.

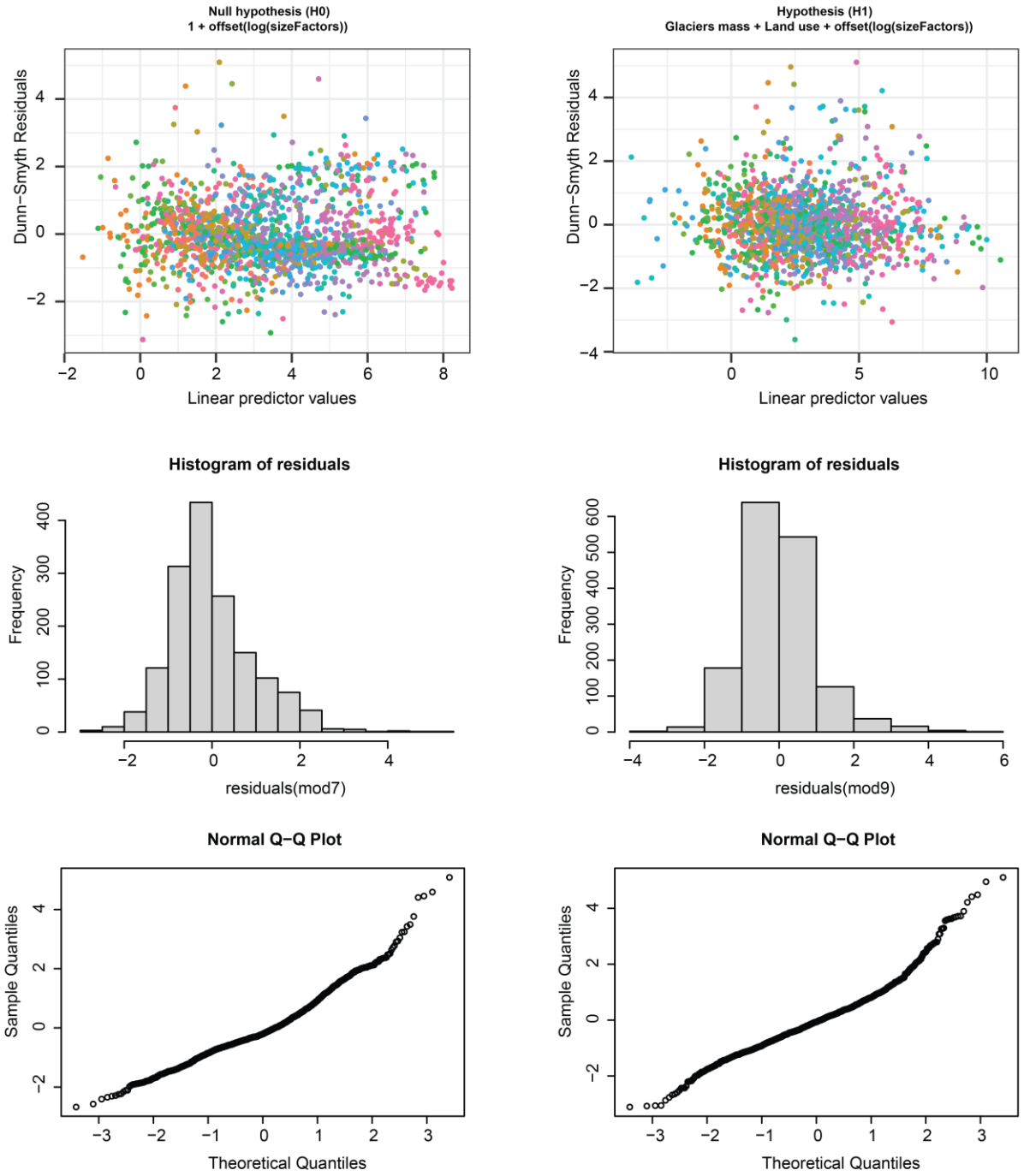

Fig. S16. Diagnostics of marginal regression models of latent factor analysis and Gaussian copula graphical network for the aquatic ecosystem. Both the null model (left panel) and the hypothesis model (right panel) display no evident patterns in the plot of residuals against linear predictor values (top row), show no significant outliers in the histogram (middle row), and strong skewness in the Q-Q plot (bottom row). These characteristics suggest that the marginal modes adhere to the basic assumptions of the Gaussian copula graphical model.

Tables S1 – S6

Table S1. Lake Naleng's shotgun sequencing, metabarcoding, and pollen analysis record similar dominant families and genera, which are among the top 20 species-rich families and genera in the Hengduan Mountains.

	Top 20 species-rich families in Hengduan Mountains	Recovered by Methods	Top 20 species-rich genera in Hengduan Mountains	Recovered by Methods
1	Asteraceae	Shotgun, Metabarcoding, Pollen	*Pedicularis* (Orobanchaceae)	Shotgun, Metabarcoding, Pollen
2	Rosaceae	Shotgun, Metabarcoding, Pollen	*Rhododendron* (Ericaceae)	Shotgun, Metabarcoding, Pollen
3	Poaceae	Shotgun, Metabarcoding, Pollen	*Saxifraga* (Saxifragaceae)	Shotgun, Metabarcoding, Pollen
4	Ranunculaceae	Shotgun, Metabarcoding, Pollen	*Gentiana* (Gentianaceae)	Shotgun, Metabarcoding, Pollen
5	Ericaceae	Shotgun, Metabarcoding, Pollen	*Aconitum* (Ranunculaceae)	Shotgun, Metabarcoding, Pollen
6	Fabaceae	Shotgun, Metabarcoding, Pollen	*Primula* (Primulaceae)	Shotgun, Metabarcoding, Pollen
7	Lamiaceae	Shotgun, Metabarcoding, Pollen	*Salix* (Salicaceae)	Shotgun, /, Pollen
8	Orchidaceae	Shotgun, / , /	*Carex* (Cyperaceae)	Shotgun, Metabarcoding
9	Orobanchaceae	Shotgun, Metabarcoding, Pollen	*Corydalis* (Papaveraceae)	Shotgun, Metabarcoding, Pollen
10	Apiaceae	Shotgun, Metabarcoding, Pollen	*Saussurea* (Asteraceae)	Shotgun, Metabarcoding, Pollen
11	Gentianaceae	Shotgun, Metabarcoding, Pollen	*Delphinium* (Ranunculaceae)	Shotgun, Metabarcoding
12	Primulaceae	Shotgun, Metabarcoding, Pollen	*Rubus* (Rosaceae)	Shotgun, /, Pollen
13	Cyperaceae	Shotgun, Metabarcoding, Pollen	*Astragalus* (Fabaceae)	Shotgun, Metabarcoding, Pollen
14	Saxifragaceae	Shotgun, Metabarcoding, Pollen	*Berberis* (Berberidaceae)	/, /, Pollen
15	Caryophyllaceae	Shotgun, Metabarcoding, Pollen	*Sedum* (Crassulaceae)	Shotgun, Pollen
16	Salicaceae	Shotgun, Metabarcoding, Pollen	*Arenaria* (Caryophyllaceae)	/
17	Papaveraceae	Shotgun, Metabarcoding, Pollen	*Ligularia* (Asteraceae)	/
18	Brassicaceae	Shotgun, Metabarcoding, Pollen	*Poa* (Poaceae)	/
19	Crassulaceae	Shotgun, Metabarcoding, Pollen	*Potentilla* (Rosaceae)	Shotgun, Metabarcoding, Pollen
20	Liliaceae	, / , /, Pollen	*Aster* (Asteraceae)	Shotgun, Pollen
	Account for counts% of corresponding data	93.5, 87.6, 75.8		

Source for list of top 20 species-rich families and genera in the Hengduan Mountains from ref (*131*).

Table S2. Identification of influential nodes (taxa) of the weighted network for the terrestrial ecosystem.

Module	Taxa	Kleinberg's hub centrality scores	Community
Pre-14 ka (high stress)	**Asteraceae**	1	Terrestrial plants
Pre-14 ka (high stress)	**Polygonaceae**	0.909	Terrestrial plants
Pre-14 ka (high stress)	***Saxifraga***	0.884	Terrestrial plants
Pre-14 ka (high stress)	***Pedicularis***	0.801	Terrestrial plants
Pre-14 ka (high stress)	Crassulaceae	0.78	Terrestrial plants
Pre-14 ka (high stress)	Bovidae	0.76	Terrestrial mammals
Pre-14 ka (high stress)	*Ochotona*	0.605	Terrestrial mammals
Pre-14 ka (high stress)	*Rhodiola*	0.495	Terrestrial plants
Pre-14 ka (high stress)	*Potentilla*	0.455	Terrestrial plants
Post-14 ka (low stress)	**Rosaceae**	1	Terrestrial plants
Post-14 ka (low stress)	***Salvia***	0.993	Terrestrial plants
Post-14 ka (low stress)	***Equus***	0.933	Terrestrial mammals
Post-14 ka (low stress)	***Capra***	0.928	Terrestrial mammals
Post-14 ka (low stress)	***Cervus***	0.921	Terrestrial mammals
Post-14 ka (low stress)	**Fabaceae**	0.915	Terrestrial plants
Post-14 ka (low stress)	**Poaceae**	0.909	Terrestrial plants
Post-14 ka (low stress)	**Papaveraceae**	0.867	Terrestrial plants
Post-14 ka (low stress)	*Salix*	0.774	Terrestrial plants
Post-14 ka (low stress)	Salicaceae	0.732	Terrestrial plants
Post-14 ka (low stress)	*Ephedra*	0.713	Terrestrial plants
Post-14 ka (low stress)	*Rhododendron*	0.707	Terrestrial plants
Post-14 ka (low stress)	*Carex*	0.648	Terrestrial plants
Post-14 ka (low stress)	*Bos*	0.632	Terrestrial mammals
Post-14 ka (low stress)	Cricetidae	0.612	Terrestrial mammals
Post-14 ka (low stress)	Apiaceae	0.582	Terrestrial plants
Post-14 ka (low stress)	Cyperaceae	0.531	Terrestrial plants
Post-14 ka (low stress)	Solanaceae	0.359	Terrestrial plants

Keystone taxa (Kleinberg's hub centrality scores ≥ 0.8) are marked in bold.

Table S3. Identification of influential nodes (taxa) of the weighted network for the aquatic ecosystem.

Module	Taxa	Kleinberg's hub centrality scores	Community
Pre-14 ka (high stress)	***Nannochloropsis***	1	Aquatic algae
Pre-14 ka (high stress)	***Pseudanabaena***	0.912	Aquatic cyanobacteria
Pre-14 ka (high stress)	***Anabaena***	0.817	Aquatic cyanobacteria
Pre-14 ka (high stress)	Leptolyngbya	0.792	Aquatic cyanobacteria
Pre-14 ka (high stress)	Oscillatoriaceae	0.773	Aquatic cyanobacteria
Pre-14 ka (high stress)	Leptolyngbyaceae	0.762	Aquatic cyanobacteria
Pre-14 ka (high stress)	Nostocaceae	0.745	Aquatic cyanobacteria
Pre-14 ka (high stress)	Chamaesiphon	0.716	Aquatic cyanobacteria
Pre-14 ka (high stress)	*Nostoc*	0.683	Aquatic cyanobacteria
Pre-14 ka (high stress)	Monodopsidaceae	0.655	Aquatic cyanobacteria
Pre-14 ka (high stress)	*Oscillatoria*	0.63	Aquatic cyanobacteria
Pre-14 ka (high stress)	*Calothrix*	0.598	Aquatic cyanobacteria
Pre-14 ka (high stress)	Microcoleaceae	0.549	Aquatic cyanobacteria
Pre-14 ka (high stress)	Coleofasciculaceae	0.521	Aquatic cyanobacteria
Pre-14 ka (high stress)	Pseudanabaenaceae	0.39	Aquatic cyanobacteria
Post-14 ka (low stress)	**Poeciliidae**	1	Aquatic fish
Post-14 ka (low stress)	**Percidae**	0.9	Aquatic fish
Post-14 ka (low stress)	***Myriophyllum***	0.85	Aquatic plants
Post-14 ka (low stress)	***Triplophysa***	0.826	Aquatic fish
Post-14 ka (low stress)	**Salmonidae**	0.823	Aquatic fish
Post-14 ka (low stress)	***Planktothrix***	0.819	Aquatic cyanobacteria
Post-14 ka (low stress)	Sciaenidae	0.776	Aquatic fish
Post-14 ka (low stress)	Cyprinidae	0.751	Aquatic fish
Post-14 ka (low stress)	Cichlidae	0.731	Aquatic fish
Post-14 ka (low stress)	Hydrocharitaceae	0.713	Aquatic plants
Post-14 ka (low stress)	Catostomidae	0.688	Aquatic fish
Post-14 ka (low stress)	*Cyanobium*	0.607	Aquatic cyanobacteria
Post-14 ka (low stress)	*Lutra*	0.581	Aquatic mammals
Post-14 ka (low stress)	*Hippuris*	0.58	Aquatic plants
Post-14 ka (low stress)	*Stuckenia*	0.578	Aquatic plants
Post-14 ka (low stress)	Calotrichaceae	0.566	Aquatic cyanobacteria
Post-14 ka (low stress)	Microcystaceae	0.566	Aquatic cyanobacteria
Post-14 ka (low stress)	Synechococcus	0.537	Aquatic cyanobacteria
Post-14 ka (low stress)	Potamogetonaceae	0.511	Aquatic plants
Post-14 ka (low stress)	Clupeidae	0.46	Aquatic fish
Post-14 ka (low stress)	Synechococcaceae	0.365	Aquatic cyanobacteria
Post-14 ka (low stress)	*Microcystis*	0.348	Aquatic cyanobacteria
Post-14 ka (low stress)	*Potamogeton*	0.268	Aquatic plants
Post-14 ka (low stress)	Prochlorococcaceae	0.237	Aquatic cyanobacteria

Keystone taxa (Kleinberg's hub centrality scores ≥ 0.8) are marked in bold

Table S4. The reads in sediments and blanks per sequencing pool.

	Read counts			Percent / %		
Library batches	**Sediments**	**Extraction blanks**	**Library blanks**	**Sediments**	**Extraction blanks**	**Library blanks**
SL064L	24,953,946	268	170	99.998	0.001	0.001
SL066L	21,054,767	2,537	1486	99.981	0.012	0.007
SL067L	2,624,963	5,207	3,991	99.651	0.198	0.152
JK125L	3,678,612	7,535	/	99.8	0.2	/
JK126L	39,550,879	2135	/	99.995	0.005	/
JK130L	15,759,638	1,806	225	99.987	0.011	0.001

Table S5. Multicollinearity evaluation and redundancy analysis (RDA) for terrestrial vegetation and mammal data.

	RDA with single environmental variable				Multicollinearity evaluation					
Categories	**Variables**	**Df**	**Explained (adj.r.squared) / %**	**P-value**	**Variables_01**	**VIF_01**	**Variables_02**	**VIF_02**	**Variables_03**	**VIF_03**
Vegetation	Temperature	38	44.9	0.001	Temperature	35.6	/	/	/	/
	Glacier extent	38	37.3	0.001	Glacier	9.3	**Glacier**	2.9	/	/
	Permafrost	38	40.1	0.001	Permafrost	18.6	**Permafrost**	1.9	/	/
	Herbivory	38	21.4	0.001	Herbivory	2.4	**Herbivory**	2.3	/	/
	Land use	38	10.8	0.003	Land use	2.1	**Land use**	1.3	/	/
Mammalian	Temperature	38	33.3	0.001	Temperature	35	/	/	/	/
	Glacier extent	38	33.9	0.001	Glacier	11	Glacier	5	**Glacier**	2
	Permafrost	38	24.2	0.001	Permafrost	20	Permafrost	6	**Permafrost**	2
	PC1	38	35.2	0.001	PC1	13	PC1	13	/	/
	Land use	38	3.8	0.001	Land use	2	Land use	1	**Land use**	1
Vegetation (taxa with abundance >= 2,450)	Temperature	38	71.9	0.001	Temperature	35.6	/	/	/	/
	Glacier extent	38	62.6	0.001	Glacier	9.3	**Glacier**	2.9	/	/
	Permafrost	38	61.8	0.001	Permafrost	18.6	**Permafrost**	1.9	/	/
	Herbivory	38	37.7	0.001	Herbivory	2.4	**Herbivory**	2.3	/	/
	Land use	38	15.1	0.008	Land use	2.1	**Land use**	1.3	/	/
Mammalian (taxa with abundance >= 2,450)	Temperature	38	61.6	0.001	Temperature	35	/	/	/	/
	Glacier extent	38	64.5	0.001	Glacier	11	Glacier	5	**Glacier**	2
	Permafrost	38	63.4	0.001	Permafrost	20	Permafrost	6	**Permafrost**	2
	PC1	38	64.3	0.001	PC1	13	PC1	13	/	/
	Land use	38	5.4	0.069	Land use	2	Land use	1	**Land use**	1

Vegetation and mammalian: 'regularized log' transformed shotgun DNA data (in this study).
Glacier extent: simulated glacier extent covering the lake catchment / km^3 was extracted from source data (*45*).
Permafrost: simulated permafrost extent covering the glacier-free lake catchment / % (in this study).
Large herbivory: percentage of *Bos* shotgun DNA against terrestrial mammalian shotgun DNA (in this study).
PC1: values of first axis of sample scores extracted from principal component analysis of vegetation compositional changes (in this study).
Land use: percentages of *Rumex* and *Sanguisorba* relative to the pollen grains of terrestrial seed-bearing plants) recorded in Lake Naleng (*25*, *50*).
All environmental factors are standardized using 'decostand(method = "standardize")' in the 'vegan' package (*121*).
adj.r.squared: adjusted R^2.
P-value: F-test with 999 permutations.
Values are rounded to one decimal place except for *P*-values.
Independent and significant variables are marked in bold for variation partitioning analysis.

Table S6. Multicollinearity evaluation and redundancy analysis (RDA) for the aquatic ecosystem.

	RDA with single environmental variable			Multicollinearity evaluation	
Categories	**Variables**	**Explained (adj.r.squared) / %**	***P*-value**	**Variables_01**	**VIF_01**
Aquatic ecosystem	Temperature	49.6	0.001	/	/
	Glacier mass	54.3	0.001	**Glacier mass**	1.1
	Land use	13.8	0.004	**Land use**	1.1
Aquatic ecosystem (taxa with abundance >= 50)	Temperature	49.8	0.001	/	/
	Glacier mass	54.7	0.001	**Glacier mass**	1.1
	Land use	13.9	0.003	**Land use**	1.1

Glacier mass: simulated glacier volume (km^3) x density of ice (Gt/km^3) were calculated from source data (*45*).
PC1: values of PC1 extracted from principal component analysis of vegetation (in this study).
Land use: percentages of *Rumex* and *Sanguisorba* relative to the pollen grains of terrestrial seed-bearing plants recorded in Lake Naleng (*25*, *50*).
All environmental factors are standardized using 'decostand(method = "standardize")' in the 'vegan' package (*121*).
P-value: F-test with 999 permutations
Values are rounded one decimal place except for *P*-values.
Independent and significant variables are marked in bold for variation partitioning analysis.

Legends for data S1 – S3

Data S1. The final sedaDNA shotgun count data used for taxonomic composition, ordination, and network analyses, along with related environmental variables, for the terrestrial ecosystem.

Data S2. The final sedaDNA shotgun count data used for taxonomic composition, ordination, and network analyses, along with related environmental variables, for the aquatic ecosystem.

Data S3. The sedaDNA shotgun sequencing information for 40 lake sediments and 12 controls.

REFERENCES AND NOTES

1. C. Körner, “Mountain biodiversity, its causes and function: An overview” in *Mountain Biodiversity*, C. Körner, E. M. Spehn, Eds. (Routledge, 2019), pp. 3–20.

2. M. Stibal, J. A. Bradley, A. Edwards, S. Hotaling, K. Zawierucha, J. Rosvold, S. Lutz, K. A. Cameron, J. A. Mikucki, T. J. Kohler, M. Šabacká, A. M. Anesio, Glacial ecosystems are essential to understanding biodiversity responses to glacier retreat. *Nat. Ecol. Evol.* **4**, 686–687 (2020).

3. X. Jin, H. Jin, G. Iwahana, S. S. Marchenko, D. Luo, X. Li, S. Liang, Impacts of climate-induced permafrost degradation on vegetation: A review. *Adv. Clim. Change Res.* **12**, 29–47 (2021).

4. M. Li, J. Wu, Y. Feng, B. Niu, Y. He, X. Zhang, Climate variability rather than livestock grazing dominates changes in alpine grassland productivity across Tibet. *Front. Ecol. Evol.* **9**, 631024 (2021).

5. Mountain Research Initiative EDW Working Group, Elevation-dependent warming in mountain regions of the world. *Nat. Clim. Change* **5**, 424–430 (2015).

6. D. Zou, L. Zhao, Y. Sheng, J. Chen, G. Hu, T. Wu, J. Wu, C. Xie, X. Wu, Q. Pang, W. Wang, E. Du, W. Li, G. Liu, J. Li, Y. Qin, Y. Qiao, Z. Wang, J. Shi, G. Cheng, A new map of permafrost distribution on the Tibetan Plateau. *Cryosphere* **11**, 2527–2542 (2017).

7. M. Yang, X. Wang, G. Pang, G. Wan, Z. Liu, The Tibetan Plateau cryosphere: Observations and model simulations for current status and recent changes. *Earth Sci. Rev.* **190**, 353–369 (2019).

8. B. Verrall, C. M. Pickering, Alpine vegetation in the context of climate change: A global review of past research and future directions. *Sci. Total Environ.* **748**, 141344 (2020).

9. D. Rhode, D. B. Madsen, P. Jeffrey Brantingham, T. Dargye, “Yaks, yak dung, and prehistoric human habitation of the Tibetan Plateau” in *Late Quaternary Climate Change and Human Adaptation in Arid China*, D. B. Madsen, F. Chen, X. Gao, Eds. (Developments in Quaternary Sciences, Elsevier, 2007), pp. 205–224.

10. Z. Tang, Z. Wang, C. Zheng, J. Fang, Biodiversity in China’s mountains. *Front. Ecol. Environ.* **4**, 347–352 (2006).

11. D. R. Rounce, R. Hock, D. E. Shean, Glacier mass change in high mountain Asia through 2100 using the open-source Python Glacier Evolution Model (PyGEM). *Front. Earth Sci.* **7**, 331 (2020).

12. G. Zhang, Z. Nan, N. Hu, Z. Yin, L. Zhao, G. Cheng, C. Mu, Qinghai-Tibet Plateau permafrost at risk in the late 21st century. *Earth's Future* **10**, e2022EF002652 (2022).

13. S. Zhou, J. Li, J. Zhao, J. Wang, J. Zheng, "*Quaternary glaciations: Extent and chronology in China" in Quaternary Glaciations - Extent and Chronology*, J. Ehlers, P. L. Gibbard, P. D. Hughes, Eds. (Developments in Quaternary Sciences, Elsevier, 2011), pp. 981–1002.

14. H. Jin, J. Vandenberghe, D. Luo, S. A. Harris, R. He, X. Chen, X. Jin, Q. Wang, Z. Zhang, V. Spektor, Q. Wu, S. Wang, Quaternary permafrost in China: Framework and discussions. *Quaternary* **3**, 32 (2020).

15. L. Tang, C. Shen, H. Lu, C. Li, Q. Ma, Fifty years of Quaternary palynology in the Tibetan Plateau. *Sci. China Earth Sci.* **64**, 1825–1843 (2021).

16. S. A. Zimov, V. I. Chuprynin, A. P. Oreshko, F. S. Chapin III, J. F. Reynolds, M. C. Chapin, Steppe-tundra transition: A herbivore-driven biome shift at the end of the Pleistocene. *Am. Nat.* **146**, 765–794 (1995).

17. S. A. Zimov, N. S. Zimov, A. N. Tikhonov, F. S. Chapin, Mammoth steppe: A high-productivity phenomenon. *Quat. Sci. Rev.* **57**, 26–45 (2012).

18. Y. Malhi, C. E. Doughty, M. Galetti, F. A. Smith, J.-C. Svenning, J. W. Terborgh, Megafauna and ecosystem function from the Pleistocene to the Anthropocene. *Proc. Natl. Acad. Sci. U.S.A.* **113**, 838–846 (2016).

19. Z. Wang, X. Shen, B. Liu, J. Su, T. Yonezawa, Y. Yu, S. Guo, S. Y. W. Ho, C. Vilà, M. Hasegawa, J. Liu, Phylogeographical analyses of domestic and wild yaks based on mitochondrial DNA: New data and reappraisal. *J. Biogeogr.* **37**, 2332–2344 (2010).

20. M. Macias-Fauria, P. Jepson, N. Zimov, Y. Malhi, Pleistocene Arctic megafaunal ecological engineering as a natural climate solution?. *Philos. Trans. R. Soc. Lond. B Biol. Sci.* **375**, 20190122 (2020).

21. X. L. Zhang, B. B. Ha, S. J. Wang, Z. J. Chen, J. Y. Ge, H. Long, W. He, W. Da, X. M. Nian, M. Yi, X.-Y. Zhou, P. Q. Zhang, Y. Jin, O. Bar-Yosef, J. W. Olsen, X. Gao, The earliest human occupation of the high-altitude Tibetan Plateau 40 thousand to 30 thousand years ago. *Science* **362**, 1049–1051 (2018).

22. F. H. Chen, G. H. Dong, D. J. Zhang, X. Y. Liu, X. Jia, C. B. An, M. M. Ma, Y. W. Xie, L. Barton, X. Y. Ren, Z. J. Zhao, X. H. Wu, M. K. Jones, Agriculture facilitated permanent human occupation of the Tibetan Plateau after 3600 B.P. *Science* **347**, 248–250 (2015).

23. Q. Qiu, L. Wang, K. Wang, Y. Yang, T. Ma, Z. Wang, X. Zhang, Z. Ni, F. Hou, R. Long, R. Abbott, J. Lenstra, J. Liu, Yak whole-genome resequencing reveals domestication signatures and prehistoric population expansions. *Nat. Commun.* **6**, 10283 (2015).

24. F. Schlütz, F. Lehmkuhl, Holocene climatic change and the nomadic Anthropocene in Eastern Tibet: Palynological and geomorphological results from the Nianbaoyeze Mountains. *Quat. Sci. Rev.* **28**, 1449–1471 (2009).

25. A. Kramer, U. Herzschuh, S. Mischke, C. Zhang, Holocene treeline shifts and monsoon variability in the Hengduan Mountains (southeastern Tibetan Plateau), implications from palynological investigations. *Palaeogeogr. Palaeoclimatol. Palaeoecol.* **286**, 23–41 (2010).

26. G. Miehe, P.-M. Schleuss, E. Seeber, W. Babel, T. Biermann, M. Braendle, F. Chen, H. Coners, T. Foken, T. Gerken, H.-F. Graf, G. Guggenberger, S. Hafner, M. Holzapfel, J. Ingrisch, Y. Kuzyakov, Z. Lai, L. Lehnert, C. Leuschner, X. Li, J. Liu, S. Liu, Y. Ma, S. Miehe, V. Mosbrugger, H. J. Noltie, J. Schmidt, S. Spielvogel, S. Unteregelsbacher, Y. Wang, S. Willinghöfer, X. Xu, Y. Yang, S. Zhang, L. Opgenoorth, K. Wesche, The *Kobresia pygmaea* ecosystem of the Tibetan highlands – Origin, functioning and degradation of the world's largest pastoral alpine ecosystem: *Kobresia* pastures of Tibet. *Sci. Total Environ.* **648**, 754–771 (2019).

27. X. Xiao, A. Yao, A. Hillman, J. Shen, S. G. Haberle, Vegetation, climate and human impact since 20 ka in central Yunnan Province based on high-resolution pollen and charcoal records from Dianchi, southwestern China. *Quat. Sci. Rev.* **236**, 106297 (2020).

28. G. Miehe, S. u. Hasson, B. Glaser, S. Mischke, J. Böhner, W. O. van der Knaap, J. F. N. van Leeuwen, L. Duo, S. Miehe, T. Haberzettl, Föhn, fire and grazing in Southern Tibet? A 20,000-year multi-proxy record in an alpine ecotonal ecosystem. *Quat. Sci. Rev.* **256**, 106817 (2021).

29. L. W. Lehnert, K. Wesche, K. Trachte, C. Reudenbach, J. Bendix, Climate variability rather than overstocking causes recent large scale cover changes of Tibetan pastures. *Sci. Rep.* **6**, 24367 (2016).

30. F. Tian, W. Qin, R. Zhang, U. Herzschuh, J. Ni, C. Zhang, S. Mischke, X. Cao, Palynological evidence for the temporal stability of the plant community in the Yellow River source area over the last 7,400 years. *Veg. Hist. Archaeobotany* **31**, 549–558 (2022).

31. K. Bauer, Y. Nyima, Laws and regulations impacting the enclosure movement on the Tibetan Plateau of China. *HIMALAYA J. Assoc. Nepal Himal. Stud.* **30**, 23–37 (2011).

32. B. Aichner, U. Herzschuh, H. Wilkes, A. Vieth, J. Böhner, δD values of *n*-alkanes in Tibetan lake sediments and aquatic macrophytes – A surface sediment study and application to a 16ka record from Lake Koucha. *Org. Geochem.* **41**, 779–790 (2010).

33. U. Herzschuh, S. Mischke, H. Meyer, B. Plessen, C. Zhang, Lake nutrient variability inferred from elemental (C, N, S) and isotopic ($\delta^{13}C$, $\delta^{15}N$) analyses of aquatic plant macrofossils. *Quat. Sci. Rev.* **29**, 2161–2172 (2010).

34. Z. Baiping, C. Xiaodong, L. Baolin, Y. Yonghui, Biodiversity and conservation in the Tibetan Plateau. *J. Geogr. Sci.* **12**, 135–143 (2002).

35. U. Herzschuh, C. Zhang, S. Mischke, R. Herzschuh, F. Mohammadi, B. Mingram, H. Kürschner, F. Riedel, A late Quaternary lake record from the Qilian Mountains (NW China): Evolution of the primary production and the water depth reconstructed from macrofossil, pollen, biomarker, and isotope data. *Glob. Planet. Change* **46**, 361–379 (2005).

36. J. Saini, F. Günther, B. Aichner, S. Mischke, U. Herzschuh, C. Zhang, R. Mäusbacher, G. Gleixner, Climate variability in the past ~19,000 yr in NE Tibetan Plateau inferred from biomarker and stable isotope records of Lake Donggi Cona. *Quat. Sci. Rev.* **157**, 129–140 (2017).

37. B. Aichner, B. Wünnemann, A. Callegaro, M. T. J. van der Meer, D. Yan, Y. Zhang, C. Barbante, D. Sachse, Asynchronous responses of aquatic ecosystems to hydroclimatic forcing on the Tibetan Plateau. *Commun. Earth Environ.* **3**, 3 (2022).

38. S. Huo, H. Zhang, J. Wang, J. Chen, F. Wu, Temperature and precipitation dominates millennium changes of eukaryotic algal communities in Lake Yamzhog Yumco, Southern Tibetan Plateau. *Sci. Total Environ.* **829**, 154636 (2022).

39. A. I. T. Tulloch, I. Chadès, Y. Dujardin, M. J. Westgate, P. W. Lane, D. Lindenmayer, Dynamic species co-occurrence networks require dynamic biodiversity surrogates. *Ecography* **39**, 1185–1196 (2016).

40. A. D. Muscente, A. Prabhu, H. Zhong, A. Eleish, M. B. Meyer, P. Fox, R. M. Hazen, A. H. Knoll, Quantifying ecological impacts of mass extinctions with network analysis of fossil communities. *Proc. Natl. Acad. Sci. U.S.A.* **115**, 5217–5222 (2018).

41. M. D. Bertness, R. Callaway, Positive interactions in communities. *Trends Ecol. Evol.* **9**, 191–193 (1994).

42. Y. Wang, J. Sun, B. Liu, J. Wang, T. Zeng, Cushion plants as critical pioneers and engineers in alpine ecosystems across the Tibetan Plateau. *Ecol. Evol.* **11**, 11554–11558 (2021).

43. Y.-Z. Zhang, L.-S. Qian, X.-F. Chen, L. Sun, H. Sun, J.-G. Chen, Diversity patterns of cushion plants on the Qinghai-Tibet Plateau: A basic study for future conservation efforts on alpine ecosystems. *Plant Divers.* **44**, 231–242 (2022).

44. F. Anthelme, L. A. Cavieres, O. Dangles, Facilitation among plants in alpine environments in the face of climate change. *Front. Plant Sci.* **5**, 387 (2014).

45. S. Liu, S. Kruse, D. Scherler, R. H. Ree, H. H. Zimmermann, K. R. Stoof-Leichsenring, L. S. Epp, S. Mischke, U. Herzschuh, Sedimentary ancient DNA reveals a threat of warming-induced alpine habitat loss to Tibetan Plateau plant diversity. *Nat. Commun.* **12**, 2995 (2021).

46. J. P. Smol, H. J. B. Birks, A. F. Lotter, S. Juggins, "The march towards the quantitative analysis of palaeolimnological data" in *Tracking Environmental Change Using Lake Sediments*, H. J. B. Birks, A. F. Lotter, S. Juggins, J. P. Smol, Eds. (Springer Netherlands,, 2012), vol. 5, chap. 1.

47. W. Jia, S. Anslan, F. Chen, X. Cao, H. Dong, K. Dulias, Z. Gu, L. Heinecke, H. Jiang, S. Kruse, W. Kang, K. Li, S. Liu, X. Liu, Y. Liu, J. Ni, A. Schwalb, K. R. Stoof-Leichsenring, W. Shen, F. Tian, J. Wang, Y. Wang, Y. Wang, H. Xu, X. Yang, D. Zhang, U. Herzschuh, Sedimentary ancient DNA reveals past ecosystem and biodiversity changes on the Tibetan Plateau: Overview and prospects. *Quat. Sci. Rev.* **293**, 107703 (2022).

48. K. H. Kjær, M. Winther Pedersen, B. De Sanctis, B. De Cahsan, T. S. Korneliussen, C. S. Michelsen, K. K. Sand, S. Jelavić, A. H. Ruter, A. M. A. Schmidt, K. K. Kjeldsen, A. S. Tesakov, I. Snowball, J. C. Gosse, I. G. Alsos, Y. Wang, C. Dockter, M. Rasmussen, M. E. Jørgensen, B. Skadhauge, A. Prohaska, J. Å. Kristensen, M. Bjerager, M. E. Allentoft, E. Coissac; PhyloNorway Consortium, A. Rouillard, A. Simakova, A. Fernandez-Guerra, C. Bowler, M. Macias-Fauria, L. Vinner, J. J. Welch, A. J. Hidy, M. Sikora, M. J. Collins, R. Durbin, N. K. Larsen, E. Willerslev, A 2-million-year-old ecosystem in Greenland uncovered by environmental DNA. *Nature* **612**, 283–291 (2022).

49. Y. Wang, T. S. Korneliussen, L. E. Holman, A. Manica, M. W. Pedersen, *ngs*LCA—A toolkit for fast and flexible lowest common ancestor inference and taxonomic profiling of metagenomic data. *Methods Ecol. Evol.* **13**, 2699–2708 (2022).

50. A. Kramer, U. Herzschuh, S. Mischke, C. Zhang, Late glacial vegetation and climate oscillations on the southeastern Tibetan Plateau inferred from the Lake Naleng pollen profile. *Quatern. Res.* **73**, 324–335 (2010).

51. B. Kang, J. Deng, Y. Wu, L. Chen, J. Zhang, H. Qiu, Y. Lu, D. He, Mapping China's freshwater fishes: Diversity and biogeography. *Fish Fish.* **15**, 209–230 (2014).

52. L. Zhang, Q. Wang, L. Yang, F. Li, B. P. L. Chan, Z. Xiao, S. Li, D. Song, Z. Piao, P. Fan, The neglected otters in China: Distribution change in the past 400 years and current conservation status. *Biol. Conserv.* **228**, 259–267 (2018).

53. Y. Lammers, P. D. Heintzman, I. G. Alsos, Environmental palaeogenomic reconstruction of an Ice Age algal population. *Commun. Biol.* **4**, 200 (2021).

54. J. Huisman, G. A. Codd, H. W. Paerl, B. W. Ibelings, J. M. H. Verspagen, P. M. Visser, Cyanobacterial blooms. *Nat. Rev. Microbiol.* **16**, 471–483 (2018).

55. J. Courtin, A. Perfumo, A. A. Andreev, T. Opel, K. R. Stoof-Leichsenring, M. E. Edwards, J. B. Murton, U. Herzschuh, Pleistocene glacial and interglacial ecosystems inferred from ancient DNA analyses of permafrost sediments from Batagay megaslump, East Siberia. *Environ. DNA* **4**, 1265–1283 (2022).

56. M. W. Pedersen, A. Ruter, C. Schweger, H. Friebe, R. A. Staff, K. K. Kjeldsen, M. L. Z. Mendoza, A. B. Beaudoin, C. Zutter, N. K. Larsen, B. A. Potter, R. Nielsen, R. A. Rainville, L. Orlando, D. J. Meltzer, K. H. Kjær, E. Willerslev, Postglacial viability and colonization in North America's ice-free corridor. *Nature* **537**, 45–49 (2016).

57. L. Parducci, I. G. Alsos, P. Unneberg, M. W. Pedersen, L. Han, Y. Lammers, J. S. Salonen, M. M. Väliranta, T. Slotte, B. Wohlfarth, Shotgun environmental DNA, pollen, and macrofossil analysis of Lateglacial lake sediments from southern Sweden. *Front. Ecol. Evol.* **7**, 189 (2019).

58. Y. Wang, M. W. Pedersen, I. G. Alsos, B. De Sanctis, F. Racimo, A. Prohaska, E. Coissac, H. L. Owens, M. K. F. Merkel, A. Fernandez-Guerra, A. Rouillard, Y. Lammers, A. Alberti, F. Denoeud, D. Money, A. H. Ruter, H. McColl, N. K. Larsen, A. A. Cherezova, M. E. Edwards, G. B. Fedorov, J. Haile, L. Orlando, L. Vinner, T. S. Korneliussen, D. W. Beilman, A. A. Bjørk, J. Cao, C. Dockter, J. Esdale, G. Gusarova, K. K. Kjeldsen, J. Mangerud, J. T. Rasic, B. Skadhauge, J. I. Svendsen, A. Tikhonov, P. Wincker, Y. Xing, Y. Zhang, D. G. Froese, C. Rahbek, D. B. Nogues, P. B. Holden, N. R. Edwards, R. Durbin, D. J. Meltzer, K. H. Kjær, P. Möller, E. Willerslev, Late Quaternary dynamics of Arctic biota from ancient environmental genomics. *Nature* **600**, 86–92 (2021).

59. K. Li, K. R. Stoof-Leichsenring, S. Liu, W. Jia, M. Liao, X. Liu, J. Ni, U. Herzschuh, Plant sedimentary DNA as a proxy for vegetation reconstruction in eastern and northern Asia. *Ecol. Indic.* **132**, 108303 (2021).

60. Z. Wende, G. Hou, J. Gao, X. Chen, S. Jin, Z. Lancuo, Reconstruction of cultivated land in the northeast margin of Qinghai–Tibetan Plateau and anthropogenic impacts on palaeo-environment during the mid-Holocene. *Front. Earth Sci.* **9**, 681995 (2021.

61. A. E. Adams, E. M. Besozzi, G. Shahrokhi, M. A. Patten, A case for associational resistance: Apparent support for the stress gradient hypothesis varies with study system. *Ecol. Lett.* **25**, 202–217 (2022).

62. J. M. Kleinberg, Authoritative sources in a hyperlinked environment. *J. ACM* **46**, 604–632 (1999).

63. G. Yang, M. Ryo, J. Roy, D. R. Lammel, M.-B. Ballhausen, X. Jing, X. Zhu, M. C. Rillig, Multiple anthropogenic pressures eliminate the effects of soil microbial diversity on ecosystem functions in experimental microcosms. *Nat. Commun.* **13**, 4260 (2022).

64. C. V. Robinson, T. M. Porter, V. C. Maitland, M. T. G. Wright, M. Hajibabaei, Multi-marker metabarcoding resolves subtle variations in freshwater condition: Bioindicators, ecological traits, and trophic interactions. *Ecol. Indic.* **145**, 109603 (2022).

65. G. Bao, K. Suetsugu, H. Wang, X. Yao, L. Liu, J. Ou, C. Li, Effects of the hemiparasitic plant *Pedicularis kansuensis* on plant community structure in a degraded grassland. *Ecol. Res.* **30**, 507–515 (2015).

66. L. A. Cavieres, E. I. Badano, Do facilitative interactions increase species richness at the entire community level? *J. Ecol.* **97**, 1181–1191 (2009).

67. J. Ebersbach, J. Schnitzler, A. Favre, A. N. Muellner-Riehl, Evolutionary radiations in the species-rich mountain genus *Saxifraga* L. *BMC Evol. Biol.* **17**, 119 (2017).

68. X. Jing, L. Ding, J. Zhou, X. Huang, A. Degen, R. Long, The adaptive strategies of yaks to live in the Asian highlands. *Anim. Nutr.* **9**, 249–258 (2022).

69. A. Kramer, U. Herzschuh, S. Mischke, C. Zhang, Late Quaternary environmental history of the south-eastern Tibetan Plateau inferred from the Lake Naleng non-pollen palynomorph record. *Veg. Hist. Archaeobotany* **19**, 453–468 (2010).

70. N. Guo, Q. Wu, F. Shi, J. Niu, T. Zhang, A. A. Degen, Q. Fang, L. Ding, Z. Shang, Z. Zhang, R. Long, Seasonal dynamics of diet–gut microbiota interaction in adaptation of yaks to life at high altitude. *Npj Biofilms Microbiomes* **7**, 38 (2021).

71. S. K. Basumatary, H. Singh, E. N. van Asperen, S. Tripathi, H. G. McDonald, A. K. Pokharia, Coprophilous and non-coprophilous fungal spores of *Bos mutus* modern dung from the Indian Himalaya: Implications to temperate paleoherbivory and paleoecological analysis. *Rev. Palaeobot. Palynol.* **277**, 104208 (2020).

72. E. Willerslev, J. Davison, M. Moora, M. Zobel, E. Coissac, M. E. Edwards, E. D. Lorenzen, M. Vestergård, G. Gussarova, J. Haile, J. Craine, L. Gielly, S. Boessenkool, L. S. Epp, P. B. Pearman, R. Cheddadi, D. Murray, K. A. Bråthen, N. Yoccoz, H. Binney, C. Cruaud, P. Wincker, T. Goslar, I. G. Alsos, E. Bellemain, A. K. Brysting, R. Elven, J. H. Sønstebø, J. Murton, A. Sher, M. Rasmussen, R. Rønn, T. Mourier, A. Cooper, J. Austin, P. Möller, D. Froese, G. Zazula, F. Pompanon, D. Rioux, V. Niderkorn, A. Tikhonov, G. Savvinov, R. G. Roberts, R. D. E. MacPhee, M. T. P. Gilbert, K. H. Kjær, L. Orlando, C. Brochmann, P. Taberlet, Fifty thousand years of Arctic vegetation and megafaunal diet. *Nature* **506**, 47–51 (2014).

73. I. C. Barrio, D. S. Hik, C. G. Bueno, J. F. Cahill, Extending the stress-gradient hypothesis – is competition among animals less common in harsh environments? *Oikos* **122**, 516–523 (2013).

74. T. J. Murchie, A. J. Monteath, M. E. Mahony, G. S. Long, S. Cocker, T. Sadoway, E. Karpinski, G. Zazula, R. D. E. MacPhee, D. Froese, H. N. Poinar, Collapse of the mammoth-steppe in central Yukon as revealed by ancient environmental DNA. *Nat. Commun.* **12**, 7120 (2021).

75. E. Politti, W. Bertoldi, A. Gurnell, A. Henshaw, Feedbacks between the riparian Salicaceae and hydrogeomorphic processes: A quantitative review. *Earth Sci. Rev.* **176**, 147–165 (2018).

76. C. Yang, T. Yan, Y. Sun, F. Hou, Shrub cover impacts on yak growth performance and herbaceous forage quality on the Qinghai-Tibet Plateau, China. *Rangel. Ecol. Manag.* **75**, 9–16 (2021).

77. A. J. Monteath, B. V. Gaglioti, M. E. Edwards, D. Froese, Late Pleistocene shrub expansion preceded megafauna turnover and extinctions in eastern Beringia. *Proc. Natl. Acad. Sci. U.S.A.* **118**, e2107977118 (2021).

78. J. d'Alpoim Guedes, Rethinking the spread of agriculture to the Tibetan Plateau. *Holocene* **25**, 1498–1510 (2015).

79. P. Rozwalak, P. Podkowa, J. Buda, P. Niedzielski, S. Kawecki, R. Ambrosini, R. S. Azzoni, G. Baccolo, J. L. Ceballos, J. Cook, B. Di Mauro, G. F. Ficetola, A. Franzetti, D. Ignatiuk, P. Klimaszyk, E. Łokas, M. Ono, I. Parnikoza, M. Pietryka, F. Pittino, E. Poniecka, D. L. Porazinska, D. Richter, S. K. Schmidt, P. Sommers, J. Souza-Kasprzyk, M. Stibal, W. Szczuciński, J. Uetake, Ł. Wejnerowski, J. C. Yde, N. Takeuchi, K. Zawierucha, Cryoconite-From minerals and organic matter to bioengineered sediments on glacier's surfaces. *Sci. Total Environ.* **807**, 150874 (2022).

80. K. Liu, Y. Liu, B. Han, B. Xu, L. Zhu, J. Ju, N. Jiao, J. Xiong, Bacterial community changes in a glacial-fed Tibetan lake are correlated with glacial melting. *Sci. Total Environ.* **651**, 2059–2067 (2019).

81. K. Liu, Y. Liu, A. Hu, F. Wang, Z. Zhang, Q. Yan, M. Ji, T. J. Vick-Majors, Fate of glacier surface snow-originating bacteria in the glacier-fed hydrologic continuums. *Environ. Microbiol.* **23**, 6450–6462 (2021).

82. J. Kleinteich, K. Hanselmann, F. Hildebrand, A. Kappler, C. Zarfl, Glacier melt-down changes habitat characteristics and unique microbial community composition and physiology in alpine lake sediments. *FEMS Microbiol. Ecol.* **98**, fiac075 (2022).

83. M. Bruno, P. M. B. Gucci, E. Pierdominici, P. Sestili, A. Ioppolo, N. Sechi, L. Volterra, Microcystin-like toxins in different freshwater species of *Oscillatoria*. *Toxicon* **30**, 1307–1311 (1992).

84. S. P. Hammarlund, W. R. Harcombe, Refining the stress gradient hypothesis in a microbial community. *Proc. Natl. Acad. Sci. U.S.A.* **116**, 15760–15762 (2019).

85. E. Hesse, S. O'Brien, A. M. Luján, D. Sanders, F. Bayer, E. M. van Veen, D. J. Hodgson, A. Buckling, Stress causes interspecific facilitation within a compost community. *Ecol. Lett.* **24**, 2169–2177 (2021).

86. K. R. Stoof-Leichsenring, S. Huang, S. Liu, W. Jia, K. Li, X. Liu, L. A. Pestryakova, U. Herzschuh, Sedimentary DNA identifies modern and past macrophyte diversity and its environmental drivers in high-latitude and high-elevation lakes in Siberia and China. *Limnol. Oceanogr.* **67**, 1126–1141 (2022).

87. J. Tao, D. He, M. J. Kennard, C. Ding, S. E. Bunn, C. Liu, Y. Jia, R. Che, Y. Chen, Strong evidence for changing fish reproductive phenology under climate warming on the Tibetan Plateau. *Glob. Chang. Biol.* **24**, 2093–2104 (2018).

88. C. Liu, L. Comte, W. Xian, Y. Chen, J. D. Olden, Current and projected future risks of freshwater fish invasions in China. *Ecography* **42**, 2074–2083 (2019).

89. C. Ayres, P. García, Features of the predation of the Eurasian otter upon toads in north-western Spain. *Mamm. Biol.* **76**, 90–92 (2011).

90. S. Nakai, S. Yamada, M. Hosomi, Anti-cyanobacterial fatty acids released from *Myriophyllum spicatum*. *Hydrobiologia* **543**, 71–78 (2005).

91. Z. A. Mohamed, Macrophytes-cyanobacteria allelopathic interactions and their implications for water resources management—A review. *Limnologica* **63**, 122–132 (2017).

92. L. Randsalu-Wendrup, D. J. Conley, J. Carstensen, S. C. Fritz, Paleolimnological records of regime shifts in lakes in response to climate change and anthropogenic activities. *J. Paleolimnol.* **56**, 1–14 (2016).

93. X. Lu, K. C. Kelsey, Y. Yan, J. Sun, X. Wang, G. Cheng, J. C. Neff, Effects of grazing on ecosystem structure and function of alpine grasslands in Qinghai–Tibetan Plateau: A synthesis. *Ecosphere* **8**, e01656 (2017).

94. K. A. Hopping, A. K. Knapp, T. Dorji, J. A. Klein, Warming and land use change concurrently erode ecosystem services in Tibet. *Glob. Chang. Biol.* **24**, 5534–5548 (2018).

95. Y. Wang, W. Lv, K. Xue, S. Wang, L. Zhang, R. Hu, H. Zeng, X. Xu, Y. Li, L. Jiang, Y. Hao, J. Du, J. Sun, T. Dorji, S. Piao, C. Wang, C. Luo, Z. Zhang, X. Chang, M. Zhang, Y. Hu, T. Wu, J. Wang, B. Li, P. Liu, Y. Zhou, A. Wang, S. Dong, X. Zhang, Q. Gao, H. Zhou, M. Shen, A. Wilkes, G. Miehe, X. Zhao, H. Niu, Grassland changes and adaptive management on the Qinghai–Tibetan Plateau. *Nat. Rev. Earth Environ.* **3**, 668–683 (2022).

96. S. Opitz, C. Zhang, U. Herzschuh, S. Mischke, Climate variability on the south-eastern Tibetan Plateau since the Lateglacial based on a multiproxy approach from Lake Naleng – comparing pollen and non-pollen signals. *Quat. Sci. Rev.* **115**, 112–122 (2015).

97. Z. Wang, Q. Wang, L. Zhao, X. Wu, G. Yue, D. Zou, Z. Nan, G. Liu, Q. Pang, H. Fang, T. Wu, J. Shi, K. Jiao, Y. Zhao, L. Zhang, Mapping the vegetation distribution of the permafrost zone on the Qinghai-Tibet Plateau. *J. Mt. Sci.* **13**, 1035–1046 (2016).

98. I. Larridon, A linear classification of Cyperaceae. *Kew Bull.* **77**, 309–315 (2022).

99. S. Strasky, A. A. Graf, Z. Zhao, P. W. Kubik, H. Baur, C. Schlüchter, R. Wieler, Late Glacial ice advances in southeast Tibet. *J. Asian Earth Sci.* **34**, 458–465 (2009).

100. F. Chen, J. Zhang, J. Liu, X. Cao, J. Hou, L. Zhu, X. Xu, X. Liu, M. Wang, D. Wu, L. Huang, T. Zeng, S. Zhang, W. Huang, X. Zhang, K. Yang, Climate change, vegetation history, and landscape responses on the Tibetan Plateau during the Holocene: A comprehensive review. *Quat. Sci. Rev.* **243**, 106444 (2020).

101. P. A. Meyers, Preservation of elemental and isotopic source identification of sedimentary organic matter. *Chem. Geol.* **114**, 289–302 (1994).

102. M.-T. Gansauge, T. Gerber, I. Glocke, P. Korlević, L. Lippik, S. Nagel, L. M. Riehl, A. Schmidt, M. Meyer, Single-stranded DNA library preparation from highly degraded DNA using T4 DNA ligase. *Nucleic Acids Res.* **45**, e79 (2017).

103. M. T. Gansauge, M. Meyer, Single-stranded DNA library preparation for the sequencing of ancient or damaged DNA. *Nat. Protoc.* **8**, 737–748 (2013).

104. S. Andrews, FastQC: A quality control tool for high throughput sequence data. (2010). https://bioinformatics.babraham.ac.uk/projects/fastqc/.

105. S. Chen, Y. Zhou, Y. Chen, J. Gu, Fastp: An ultra-fast all-in-one FASTQ preprocessor. *Bioinformatics* **34**, i884–i890 (2018).

106. B. Langmead, S. L. Salzberg, Fast gapped-read alignment with Bowtie 2. *Nat. Methods* **9**, 357–359 (2012).

107. J. Dabney, M. Meyer, S. Pääbo, Ancient DNA Damage. *Cold Spring Harb. Perspect. Biol.* **5**, a012567 (2013).

108. H. Jónsson, A. Ginolhac, M. Schubert, P. L. F. Johnson, L. Orlando, MapDamage2.0: Fast approximate Bayesian estimates of ancient DNA damage parameters. *Bioinformatics* **29**, 1682–1684 (2013).

109. J. He, H. Lin, R. Wang, C. Dai, H. Yu, J. Tu, J. Yu, H. Jiang, Joint effects of environmental filtering and dispersal limitation on the species assemblage of the Tibetan Plateau. *J. Biogeogr.* **49**, 640–653 (2022).

110. X.-H. Li, X.-X. Zhu, Y. Niu, H. Sun, Phylogenetic clustering and overdispersion for alpine plants along elevational gradient in the Hengduan Mountains Region, southwest China. *J. Syst. Evol.* **52**, 280–288 (2014).

111. J. Xu, Y. Chen, L. Zhang, Y. Chai, M. Wang, Y. Guo, T. Li, M. Yue, Using phylogeny and functional traits for assessing community assembly along environmental gradients: A deterministic process driven by elevation. *Ecol. Evol.* **7**, 5056–5069 (2017).

112. M. I. Love, W. Huber, S. Anders, Moderated estimation of fold change and dispersion for RNA-seq data with DESeq2. *Genome Biol.* **15**, 550 (2014).

113. J. D. Shakun, P. U. Clark, F. He, S. A. Marcott, A. C. Mix, Z. Liu, B. Otto-Bliesner, A. Schmittner, E. Bard, Global warming preceded by increasing carbon dioxide concentrations during the last deglaciation. *Nature* **484**, 49–54 (2012).

114. S. A. Marcott, J. D. Shakun, P. U. Clark, A. C. Mix, A reconstruction of regional and global temperature for the past 11,300 years. *Science* **339**, 1198–1201 (2013).

115. Z. Xie, X. Le Roux, C. Wang, Z. Gu, M. An, H. Nan, B. Chen, F. Li, Y. Liu, G. Du, H. Feng, X. Ma, Identifying response groups of soil nitrifiers and denitrifiers to grazing and associated soil environmental drivers in Tibetan alpine meadows. *Soil Biol. Biochem.* **77**, 89–99 (2014).

116. M. Court-Picon, A. Buttler, J.-L. de Beaulieu, Modern pollen/vegetation/land-use relationships in mountain environments: An example from the Champsaur valley (French Alps). *Veg. Hist. Archaeobotany* **15**, 151–168 (2006).

117. M. Ma, J. I. Walck, Z. Ma, L. Wang, G. Du, Grazing disturbance increases transient but decreases persistent soil seed bank. *Ecol. Appl.* **28**, 1020–1031 (2018).

118. C. M. Pauler, J. Isselstein, T. Braunbeck, M. K. Schneider, Influence of highland and production-oriented cattle breeds on pasture vegetation: A pairwise assessment across broad environmental gradients. *Agric. Ecosyst. Environ.* **284**, 106585 (2019).

119. J. Fox, S. Weisberg, "Diagnosing problems in linear and generalized linear models" in *An R Companion to Applied Regression* (SAGE Publications Inc.,, ed. 2, 2011), pp. 285–328.

120. P. R. Peres-Neto, P. Legendre, S. Dray, D. Borcard, Variation partitioning of species data matrices: Estimation and comparison of fractions. *Ecology* **87**, 2614–2625 (2006).

121. J. Oksanen, F. G. Blanchet, M. Friendly, R. Kindt, P. Legendre, D. McGlinn, P. R. Minchin, R. B. O'Hara, G. L. Simpson, P. Solymos, M. H. H. Stevens, E. Szoecs, H. Wagner, vegan: Community Ecology Package. (2019). https://CRAN.R-project.org/package=vegan.

122. F. Valladares, C. C. Bastias, O. Godoy, E. Granda, A. Escudero, Species coexistence in a changing world. *Front. Plant Sci.* **6**, 866 (2015).

123. G. C. Popovic, D. I. Warton, F. J. Thomson, F. K. C. Hui, A. T. Moles, Untangling direct species associations from indirect mediator species effects with graphical models. *Methods Ecol. Evol.* **10**, 1571–1583 (2019).

124. G. C. Popovic, F. K. C. Hui, D. I. Warton, A general algorithm for covariance modeling of discrete data. *J. Multivar. Anal.* **165**, 86–100 (2018).

125. G. Csardi, T. Nepusz, The igraph software package for complex network research. *InterJournal Complex Syst.* **1695**, 1–9 (2006).

126. R Core Team, R: A Language and Environment for Statistical Comput. Secur., version 4.1.2 (2021). https://R-project.org/.

127. X. Li, L. Wang, D. Chen, K. Yang, B. Xue, L. Sun, Near-surface air temperature lapse rates in the mainland China during 1962-2011. *J. Geophys. Res. Atmospheres* **118**, 7505–7515 (2013).

128. GBIF.org, GBIF occurrence download: Tracheophyta, (2022). https://doi.org/10.15468/dl.8ruwan.

129. A. R. Brach, H. Song, eFloras: New directions for online floras exemplified by the Flora of China Project. *TAXON* **55**, 188–192 (2006).

130. H. Yu, A. Favre, X. Sui, Z. Chen, W. Qi, G. Xie, Mapping the genetic patterns of plants in the region of the Qinghai–Tibet Plateau: Implications for conservation strategies. *Divers. Distrib.* **25**, 310–324 (2019).

131. H. Yu, S. Miao, G. Xie, X. Guo, Z. Chen, A. Favre, Contrasting Floristic Diversity of the Hengduan Mountains, the Himalayas and the Qinghai-Tibet Plateau Sensu Stricto in China. *Front. Ecol. Evol.* **8**, 136 (2020).

132. Y. Zhang, B. Li, D. Zheng, Datasets of the boundary and area of the Tibetan Plateau. *Acta Geogr. Sin.* **64**, 164–168 (2014).

133. X. Li, W. Fu, H. Shen, C. Huang, L. Zhang, Monitoring snow cover variability (2000–2014) in the Hengduan Mountains based on cloud-removed MODIS products with an adaptive spatio-temporal weighted method. *J. Hydrol.* **551**, 314–327 (2017).

134. E. Pebesma, S. B. Roger, S classes and methods for spatial data: The sp package. *R News* **5**, 9–13 (2005).

135. R. Bivand, E. J. Pebesma, V. Gómez-Rubio, “Further methods for handling spatial data” in *Applied Spatial Data Analysis with R* (Use R!, Springer,, ed. 2, 2013), pp. 140–142.

136. R. J. Hijmans, raster: Geographic data analysis and modeling. R package version 31-5 (2020). https://rspatial.org/raster.

137. QGIS.org, QGIS geographic information system, version 3.24.1-Tisler, QGIS Association (2022). http://qgis.org.

138. S. A. Chamberlain, E. Szöcs, Taxize: Taxonomic search and retrieval in R. *F1000Res.* **2**, 191 (2013).

139. A. T. Smith, Y. Xie, R. S. Hoffmann, F. Gemma, Eds., *Mammals of China* (Princeton University Press, 2013).

140. GBIF.org, GBIF occurrence download: Mammalia, (2022). https://doi.org/10.15468/dl.7473xu.

141. Y. Xing, C. Zhang, E. Fan, Y. Zhao, Freshwater fishes of China: Species richness, endemism, threatened species and conservation. *Divers. Distrib.* **22**, 358–370 (2016).

142. GBIF.org, GBIF occurrence download: Freshwater fish, (2023). https://doi.org/10.15468/dl.cq3ytx.

143. M. Yang, F. E. Nelson, N. I. Shiklomanov, D. Guo, G. Wan, Permafrost degradation and its environmental effects on the Tibetan Plateau: A review of recent research. *Earth Sci. Rev.* **103**, 31–44 (2010).

144. Q. Lu, D. Zhao, S. Wu, Simulated responses of permafrost distribution to climate change on the Qinghai–Tibet Plateau. *Sci. Rep.* **7**, 3845 (2017).

145. G. Hu, L. Zhao, R. Li, X. Wu, T. Wu, Q. Pang, G. y. Liu, C. Xie, A model for obtaining ground temperature from air temperature in permafrost regions on the Qinghai-Tibetan Plateau. *Catena* **189**, 104470 (2020).

146. S. E. Fick, R. J. Hijmans, WorldClim 2: New 1-km spatial resolution climate surfaces for global land areas. *Int. J. Climatol.* **37**, 4302–4315 (2017).

147. T. Watanabe, Soil Erosion on Yak-Grazing Steps in the Langtang Himal, Nepal. *Mt. Res. Dev.* **14**, 171–179 (1994).

148. Y. Chen, Y. Deng, J. Ding, H. Hu, T. Xu, F. Li, G. Yang, Y. Yang, Distinct microbial communities in the active and permafrost layers on the Tibetan Plateau. *Mol. Ecol.* **26**, 6608–6620 (2017).

149. C. L. Freeman, L. Dieudonné, O. B. A. Agbaje, M. Žure, J. Q. Sanz, M. Collins, K. K. Sand, Survival of environmental DNA in sediments: Mineralogic control on DNA taphonomy. *Environ. DNA* **5**, 1691–1705 (2023).

150. K. K. Sand, S. Jelavić, K. H. Kjær, A. Prohaska, Importance of eDNA taphonomy and sediment provenance for robust ecological inference: Insights from interfacial geochemistry. *Environ. DNA* **6**, e519 (2024).

151. C. Zhang, S. Mischke, A Lateglacial and Holocene lake record from the Nianbaoyeze Mountains and inferences of lake, glacier and climate evolution on the eastern Tibetan Plateau. *Quat. Sci. Rev.* **28**, 1970–1983 (2009).

152. Y. Wang, X. Liu, S. Mischke, U. Herzschuh, Environmental constraints on lake sediment mineral compositions from the Tibetan Plateau and implications for paleoenvironment reconstruction. *J. Paleolimnol.* **47**, 71–85 (2012).

153. A. B. G. Janssen, S. Teurlincx, S. An, J. H. Janse, H. W. Paerl, W. M. Mooij, Alternative stable states in large shallow lakes? *J. Great Lakes Res.* **40**, 813–826 (2014).

154. A. Laug, A. Schwarz, S. Lauterbach, S. Engels, A. Schwalb, Ecosystem shifts at two mid-Holocene tipping points in the alpine Lake Son Kol (Kyrgyzstan, Central Asia). *Holocene* **30**, 1410–1419 (2020).

155. H. J. Kanbar, F. Olajos, G. Englund, M. Holmboe, Geochemical identification of potential DNA-hotspots and DNA-infrared fingerprints in lake sediments. *Appl. Geochem.* **122**, 104728 (2020).